NOTICE

AVIS

Canada

UNIVERSITY OF ALBERTA

SORPTION RATES AND BANDBROADENING ON A POROUS POLYMERIC
HPLC PACKING

BY

LAURIE M. LITWINSON

A THESIS SUBMITTED TO THE FACULTY OF GRADUATE STUDIES AND
RESEARCH IN PARTIAL FULFILLMENT OF THE REQUIREMENTS FOR THE
DEGREE OF
MASTER OF SCIENCE

DEPARTMENT OF CHEMISTRY

EDMONTON, ALBERTA
SPRING, 1992

Canada

UNIVERSITY OF ALBERTA

RELEASE FORM

NAME OF AUTHOR: LAURIE M. LITWINSON

TITLE OF THESIS: SORPTION RATES AND BANDBROADENING ON

A POROUS POLYMERIC HPLC PACKING

DEGREE FOR WHICH THESIS WAS PRESENTED: M.Sc.

YEAR THIS DEGREE GRANTED: 1991

Permission is hereby granted to the University of Alberta Library to reproduce single copies of this thesis and to lend or sell such copies for private, scholarly or scientific purposes only.

The author reserves all other publication and other rights in association with the copyright in the thesis, and except as hereinbefore provided neither the thesis nor any substantial portion thereof may be printed or otherwise reproduced in any material form whatever without the author's prior written permission.
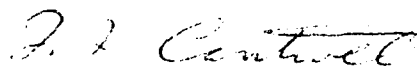
#301 - 555 Austin Ave.
Coquitlam, B.C.
V3K 6R8

DATE: 13 Nov 1991
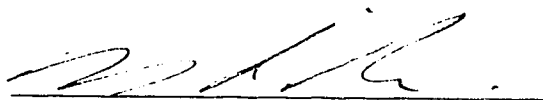
UNIVERSITY OF ALBERTA

FACULTY OF GRADUATE STUDIES AND RESEARCH

The undersigned certify that they have read. and recommed to the Faculty of Graduate Studies and Research for acceptance. a thesis entitled. SORPTION RATES AND BANDBROADENING ON A POROUS POLYMERIC HPLC PACKING submitted by LAURIE M. LITWINSON in partial fulfillment of the requirements for the degree of MASTER OF SCIENCE.

F.F. Cantwell, Supervisor

N. Dovichi

P. Huck

DATE: 6 Nov 1991

This thesis is dedicated to my mother and the memory of my father

"You are the wind beneath my wings"

ABSTRACT

Although the polymeric phase Hamilton PRP-1, which is a styrene divinylbenzene copolymer, is chemically more stable than silica-based reversed phases, it produces broad asymmetric peaks with certain compounds, such as naphthalene and other polyaromatics. Slow sorption-desorption rates on PRP-1 are investigated as a possible cause of the inefficiency.

A shallow bed apparatus is designed to measure rates of sorption on microparticulate HPLC packings. Milligram amounts of sorbent are contained in a slider valve and are subject to exposure to a flowing sample solution for times greater than about 0.4 s. A sorption rate curve, a plot of the concentration of sample in the stationary phase against exposure time, is produced. For sorption of naphthalene on PRP-1, the curve rises sharply then approaches equilibrium at 60 s relatively slowly. It is well fit by a tri-exponential rate equation.

An HPLC analytical column containing PRP-1 is modelled by a series of three hypothetical columns, each corresponding to a separate kinetic process described by one of the terms in the tri-exponential rate equation. Each hypothetical column acts on an impulse function to produce a probability distribution referred to as P1, P2, and P3, corresponding to the broadening caused by the fastest, intermediate and slowest sorption processes respectively. If a sample is injected into a series of the hypothetical columns, the overall predicted elution profile is a convolution of the three distributions.

For PRP-1, the observed elution peak of naphthalene is semi-quantitatively predicted by P1 and P2. The tail of the peak, predicted by inclusion of P3, is not well modelled because of uncertainties in P3 and because the extent of tailing appears to be dependent on column history.

The sorption rate curve of naphthalene on Partisil-10 ODS-3, a silica-based

packing is very different from that on PRP-1. There is a marked absence of a very slow sorption process that, on PRP-1, is observed to affect the curve mainly after the 10 s time. Because the rates on Partisil are too fast to be accurately measured, the sorption rate data does not accurately predict real elution profiles in this case.

ACKNOWLEDGEMENTS

TABLE OF CONTENTS

* * * * * *

LIST OF FIGURES

LIST OF SYMBOLS

A	Pre-exponential factor in EMG function
$A_{hold-up}$	Area of peak due to amount of unretained compound in hold-up volume of shallow bed
A_{inj}	Area of peak due to amount of unretained compound in injection loop of valve V3
C	Concentration of sample injected, in elution experiments
C_e	Effluent sample concentration, in breakthrough experiment
C_m	Sample concentration in the mobile phase
C_s	Sample concentration in the stationary phase
d_i	Diffusion distance
d_p	Particle diameter
D	Slope of linear portion of a sorption isotherm
D_m	Diffusion coefficient in the mobile phase
erf	Error function
EMG	Exponentially modified Gaussian
f	Fraction of mobile phase in pores of a porous stationary phase
$h(t)$	Height of a chromatographic signal with respect to time
h_{EMG}	Height of an exponentially modified Gaussian signal
H	Height equivalent of a theoretical plate
H_{couple}	Plate height due to coupling between eddy diffusion and resistance to mass transfer in the mobile phase
H_{Eddy}	Plate height due to eddy diffusion
H_{LD}	Plate height due to longitudinal diffusion
H_m	Plate height due to resistance to mass transfer in the mobile phase
H_s	Plate height due to resistance to mass transfer in the stationary phase
H_{sm}	Plate height due to resistance to mass transfer in the stagnant mobile phase

H_T	Total plate height
j_m	species j in the mobile phase
j_s	species j in the stationary phase
k'	capacity factor
k_f	Irreversible sorption rate constant
$k_{f,i}$	Irreversible sorption rate constant associated with the ith sorption process
k_i	Measured sorption rate constant due to the ith sorption process
k_r	Irreversible desorption rate constant
$k_{r,i}$	Irreversible desorption rate constant associated with the ith desorption process
L	Length of chromatographic column
M_0	Zeroth statistical moment
$M_{0,i}$	Zeroth statistical moment contribution of the ith term of the multiexponential equation describing the sorption rate curve
M_1	First statistical moment
$M_{1,i}$	First statistical moment contribution of the ith term of the multiexponential equation describing the sorption rate curve
M_2	Second statistical moment
$M_{2,i}$	Second statistical moment contribution of the ith term of the multiexponential equation describing the sorption rate curve
MW_a	molecular weight of solute
$n(t)$	Concentration of sample sorbed at time t in the shallow bed experiment, in moles sample/g packing
n_i	Pre-exponential factor of ith term in the multiexponential equation describing the sorption rate curve
n_m	Number of moles of sample in the mobile phase
n_s	Number of moles of sample in the stationary phase
n_0	Concentration of sample sorbed at infinite exposure time in the shallow bed experiment, in moles sample/g packing

N_{dummy}	Number of moles contained in the dummy hole
N_{el}	Number of moles eluted from shallow bed
$N_{hold\ up}$	Number of moles contained in hold-up volume in shallow bed
N_s	Number of moles adsorbed on the shallow bed
N_{sorb}	Number of moles sorbed on shallow bed
$P(ts)_i$	The probability distribution due to the ith sorption process with respect to time, ts
r	Radius of the shallow bed
t_f	Diffusion time
t_G	Centre of gravity of the parent Gaussian peak in an EMG function
t_m	Time to elute an unretained compound
$t_{m,i}$	Time to elute an unretained compound in a hypothetical column associated with the ith sorption process
t_r	Retention time of a sample
t_s	Time measured from the time to elute an unretained compound
T	Temperature, measured in Kelvin
u	Linear velocity through the shallow bed
u_o	Mobile phase linear velocity, in HPLC column experiments
v_{ip}	Specific interparticle volume
v_p	Specific pore volume
$v_{p,Si}$	Specific pore volume of underivatized silica
v_p'	Specific pore volume of bonded phase with respect to weight of original silica
V_a	Molar volume of solute a
$V_{hold-up}$	Actual hold-up volume of shallow bed
$V_{hold-up,T}$	Total hold-up volume of shallow bed
V_{inj}	Volume of injection loop in valve V3
V_m	Mobile phase volume
V_p	Pore volume in shallow bed

W	Weight of stationary phase in chromatographic column
Wt	Weight of packing in shallow bed
X	Distance travelled down a chromatographic column
Z	Variable in EMG function (see equation 2.31 for definition)
ϵ_{inter}	Fraction of bed volume between particles
γ	Obstruction factor
γ'	Tortuosity factor in resistance to mass transfer in the stagnant mobile phase term
η	viscosity of solvent
λ	packing factor in longitudinal diffusion term
ω	packing factor in resistance to mass transfer in the mobile phase term
ω'	density of solvent
Φ_i	Fraction of sample that passes through a hypothetical column in which the ith sorption process occurs without undergoing at least one sorption-desoption cycle; the non-interacting fraction
ρ	packing density
σ_G	Square root of the variance of the parent Gaussian peak of an EMG function
σ_x^2	Variance of a chromatographic zone in terms of distance
Ψ_s	Association factor of solvent S

LIST OF EQUATIONS

CHAPTER 1

Introduction

Modern HPLC analyses have been made routine and reliable with the
commercial availability of high quality, high efficiency columns. Most analyses are
carried out in the reverse-phase mode on columns containing a non-polar stationary
phase. The vast majority of reverse-phase columns are packed with a silica-based
bonded phase [1.1]. The physical characteristics of the silica support, including
excellent mechanical strength, excellent mass transfer properties in microparticulate
packings and widely available reagents to modify the silica surface, make it a suitable
material for manufacturing chromatographic packings [1.2]. The material does have
some limitations, however, notably its relatively poor resistance to attack in acidic or
basic solutions. The efficiency of silica-based packings also tends to deteriorate with
use of mobile phases which have a high water content, such as are appropriate for ion-
exchange separations.

Various alternate materials have been used as the support for bonded phases in
an attempt to overco.. .. the problems with the pH extremes. Other supports, such as
alumina [1.3, 1.4] and zirconia [1.2] show greater chemical stability [1.5], but are still
largely experimental as supports for RP-HPLC.

Non-polar adsorbents represent an alternate family of RP supports. This
includes carbon and organic copolymers. Carbon, in its various forms has been shown
to be energetically heterogeneous and, in the form of graphite, is mechanically fragile
and subject to long term oxidation [1.2]. One common organic polymer is polystyrene-
divinylbenzene (PS-DVB) which is marketed under trade names such as PRP-1
(Hamilton, Reno, NV), PLRP-S (Polymer Laboratories, Church Stretton, UK) and
Rogel (RSL-Alltech Europe, Eke, Belgium). Other types of polymers such as

polyaromatic esters [1.6] have been synthesized.

Originally, the copolymers were successfully applied to problems such as the separation of amines at high pH, which produces ion suppression, and the resulting separations showed better efficiencies than the same separations on silica-based packings [1.7]. The use of macroporous polymers as a stationary phase for liquid chromatography has recently been reviewed [1.8]. They are applicable in areas where silica-based packings are inadequate and they have been used in the analysis of biologically active species such as tetracyclines [1.9, 1.10, 1.11], penicillins [1.11], proteins [1.12] and erythromycin [1.13]. Some successful assays, such as the separation of Rheumatoid drugs and their metabolites in blood and plasma [1.14] are carried out at elevated pH, in this case, at pH 11. The packing used in this study, PRP-1, has been successfully used as a dynamic cation [1.15, 1.16, 1.17] and a dynamic anion exchanger [1.18, 1.19]. PRP-1 has also been used in the analysis of S-triazine herbicides [1.20].

PS-DVB packings are neutral stationary phases which can be easily modified to produce cation- or anion-exchangers by derivatization with sulphonate or amino groups [1.21]. The underivatized support is stable from pH 1 to 14 [1.22]. The relatively high amount of cross-linking makes the supports mechanically rigid. Despite these ideal characteristics, columns of polymeric packings tend to demonstrate asymmetric peaks and poor efficiency [1.21,1.23]. The efficiency has been shown to be dependent on both the identity of the sample [1.23, 1.24] and the solvent [1.23]. For instance, a planar molecule, such as 9-hydroxymethylanthracene is associated with much lower efficiency than a compound with similar retention characteristics which is linear. Aromatic compounds, in general, tend to give poor efficiency on these packings [1.21].

Figure 1.1 shows the elution chromatograms for naphthalene on two different stationary phases. Partisil-10 ODS-3 is a silica-based bonded phase and the elution profile associated with this packing is symmetrical and narrow. PRP-1 is a PS-DVB
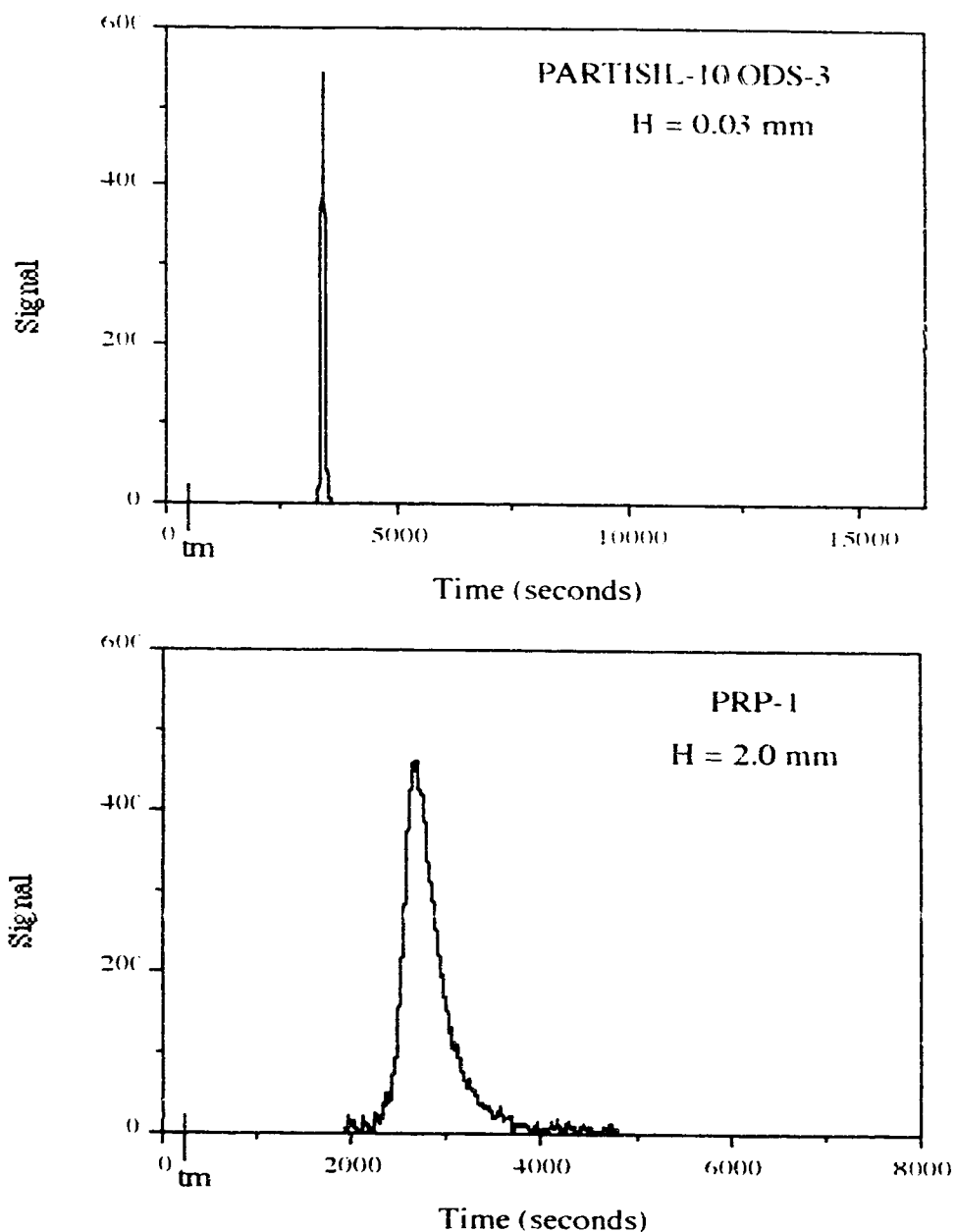
Figure 1.1   Chromatograms of naphthalene on two different kinds of HPLC

packing. The time t_m is the retention time of an unretained compound.

The signal eluting from a column containing the silica-based RP packing

(Partisil-10 ODS-3, in this case) is symmetrical and narrow with a small

plate height, H. The signal from a polymeric packing (PRP-1, in this

case) is severely broadened and highly tailed, with a large plate height.

polymeric stationary phase and the elution profile associated with it is severely broadened and asymmetrical. These peak characteristics observed with PRP-1 lead to poor resolution. poor detection limits and anomalously long analysis times.

Two alternate explanations for this phenomenon have been given. Benson and Woo initially assumed that the poor efficiency was due to π electrons in the polystyrene chains of the support. These electrons might interact strongly with orbitals of solute species. These relatively strong interactions might lead to peak broadening and asymmetry [1.21] in the same way that compounds that are strongly attracted to residual silanols in silica-based columns show these elution characteristics. Copolymers which had been derivatized at the aromatic portion would show decreased π electron interaction and this would lead to decreased tailing. While increased efficiency has been claimed for PS-DVB derivatized with nitro groups [1.25]. no plate heights or other similar measures of the quantity were quoted and conclusions are difficult from published information. Other chemically modified PS-DVB packings have been reported [1.21, 1.26].

An alternate explanation depends on the physical structure of the support. The physical characteristics. including the pore characteristics have been recently well studied for the polymeric stems [1.22, 1.24, 1.27]. These packings are termed "macroporous". and have rather large pores (>50 nm) due to the heterogeneity of the polymerization process. The average pore diameter of these packings is in the range of 5 - 10 nm and there are a large number of micropores (< 2 nm) as well [1.28]. The micropores are due to the spaces between the components of the copolymer. Poor efficiency has been linked to hindered diffusion of solutes in and out of these micropores [1.24]. This view explains not only the sample dependence but also the solvent dependence of column efficiency. For solvents like tetrahydrofuran (THF). much better efficiencies are generally obtained than if the solvent is methanol (MeOH) or acetonitrile (ACN) [1.23, 1.29]. There is also evidence that the void volume of a

column changes with the solvent, meaning that the support swells in solvents it is well wetted by, such as THF, which can interact with the aromatic rings in the polystyrene chains. As the support swells, the micropore volume increases and, with the larger pore, the hindered diffusion also decreases, leading to better efficiency.

This proposed effect of micropores on efficiency is supported by studies of porous polymer packings of varying mean pore dimensions which suggest that the efficiency is generally independent of this quantity [1,24], even though it would be reasonable to assume that with a larger pore size, diffusion rates would increase. The quantity however, does not deal with the existence of micropores which exist necessarily because of the structure of the polymer and which might be the cause of the rate limiting processes in the partition of solutes between the two phases.

This is not to suggest that only polymeric phases have micropores. Silica-based supports which are underivatized also have micropores but these are generally smaller than found in polymers because the functional groups, SiO_2, are smaller than the functional groups in the polymers. It is also conceivable that the micropores, which are already inaccessible to solute molecules in the underivatized support may be filled in the process of derivatization and/or endcapping. The mechanism of adsorption on silica-based RP-HPLC packings is probably more of a surface phenomenon than on the polymeric phases.

Whatever the physical process, there seems to be some excessive resistance to mass transfer of solutes in these packings which lead not only to peak asymmetry but also to increased peak widths for certain compounds. It is the origin of the poor efficiency which is the subject of this study.

Bandbroadening in chromatography is the result of physical processes which occur in the separation process. It is generally considered to be the result of a series of independent rate processes which affect the sample band, originally injected as an impulse, as it migrates along the column. The individual processes are examined

briefly in Chapter 2. The processes that may be dominant for the polymeric phases involve resistance to mass transfer within the particle. Included in this transfer are the rate of transfer through the stagnant mobile phase which fills the pores of the polymer and the rate of transfer between the stationary phase and the stagnant mobile phase. This rate of transfer, termed here the rate of sorption if we are describing the transfer of a solute from the mobile to the stationary phase, is of interest if we are to quantify the contribution of this transfer processes to the overall process of separation.

This study focuses on the possibility that a slow sorption rate is the major cause of the bandbroadening and tailing observed on PRP-1 when using polyaromatic sample species. The development of a technique to measure the rate of sorption is detailed and a model is used to relate the measured rate to experimental elution profiles of naphthalene. The results of the study on PRP-1 are compared to results for a parallel study on the silica-based packing, Partisil-10 ODS-3.

CHAPTER 2

Theory

2.1   Bandbroadening in Liquid Chromatography

2.1.1   Introduction

The phenomenon of bandbroadening has been extensively treated in the literature [2.1 to 2.3]. Only a brief discussion will be included here.

Ideally, sample solutions are injected onto chromatographic columns as an impulse. Physical rate processes on the column affect the sample zone and lead to non-uniform flow profiles and non-equilibrium between the various phases in the column. The relative magnitudes of these rate processes are affected by the characteristics of the experiment, such as the particle size of the packing, the diffusion characteristics of the sample molecule and the linear velocity of the mobile phase. The relative effect of various parameters on the bandbroadening can be predicted by assuming that several independent physical processes contribute to the sample zone broadening. The contribution of each process to zone broadening is equivalent to the relative plate height contribution of that process to the overall plate height for the column. The usual treatment, described below assumes that as independent processes, the effect of each is superimposed on the moving zone centre to describe the overall observed peak shape.

The height equivalent of a theoretical plate is the quantitative measure of the contribution to zone broadening. This quantity, H, is defined in equation 2.1.

$$H = \frac{\sigma_X^2}{X}$$

eqn. 2.1

The variance produced by the process, σ_X^2, in units of distance, is related to the width of the chromatographic peak. X is the distance travelled; for a sample eluting from a

column X is equal to the length of the column. Equation 2.1 can be easily converted into time or volume uni's.

2.1.2   Longitudinal Diffusion

If the sample zone is initially an impulse of infinitely narrow width, as it moves down a column, molecules in the band will tend to diffuse along the axis of the column in two directions, backward and forward. This diffusion is inversely proportional to the linear velocity of the mobile phase, u_0; the faster the stream is flowing, the less time available for the sample molecules to diffuse from the front. The contribution to plate height is directly proportional to the diffusion coefficient of the sample molecule, D_m; as the diffusion coefficient increases, the molecule diffuses faster and the longitudinal diffusion becomes more extreme. The plate height contribution due to longitudinal diffusion, H_{LD} is given by equation 2.2 [2.4].

$$H_{LD} = \frac{2\gamma D_m}{u_0}$$

eqn. 2.2

In packed beds, the longitudinal diffusion tends to be smaller than that found in open tubes of similar diameters. In packed beds, diffusion is obstructed by the particles and an unitless obstruction factor, γ, is introduced. The value of the obstruction factor is approximately 0.5 to 0.7. The obstruction factor accounts for the overall effect of packing on the diffusion characteristics of the sample molecule. More detailed accounts of the origin of the obstruction factor are available elsewhere [2.5]. In HPLC, this term tends to be negligibly small [2.6].

2.1.3   Eddy Diffusion

This term arises from changes to the sample band resulting from non-uniformity in flow of the mobile phase. The presence of particles in a column creates velocity differences of various types especially when particles are not uniformly packed or of a

large distribution of sizes. The different velocity flow streams carry along molecules, leading to broadening of the zone. The broadening, however, is not as severe as it would be in an open tube. This is a result of the lateral convective mass transfer of molecules between the flow streams of different linear velocities which tends to relax the non-uniform flow profile. The value of the contribution to the plate height can be calculated from equation 2.3 [2.7].

$$H_{eddy} = 2\lambda d_p$$

eqn. 2.3

This term is dependent on particle diameter, d_p; when the particle diameter is small, the sample molecule may spend less time in a flow stream which is faster or slower than average. The packing factor, λ, relates to the uniformity of packing of the bed and generally increases as the particle size decreases. Large particles are easier to pack uniformly in a chromatographic column [2.8]. Modern packing techniques result in columns which generally have a packing factor much less than 10. It has been measured to be approximately 2.5 for spherical particles in the particle diameter range of 5 to 35 µm [2.9]. However, λ can vary significantly from column to column [2.2].

2.1.4 Resistance to Mass Transfer in the Mobile Phase

In the mobile phase, radial diffusion of the sample across the column leads to a relaxing of the effects of non-uniform flow profile of the mobile phase on the sample zone. The finite rate of diffusional mass transfer across the column means that the non-uniform flow profile will be only partially relaxed. The plate height contribution due to this effect is calculated by equation 2.4 [2.10].

$$H_m = \frac{\omega d_p^2 u_o}{D_m}$$

eqn. 2.4

The process is related to the diffusion characteristics of the sample; as the diffusion coefficient, D_m increases, the relaxation of the non-uniform profile is more

efficient . The term depends directly on the linear velocity. u_0; if the sample spends more time in the flowing stream while travelling a given distance along the column, then diffusion across the column becomes more efficient. For small particle sizes, the plate height contribution tends to be relatively small. The contribution is also directly proportional to ω, a packing factor. As the uniformity of the bed increases, ω decreases since the various streams of moving phase become more uniform in velocity. ω is dependent on the column packing and can also vary from column to column [2.2].

In gas chromatography, where the mobile phase is a gas, the value of the diffusion coefficient is on the order of 10^{-2} to 10^{-1} cm^2/s, the plate height contribution due to resistance to mass transfer in the mobile phase is considered negligible [2.11]. In liquid chromatography, however, the diffusion coefficient of sample molecules is on the order of 10^{-6} to 10^{-5} cm^2/s and the contribution calculated from equation 2.4 is much larger.

2.1.5   Coupling of H_{eddy} and H_m in HPLC

These two contributions are associated with lateral convection and lateral diffusion respectively. Both contribute to relaxation of the flow profile established by non-uniform velocity profile. These terms are said to be coupled and the overall contribution, H_{couple}, is given by Giddings as equation 2.5 [2.12].

$$H_{couple} = \left[\frac{1}{H_{eddy}} + \frac{1}{H_m} \right]^{-1}$$

eqn. 2.5

The validity of the coupling term has been questioned by several researchers including Giddings himself [2.13] who states that "The coupling expression is simply an approximation to a very complex interaction between diffusion and convection. The process has been formulated rigorously but the boundary conditions for real granular beds are so complex that meaningful solutions have not yet been obtained." Equation

2.5 along with equations 2.3 and 2.4 allow one to predict the relative effect of changing the variables in the column (for example, d_p). The values of the constants γ, λ and ω are only estimates and the value of the plate height calculated from the above equations may be significantly different from actual plate height of a column. The contribution due the processes covered in the previous sections can be measured directly in silica columns for affinity chromatography using totally unretained compounds, which neither interact with the stationary phase by adsorption or enter the pores. The bands of these totally unretained compounds will be subject to broadening due to longitudinal diffusion and to the coupled mobile phase processes. These contributions were measured on silica gel packings which had been derivatized with an immobilized ligand for use in affinity chromatography. On 10 μm particles. these contributions are on the order of 10 to 100 μm at the usual linear velocities used in HPLC [2.14].

2.1.6.   Resistance to Mass Transfer in the Stationary Phase

Bandbroadening occurs whenever sample molecules fail to move with the centre of the sample plug. The physical or chemical reactions of adsorption and desorption can be a source of bandbroadening if they requires a finite time. As a sample zone moves down the column. the mobile phase will contain a concentration of sample that is higher than the equilibrium concentration. This provides the driving force for adsorption but if this step takes time, the sample will continue down the column without reaching equilibrium, causing the front end of the peak to stretch out. The sample zone in the stationary phase will, at this point contain a concentration less than that at equilibrium. Once the band centre passes, however, the mobile phase will contain a concentration of sample less than that predicted by the equilibrium distribution coefficient. If desorption takes time, this cause the back end of the peak to stretch out. Overall, the peak is broadened by the non-equilibrium processes associated with slow sorption-desorption kinetics.

The bandbroadening contribution is related to the rate constant for the sorption or desorption reaction. The process is often considered in terms of the irreversible desorption rate constant, k_r. The random walk model was used by Giddings to derive equation 2.6 [2.15].

$$H_s = 2 \frac{k'}{(1 + k')^2} \frac{u_o}{k_r}$$

eqn. 2.6

The time associated with this process is only the time necessary to undergo reaction, not time required to diffuse to the surface. For reverse phase packings used in HPLC, this term is often considered to be negligible [2.3].

2.1.7 Resistance to Mass Transfer in the Stagnant Mobile Phase

Porous particles are filled with mobile phase but the solution does not undergo the various convection processes associated with the flowing mobile phase. The stagnant mobile phase is probably not quickly exchanged with fresh mobile phase. Sample molecules which enter the pores of a particle must diffuse into the stagnant mobile phase to reach the surface of the stationary phase where adsorption actually occurs. The bandbroadening associated with this process must depend on the diffusion characteristics of the sample molecule. Equation 2.7 calculates the plate height contribution for this process [2.16].

$$H_{sm} = \frac{fct\ (f,\ k')\ d_p^2\ u_o}{\gamma' D_m}$$

eqn. 2.7

The tortuosity factor, γ', accounts for the increased path length the sample molecules must follow due to the winding channels within the particles. It has a value less than 1. The variable fct (f, k') is a function of f, the fraction of the mobile phase in the pores of the packing and of k', the capacity factor. The function has different forms depending on the type of stationary phase used. For spherical particles, the function is given by equation 2.8 [2.16].

$$fct(f,k') = \frac{(1 - f + k')^2}{30(1 - f)(1 + k')^2}$$

<div align="right">eqn 2.8</div>

Einstein's equation, shown in equation 2.9 which relates the square of the diffusion distance, d_f^2, to the time of diffusion, tf, can be used to replace d_p^2 and D_m in equation 2.7 with diffusion times as shown in equation 2.10 [2.17].

$$d_f^2 = 2D_m t_f$$

<div align="right">eqn 2.9</div>

$$H_{sm} = 2\ fct(f,k')\ \gamma'\ t_f = \frac{2\ fct(f,k')\ \gamma'}{k_f}$$

<div align="right">eqn 2.10</div>

Equation 2.10 relates the band broadening due to resistance to mass transfer in the stagnant mobile phase to a first-order rate constant, kf, for diffusion through the pores of the packing.

2.1.8   Total Plate Height

The previous discussion for the estimation of plate heights for chromatographic columns can be summarized in equation 2.11.

$$H = H_{LD} + \left[\frac{1}{H_{eddy}} + \frac{1}{H_m} \right]^{-1} + H_s + H_{sm}$$

<div align="right">eqn 2.11</div>

The relative contributions to the plate height have been calculated for a hypothetical HPLC column containing 10 μm spherical, porous particles for a sample having a $k' = 35$. The calculations used a linear velocity of 0.4 cm/s which corresponds to a realistic flow rate of about 2 mL/min. Detailed calculations are shown in Appendix 1. Table 2.1 summarizes the results.

The overall plate height for this column then is 0.073 mm, with the majority of the band broadening originating with the mobile phase effects in the coupled term. The parameters discussed in Appendix 1 were chosen to closely parallel parameters for the polymeric packing PRP-1 and for typical HPLC experiments on that packing.

Table 2.1   Summary of individual plate height contributions in a typical HPLC experiment with conditions described in Appendix 2.

term	plate height contribution (cm)
H_{LD}	3×10^{-5}
H_{eddy}	0.005
H_m	0.052
H_{couple}	0.0046
H_{sm}	0.0027
H_s	4.3×10^{-5}
H_{total}	0.0073

However, the predicted value of 0.073 mm grossly underestimates the observed plate height for PRP-1 columns with certain kinds of samples. This study will investigate the possibility that the some combination of the H_{sm} term and the H_s term underestimates the contribution to bandbroadening of slow mass transfer in the porous structure of the polymer. For certain molecules which are of the molecular dimensions of the micropores, their behaviour in the micropores may be lead to large values of H_{sm} and/or H_s.

2.1.9   Rate Processes and Bandbroadening

PRP-1 was previously described as a macroporous packing. Each particle has an extensive network of pores of a variety of sizes. Mercury porosimetry studies on a related macroporous polymer, Amberlite XAD-2, suggests that micropores are present [2.18]. The pores probably range in size from macropores to micropores. It has also been observed that PRP-1 is an exceptionally poor stationary phase for certain kinds of compounds, especially polyaromatics. After eliminating other possible causes for the severely broadened peaks such as high longitudinal diffusion and a non-uniform flow profile [2.19], the slow adsorption-desorption kinetics was suspected to be the primary cause of the inefficiency. Typically, adsorption onto non-polar stationary phases is considered to be a fast process since there tends to be only a small activation energy associated with the weak dispersion forces which are the primary retention mechanism. If, however, we consider the total sorption process to include the diffusion of the sample through the interior pores of the particle it is not difficult to imagine that the overall process may be slow and may lead to non-equilibrium between the mobile phase and the particle phase (including the stagnant mobile and the stationary phases).

The shallow bed method described in this thesis is designed to measure the overall rate of the total sorption process of a sample compound onto a stationary phase. The measured rate may be limited by slow diffusion through the pores and/or by

adsorption onto the actual surface.

2.2   Shallow Bed Theory

Sorption of a sample from a liquid solution onto a porous solid particle involves several steps as illustrated in Figure 2.1 [2.20, 2.21]. Film diffusion is the diffusion of sample from the bulk solution across a concentration gradient to the particle surface. For porous particles, particle diffusion involves the movement of the sample through the pores in the particle. The final step is the actual physical or chemical reaction involved in surface adsorption. Desorption can be considered occur as the reverse of the above steps [2.21].

In chromatographic columns, the manifestation of these processes will be bandbroadening if the processes are time-consuming. If film diffusion is slow, this results in a plate height contribution due to slow mass transfer in the mobile phase according to equation 2.4. In fact, film diffusion relates to only one of the physical processes included in the H_m term. The individual processes refer to mass transfer over various distances in the column; film diffusion corresponds to so-called "trans-channel" mass transfer. This is the mass transfer between flow streams of different linear velocities in the channel between two particles. This contribution is actually small at nor nal HPLC linear velocities [2.10]. If particle diffusion is slow, it might be expected that the contribution from resistance to mass transfer in the stagnant mobile phase according to equation 2.7 will be large. If the chemical or physical adsorption is slow, a large contribution due to resistance to mass transfer in the stationary phase calculated according to equation 2.6 will be expected. The slowest of the three steps illustrated in Figure 2.1 is considered to be the rate-limiting step in the overall sorption process. At this point, however, it may be noted that in the "shallow bed method", described below, film diffusion is very fast because the particle outer film is very thin so that only particle (pore) diffusion and surface adsorption-desorption are potentially
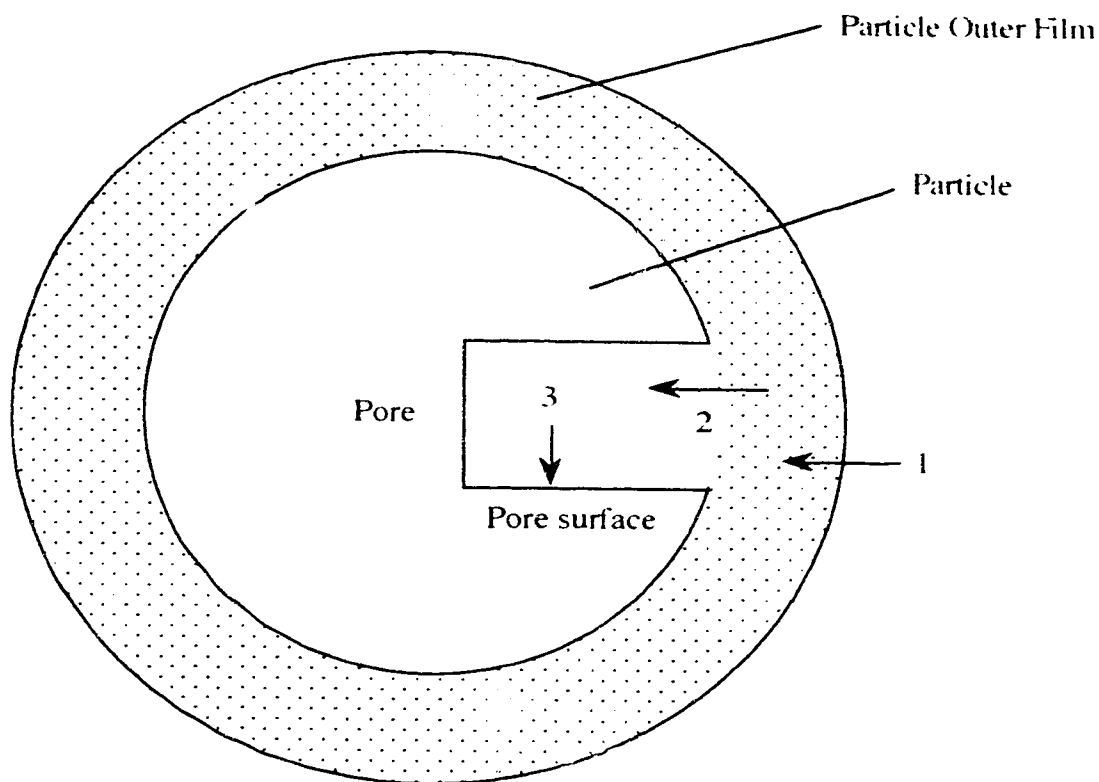
Figure 2.1 Schematic diagram of a spherical porous stationary phase particle. Three steps in the sorption process are illustrated. (1) Sample diffuses from the bulk solution across the concentration gradient surrounding the outer surface of the particle. This process is termed "film diffusion". (2) Sample diffuses through the stagnant mobile phase contained in the pore. This process is termed "particle diffusion". (3) Physical or chemical adsorption occurs onto the pore surface. Desorption can be considered to occur by the reverse of these steps.

involved. It is not necessary to determine which of these two steps is the slower, and, for convenience, the terms "sorption" and "desorption" will be used to refer to the combined process of pore-diffusion and surface adsorption-desorption.

Whatever the actual rate limiting process, the measurement of the rate of the overall sorption process is dependent on measuring the amount sorbed by an adsorbent with respect to an exposure time to a solution. For very large particles where the overall sorption rate is small, the experiment may be as technically simplistic as shaking a known amount of sorbate in a solution of known concentration for variable amounts of time and analyzing either phase for changes in concentration. This type of experiment becomes more challenging as the sorption rate becomes faster and the necessary exposure times decrease.

The rate of sorption on HPLC stationary phases has been the subject of relatively few studies. It has proven to be a bit more technically challenging. Marshall et.al. [2.22] measured the sorption rate constant in an octadecylsilica, ion pairing chromatographic system using the pressure-jump relaxation kinetics method. While the rate constant for the ion-pairing reaction preceding the adsorption was too fast to measure with the system, the adsorption step was determined also determined to be very fast. Reciprocal relaxation times for adsorption on bonded phases were determined to be of the order of 500 to 700 s^{-1}.

In this laboratory, a technique based on a fixed-bed adsorber, termed the shallow bed method, has been developed to accommodate exposure times of less than 1 s. The basic technique was originally described in 1947 [2.23] and has been used to study the kinetics of sorption on ion-exchange resins [for example, 2.24]. The design of the apparatus will be discussed in detail in Section 3.4.1. Briefly, the fixed bed consists of milligram amounts of HPLC stationary phase material held in a modified slider valve. This small bed, termed a shallow bed, can be exposed to a flowing sample stream for variable amounts of time. The sorbed sample is then eluted from the shallow

bed and the sorbed amount is plotted vs exposure time to generate a sorption rate curve.

The experiment is designed to measure the rate constant for the reversible sorption of species j from the mobile phase. designated j_m onto the stationary phase where the species is designated j_s.

$$j_m \underset{k_r}{\overset{k_f}{\rightleftharpoons}} j_s \qquad \text{eqn. 2.12}$$

The forward reaction is the sorption reaction and has an irreversible rate constant of k_f while the reverse reaction, desorption, has an irreversible rate constant of k_r. Under reversible conditions, the observed rate constant, k can be shown to be the sum of the two aforementioned irreversible constants |2.25| as shown in equation 2.13.

$$k = k_f + k_r \qquad \text{eqn. 2.13}$$

The success of the experiment depends on achieving so-called shallow bed conditions. Shallow bed conditions are said to exist when the sample concentration in the mobile phase is constant at all times including exposure time = 0. To fulfill this condition, the sample solution passes through the bed at a rapid rate. When sample is sorbed by the bed, the local concentration in the flowing sample solution will not decrease because the flow flushes the bed at a rapid rate. Shallow bed conditions simplify assumptions necessary to data analysis. No concentration gradient exists in the shallow bed either longitudinally or radially.

The fulfillment of shallow bed conditions is accomplished by the combination of two experimental conditions. First, a small length of packing is used in the shallow bed. This assures that by the time a volume element of solution reaches the lower portion of the bed, it will not have been in contact with much overlying packing and at most only a very small amount of solute will have been sorbed. The more sample sorbed by the bed, the harder it will be to maintain a constant sample concentration in the flowing phase. A concentration gradient might be established. The second

experimental consideration is the use of a high linear velocity of the sample solution through the shallow bed. This is accomplished using a constant pressure system. Minimization of resistance to flow is also necessary. The use of a very short (shallow) bed is therefore indicated.

The shallow bed method can be compared to frontal chromatography [2.26]. In frontal chromatography, which is schematically illustrated in Figure 2.2, a sample solution of concentration C_m is pumped continuously through a column. A plot of the sample concentration in the effluent, C_c, vs time is called a breakthrough curve. The shape of the breakthrough curve is often sigmoidal. The variable t_m, illustrated in Figure 2.2, is the finite time that is necessary to sweep out the void volume of the column with sample solution. In the shallow bed experiment, this step is assumed to occur instantaneously because of the very high linear velocity and very small void volume of the bed. The breakthrough curve in Figure 2.2 continues along the baseline, then rises in the typical S shaped pattern. In this region, there is a concentration gradient established longitudinally in the column. At the top of the column, the packing sorbs sample decreasing its concentration in the flowing phase. As this gradient moves down the column, the concentration continually decreases due to the sorption process. As the packing reaches equilibrium with the flowing sample, the concentration of the mobile pha   proaches a constant and the breakthrough curve levels off when all packing has reached equilibrium. The retention time of the sample, t_r, is located at the midpoint of the rising part of the elution curve. In the shallow bed experiment, the effluent concentration can be considered to be a constant at all times. In other words, the values of t_m and t_r approach zero. The curve in Figure 2.2 would therefore be inapplicable to the shallow bed. All particles in the shallow bed experience the same solution conditions at all times and will therefore undergo sorption processes at the same rate regardless of geographical location in the column.
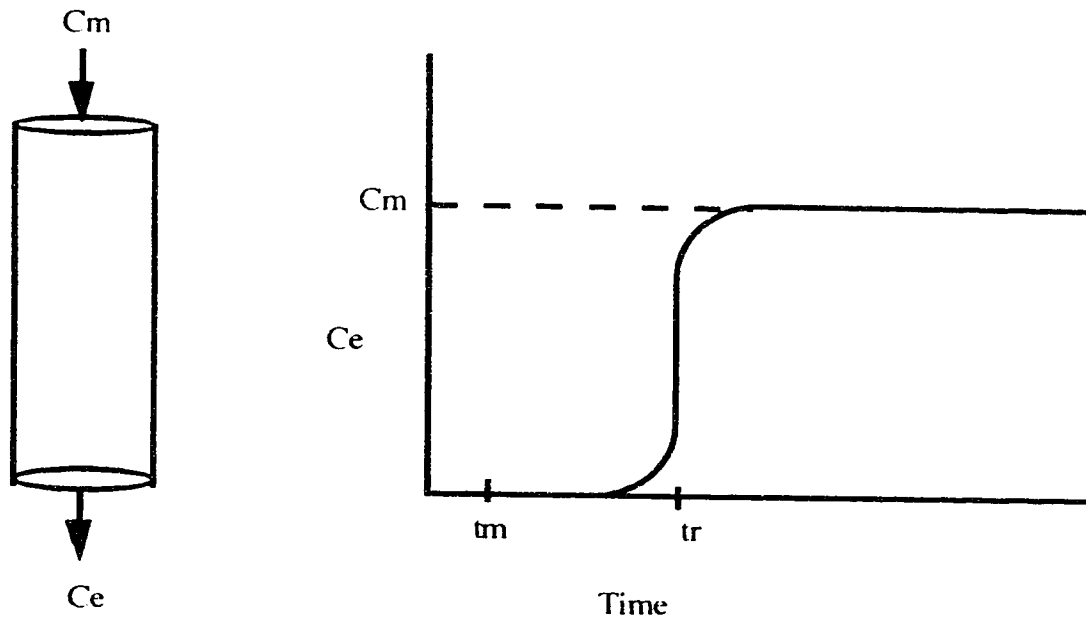
Figure 2.2   Column for frontal chromatography and breakthrough curve. A sample solution of concentration C_m is pumped continuously through the chromatographic column and the concentration in the effluent. C_e is monitored. C_e is plotted as a function of time in the breakthrough curve. The time t_m is the time for the solution to rinse out the void volume of the column. The time t_r is the retention time for the sample on the column. Equilibrium exists between the stationary and mobile phases in the plateau region of the breakthrough curve. If the column is replaced by a shallow bed, breakthrough is assumed to be achieved instantaneously. On the very short shallow bed, both t_m and t_r approach zero.

2.3 Analysis of Sorption Rate Data

2.3.1 Curve Fitting of Sorption Rate Data

The sorption rate data that result from the experiment described in this thesis can be fit, using non-linear least squares analysis, to a multi-exponential curve as shown in equation 2.14.

$$n(t) = n_o - \sum_{i=1}^{i} n_i e^{-k_i t}$$

eqn. 2.14

The use of a multi-exponential equation was suggested by the shape of the plot of the experimental data points and not by theoretical considerations. It is important to note that this curve fitting is empirical. Typical sorption rate data, a plot of moles of sample sorbed vs sorption time is shown in Figure 2.3. The solid line is a best-fit to a tri-exponential equation. Multi-exponential curves are observed in luminescence decay data for species in heterogeneous environments such as inhomogeneous surfaces [2.27]. In these situations, the various terms are associated with independent kinetic processes, each associated with different activation energies. Such curves may also be of the continuous exponential variety. In these types of curves, there is a range of rate constants instead of a set of discrete rate constants. The statistical considerations necessary to distinguish the situations are fully explored in Reference 2.28. The sorption rate data described in this thesis gave good fits to the discrete multi-exponential function and the possibility of a continuous distribution of sorption rate constants was not explored.

2.3.2 Calculation of Elution Profiles from Sorption Rate Data

We are primarily interested in predicting the shape of the profile of a sample peak eluted from a long chromatographic column packed with sorbent based on
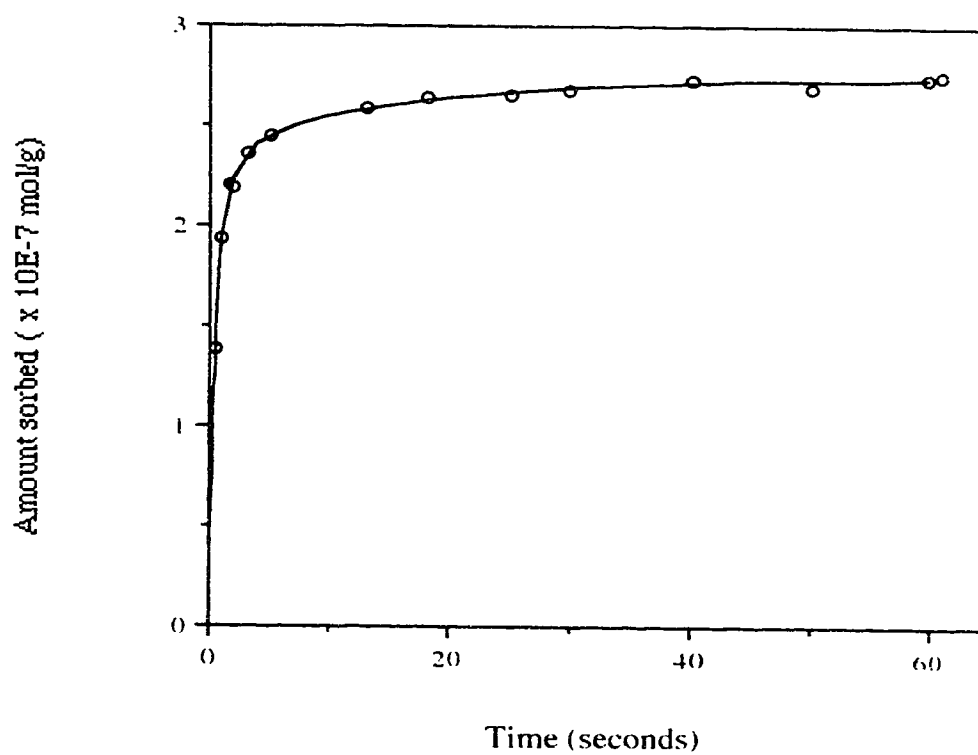
Figure 2.3   Sorption rate curve for Naphthalene on PRP-1 in 85 % MeOH. The
experimental data point (o) are overlaid by a solid line representing the
tri-exponential function that fits them.

information from the sorption rate curve for the sample obtained by the shallow bed experiment performed on the sorbent. In order to correctly predict the shape of the elution curve, it is necessary to treat each term of the multi-exponential as though it represented the rate of an independent first-order sorption process. For most of the sorption rate curves that will be presented here, there are three terms in the multi-exponential equation. This number is not imposed arbitrarily but rather is the number of terms that gives the best fit to the data points. Each of the i individual processes is associated with a first-order rate constant, k_i, and with a pre-exponential multiplier, n_i, which can be considered to be related to the number of sites associated with the ith process.

One can imagine that a chromatographic column filled with the packing of interest could be treated as a series of smaller columns in which only one of the sorption processes occurs. Each of the hypothetical smaller columns will have a length proportional to n_i/n_0, the fraction of sites associated with the process given in the multi-exponential equation. In each of the small columns, only a single first-order sorption process occurs, associated with a single sorption rate constant. Giddings has given a general equation which gives the probability distribution $P(t_s)_i$ associated with a single first-order sorption-desorption kinetic process, as shown in equation 2.15 [2.29].

$$P(t_s)_i = \left(\frac{k_{f,i}k_{r,i}t_m}{t_s} \right)^{0.5} e^{-(k_{f,i}t_m + k_{r,i}t_s)} I_1 \sqrt{4k_{f,i}k_{r,i}t_s t_m}$$

$$\text{eqn. 2.15}$$

The probability distribution plot of $P(t_s)_i$ vs t_s corresponds to an elution chromatogram for a sample on the hypothetical column associated with the ith process.

Equation 2.15 is expressed in terms of the variable t_s, which is time measured from the time an unretained compound takes to elute from the column, t_m.

$$t_s = t - t_m \qquad\qquad \text{eqn 2.16}$$

In a column, the sample is injected as an impulse. As the sample passes through the column, any physical process which results in certain molecules moving at a different velocity than the centre of the sample zone results in zone broadening. In our imaginary columns, the only source of zone broadening is slow sorption: we imagine that all other processes are negligible.

2.3.3 Data treatment for a Bi-exponential Rate Curve

The data treatment can be more easily understood by first considering the case where the sorption rate curve is in the form of a bi-exponential shown in equation 2.17.

$$n(t) = n_o - n_1 e^{-k_1 t} - n_2 e^{-k_2 t}$$

eqn. 2.17

We then suppose that there are two independent sorption processes ($i = 1$ or 2) and treat the chromatographic column as if it were two smaller columns in tandem. This thought experiment is illustrated in Figure 2.4.

In hypothetical column 1, the only sorption process that occurs is one corresponding to the first term of the bi-exponential. The process has a reversible rate constant k_1 (as obtained by non-linear least squares fit of the sorption rate curve). The value of k_1 can be used to calculate the irreversible rate constants for sorption and desorption, $k_{f,1}$ and $k_{r,1}$, which are needed to calculate the probability distribution given by equation 2.15. Using equation 2.13 and equation 2.18, the values of the two reversible rate constants can be calculated using data for k' as shown in equations 2.19 and 2.20.

$$k' = \frac{k_{f,1}}{k_{r,1}}$$

eqn. 2.18

So

$$k_{f,1} = k_1 \frac{k'}{1 + k'}$$

eqn. 2.19

and

original column

impulse ———————→ [original column] ————————→

Column 2   Column 1

impulse —→ [Column 2] ——→ [Column 1] ————→

$$t_{m.2} = t_m \frac{n_2}{n_0}$$ $$t_{m.1} = t_m \frac{n_1}{n_0}$$

$P(ts)$

II   *   I   =   III

0   5000   0   5000   0   5000
ts (s)   ts (s)   ts (s)
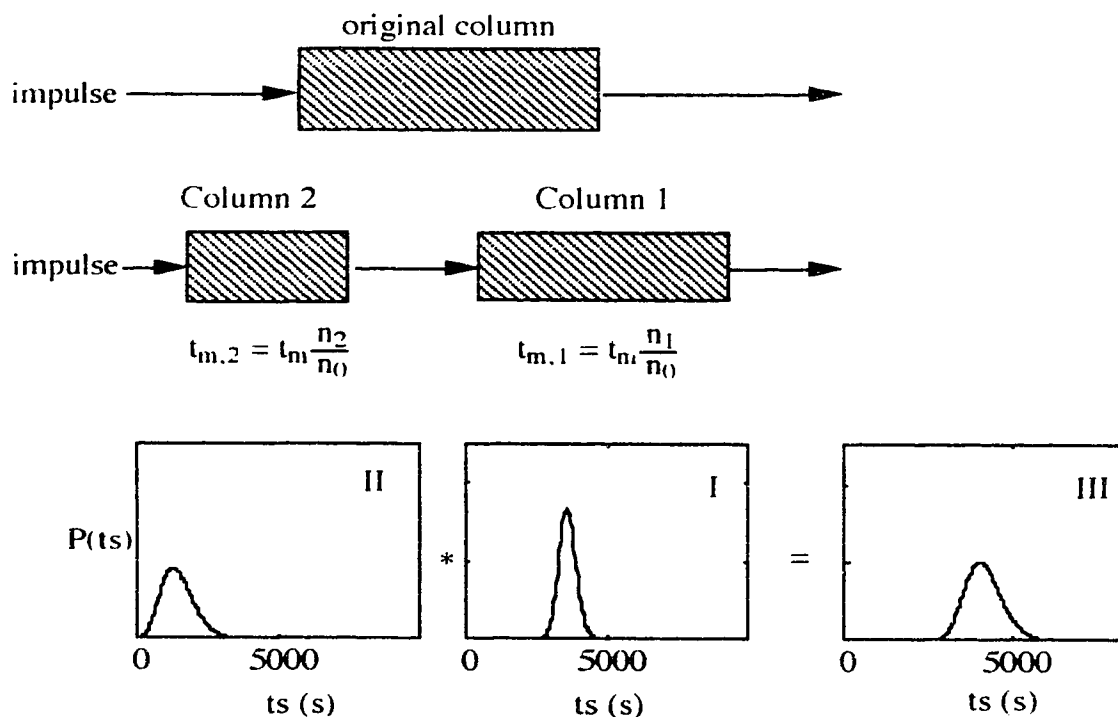
Figure 2.4   Prediction of elution peaks for a sample which has a bi-exponential rate curve on the packing in the column. The analytical column is modelled by two columns in which the two different sorption processes occur. The effect of these processes on a sample injected as an impulse is calculated for each column by equation 2.15, resulting in the profiles I and II. The overall elution peak, labelled III, is the result of the convolution of the probability distributions associated with the kinetic processes. Note that the distributions are a function of t_s which is zero at the time an unretained compound elutes from the column. In order to compare the peak III with an experimental elution profile, t_m must be added to the time axis. Details are found in Section 2.3.3.

$$k_{r,1} = k_1 \frac{1}{1 + k'}$$

eqn. 2.20

Also required for calculation of the probability distribution associated with sorption onto the sites of hypothetical column 1 is a measure of the time the mobile phase takes to pass through the column, $t_{m,1}$. It is equal to the time the mobile phase takes to pass through the entire column, t_m, multiplied by a fraction of the number of sites, n_1/n_o as shown in equation 2.21.

$$t_{m,1} = t_m \frac{n_1}{n_o}$$

eqn. 2.21

An analogous set of equation describes the hypothetical column 2. For the two columns the sum of $(t_{m,1} + t_{m,2})$ is equal to t_m for the original column.

From equation 2.15, the probability distribution associated with the sorption process in hypothetical column 1 is shown in equation 2.22.

$$P(t_s)_1 = \left(\frac{k_{f,1}k_{r,1}t_{m1}}{t_s} \right)^{0.5} e^{-(k_{f,1}t_m + k_{r,1}t_s)} I_1 \sqrt{4k_{f,1}k_{r,1}t_st_{m,1}}$$

eqn 2.22

Similar calculations can be done for a second column having only sites that undergo the second sorption process which has an observed reversible rate constant k_2. The rate constants $k_{f,2}$ and $k_{r,2}$ can be calculated from k_2 using equations analogous to equations 2.19 and 2.20 and the quantity $t_{m,2}$ can be calculated using an equation analogous to equation 2.21 along with data for n_2. The probability distribution associated with slow sorption on the second hypothetical column has the form shown in equation 2.23.

$$P(t_s)_2 = \left(\frac{k_{f,2}k_{r,2}t_{m,2}}{t_s} \right)^{0.5} e^{-(k_{f,2}t_m + k_{r,2}t_s)} I_1 \sqrt{4k_{f,2}k_{r,2}t_st_{m,2}}$$

eqn. 2.23

If these two hypothetical columns are now imagined to be attached in tandem as illustrated in Figure 2.4 and an injection is made into column 2, the sample band will undergo broadening in both columns due to the kinetic processes. (Note that the

sample band is initially considered to be an impulse of infinitely narrow width.) As the sample passes through column 2, broadening due to the slower kinetic process results in profile II. If the effluent from column 2 is directed into column 1, where broadening due to the faster kinetic process occurs, the profile exiting column 1 will be the convolution of the two distributions I and II. This profile is designated III.

One final correction to this predicted profile must be made before comparison to real chromatograms. Distribution III in Figure 2.4 is expressed in terms of t_s (defined in equation 2.16). To be expressed in real time units, the peak must be shifted down the time axis an amount t_m corresponding to the retention time of an unretained compound in the original column.

The convolution of the two probability distributions is valid providing the absolute values of $kf_{,1}$ and $kf_{,1}$ are large enough that virtually all molecules in the sample zone undergo at least one sorption-desorption cycle in each of the hypothetical columns 1 and 2, as described in Section 2.3.4, below.

2.3.4 Assumptions in Generation of Elution Profiles from Sorption Rate Data

The distributions calculated above will be the resulting profile of the effluent under two conditions:

1. if all other bandbroadening processes are negligible

2. if all molecules in the sample zone undergo the sorption-desorption processes at least once in each column.

Each of these conditions can be examined separately as follows:

Condition 1:

As was previously mentioned, slow sorption-desorption kinetics is assumed to be the major contributor to zone broadening. The relative contributions from other processes such as those described in Sections 2.1.2 to 2.1.5 can be calculated using equations shown in the above sections.

Condition 2:

Usually in chromatography, any given sample molecule will undergo the sorption-desorption cycle many times on a column. However, if sorption is particularly slow, it is conceivable that, depending on how much time the molecules spend in the mobile phase of a column, some of the molecules in the sample zone will pass through the column without undergoing the slow physical process even once. In an ideal column, these molecules would then elute as an impulse, having the same shape as the injected impulse if all other bandbroadening processes are negligible. The fraction of molecules that do not undergo the ith slow sorption process, Φ_i, is given by Giddings [2.29].

$$\Phi_i = e^{-k_{f,i} t_{m,i}}$$

<div align="right">eqn. 2.24</div>

The fraction Φ_i is the "non-interacting fraction" of sample on the column in question. It is related to the adsorption rate constant, $k_{f,i}$; as the process becomes slower and the rate constant decreases, the fraction of molecules that passes through the column without undergoing the process will necessarily increase. The fraction is also related to $t_{m,i}$ which is a measure of how long the sample molecules stay in the mobile phase. As the linear velocity of the mobile phase increases, t_m decreases. Because the sample molecules spend less time in the column, they have less time to undergo the slow sorption process. On any particular hypothetical column which has a single k_i and n_i, equation 2.15 describes the distribution only of the fraction of molecules (1 - Φ_i) which elutes with a retention time of $t_{s,i}$. The fraction Φ_i elutes as an impulse at time $t_{m,i}$. In the discussion in Section 2.3.3, above, it was assumed that $\Phi_i \sim 0$ for both hypothetical columns 1 and 2. As this fraction Φ_i increases in one or both of the hypothetical columns, the above data treatment will fail to predict reasonable elution curves. The following section describes the data treatment procedure for a bi-exponential sorption rate curve where k_i and/or $t_{m,i}$ are small in one of the columns so

that a significant fraction of molecules pass through that column without undergoing the zone broadening process.

2.3.5 Data Treatment for Bi-exponential Rate Curve where Non-interacting Fraction for One Sorption Step is Significant.

The discussion in this section draws heavily on the two-site sorption model of kinetic tailing developed by Giddings [2.29]. Consider the situation illustrated in Figure 2.5.a. A single column contains a stationary phase on which the sorption rate is sufficiently slow as to violate condition 2 described in the previous section. In this column, the rate constant k_f, is small enough to make Φ_1, the non-interacting fraction of a sample zone significant. If sample is injected into this column as an impulse, the non-interacting fraction passes through the column without being sorbed onto the stationary phase. These molecules elute in one dead volume of the column (profile I in Figure 2.5.a) at the time t_m and the shape of the zone is unchanged except for the height. The height of this impulse is Φ of the height of the original impulse. A second fraction, (1 - Φ) is shown as profile II in Figure 2.5.a, which does interact with the stationary phase in the column. This fraction will elute as a peak with a distribution $P(t_s)$, given by equation 2.15. Note that as k_f and k_r decrease, the distribution becomes increasingly broadened and increasingly asymmetrical.

Now consider the situation illustrated in Figure 2.5.b. The column described above is designated Column 2 . The characteristics of this hypothetical column are determined by the constant in the second exponential term of the bi-exponential equation (ie. n_2 and k_2). The only process that occurs in this column is the slower sorption-desorption. The sample exits Column 2 in two zones. The first is an impulse from the fraction of sample that has not yet undergone sorption. The second is a broadened zone described by $P(t_s)_2$ (equation 2.23). Both of these zones enter Column 1 which is associated with the faster sorption process and the first exponential term of
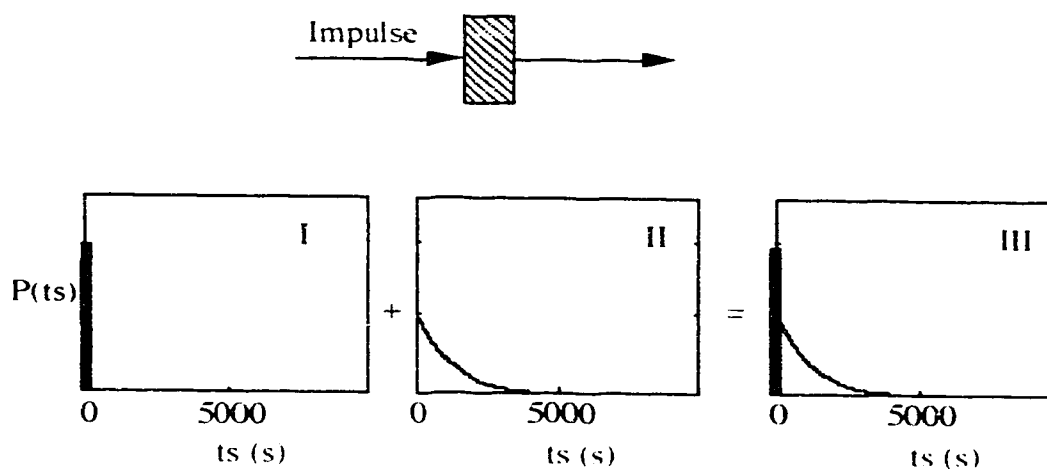
Figure 2.5.a   The output of a column in which a significant fraction of sample does
                not undergo at least sorption-desorption cycle. The non-interacting
                fraction elutes as a spike at $t_s = 0$. The profile illustrated I represents
                this impulse. assumed to have the same width as the injected impulse
                which is considered to be infinitely narrow. Note that the time $t_s = 0$
                corresponds to t_m, the retention time for an unretained compound in the
                column. The interacting fraction has a probability distribution that can
                be calculated by equation 2.15. The resulting profile is labelled II in the
                diagram above. The overall profile of a sample is the sum of the two
                fractions, labelled III above.

original column

impulse

Column 2   Column 1

impulse

$t_{m,2} = t_m \frac{n_2}{n_0}$ $t_{m,1} = t_m \frac{n_1}{n_0}$

P(ts)

0   5000   *   0   5000   =   0   5000   I

P(ts)

0   5000   *   0   5000   =   0   5000   II
ts (s)   ts (s)   ts (s)

<u>Overall Elution Profile</u>

P(ts)

0   5000   I   +   0   5000   II   =   0   5000   III
ts (s)   ts (s)   ts (s)
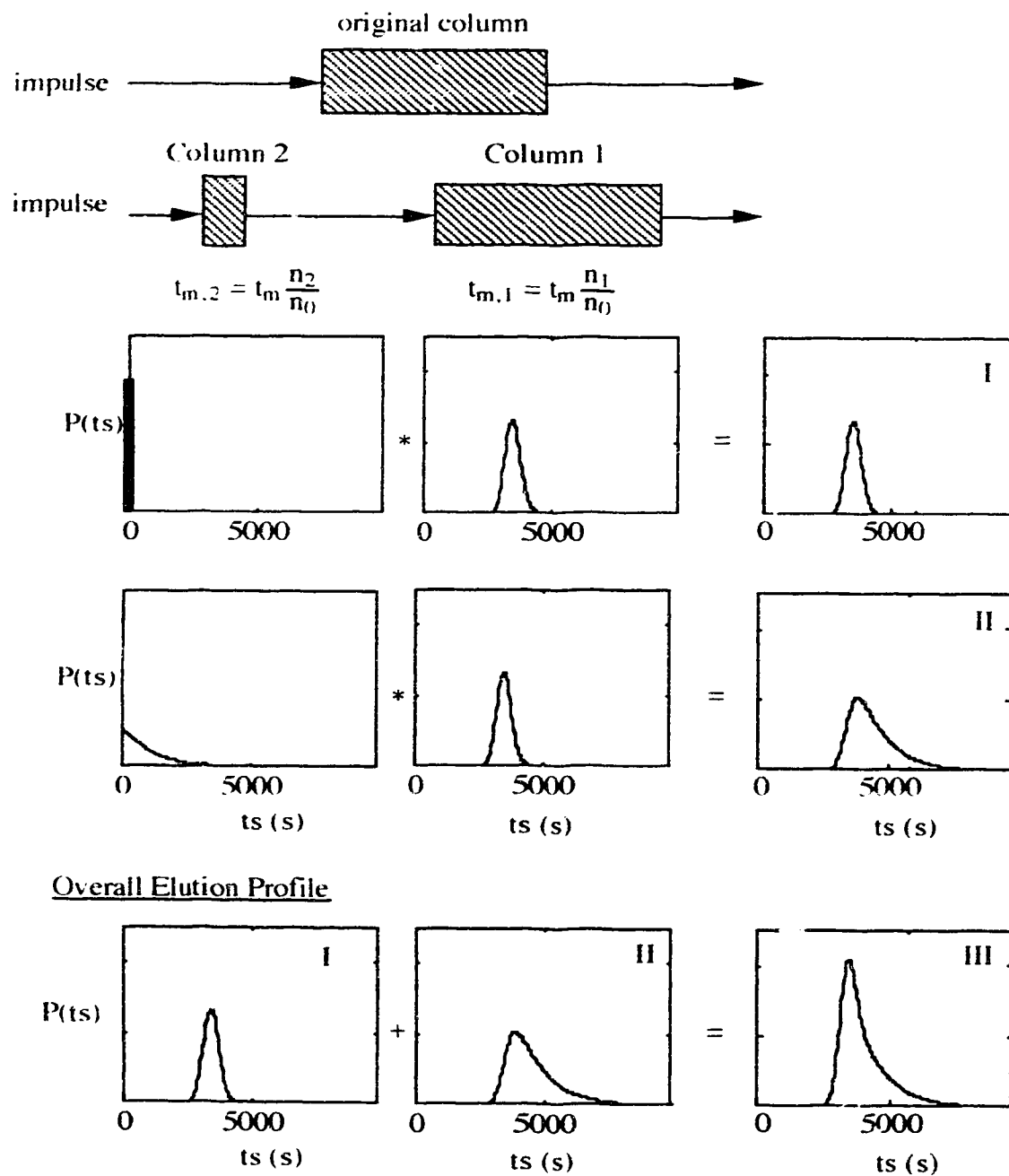
Figure 2.5.b   Prediction of the elution peak for a sample which has a bi-exponential rate curve on the packing in the analytical where there is some fraction that does not undergo the slowest sorption process. See Section 2.3.5.

the tri-exponential equation. Both of the incoming sample zones undergo broadening which is equivalent to convolution with the distribution $P(t_s)_1$ (equation 2.21). Profile I is the result of convolution of the impulse with $P(t_s)_1$ and profile II is the result of convolution of $P(t_s)_2$ with $P(t_s)_1$.

In order to predict the real chromatogram from the profiles I and II, two additional calculations are made. First, the profiles are scaled according to the non-interacting fraction. This scaling is done according to area (ie. if $\Phi_2 = 0.3$, the area under profile I must be 30 % of the total area.) The scaled profiles are then summed to form III. Once the time correction is made by adding t_m on the time axis (as discussed in Section 2.3.3), this profile is then comparable to the elution profile of the sample from a real chromatographic column containing a stationary phase whose sorption rate curve is modelled by a bi-exponential equation containing one relatively small and one relatively large sorption rate constant.

2.3.6 Data Treatment For Tri-exponential Rate Curve Where Non-interacting Fraction for One Sorption Step is Significant.

The data treatment actually used for the majority of rate curves de ... ... in this thesis falls under this category. Generally, the rate curves are tri-ex... ... in nature, which has the form shown in equation 2.25.

$$n(t) = n_o - n_1 e^{-k_1 t} - n_2 e^{-k_2 t} - n_3 e^{-k_3 t}$$

eqn. 2.25

The thought experiment previously described is modified so that the chromatographic column is modelled by a series of three columns of varying lengths. This situation is illustrated in Figure 2.6. In the first column, labelled Column 3, the sorption rate is the slowest and a significant fraction of a sample zone will not interact with the stationary phase in this column. The output from the first column is as
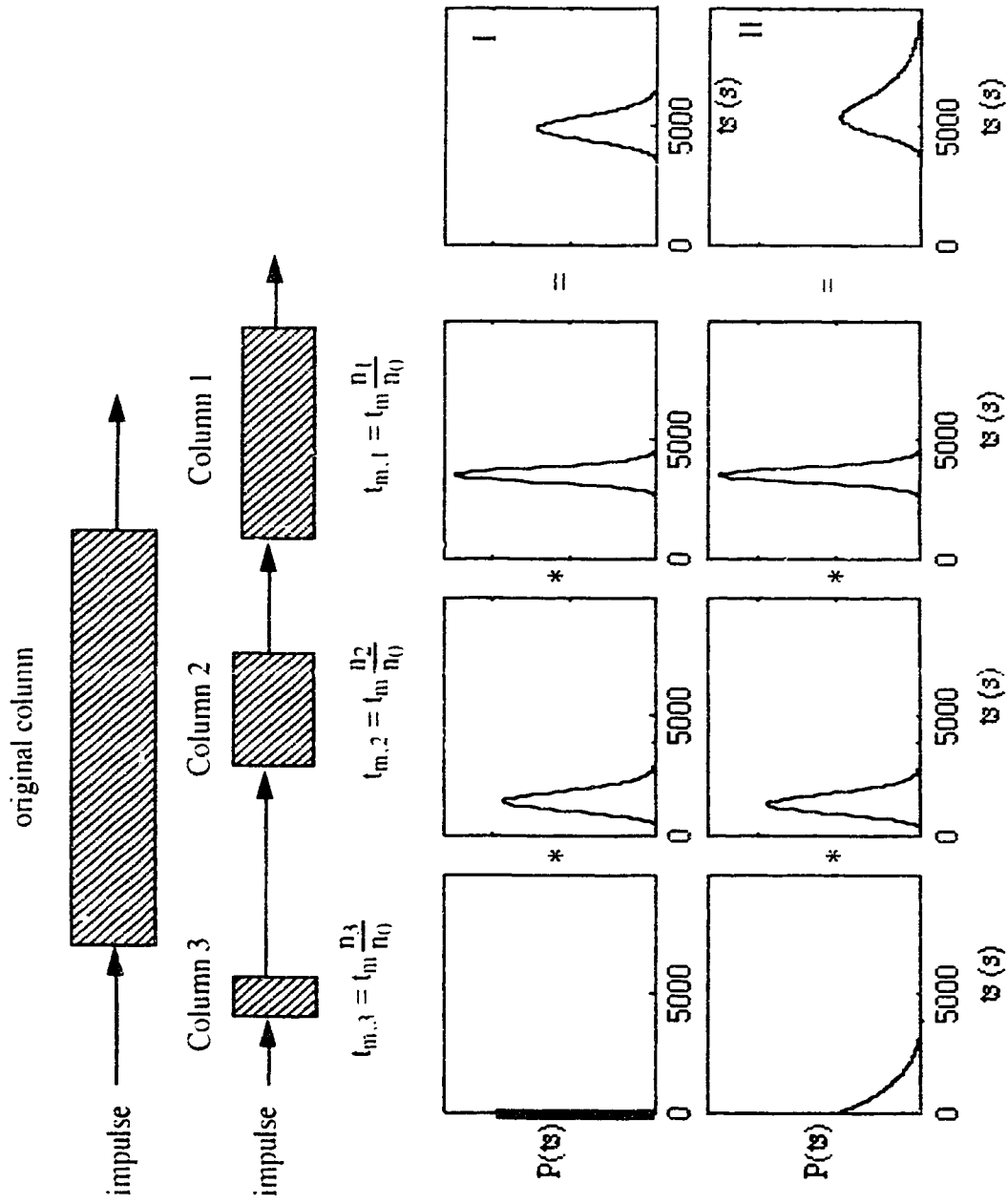
Figure 2.6.a   See caption for Figure 2.6.b for explanation.

Overall Elution Profile
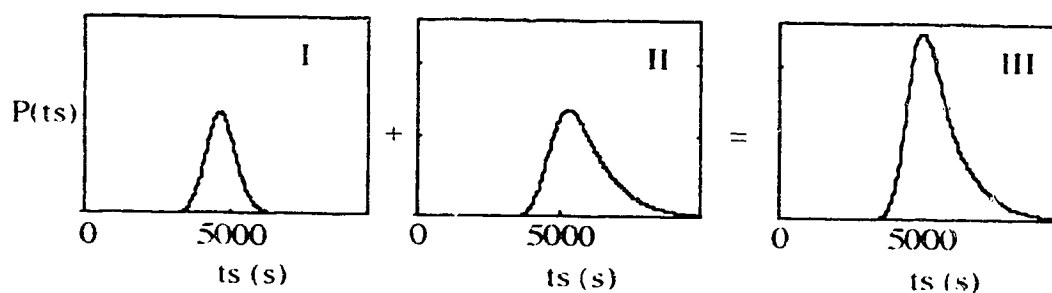
Figure 2.6.b   Prediction of the elution profile for a sample which has a tri-exponential

sorption rate curve on the packing in the analytical column. The profiles

I and II represe⁻ the two sample zones which elute from the series of

hypothetical columns, as shown in Figure 2.6.a. Profile I is broadened

due to kinetic processes occurring only on columns 1 and 2. Profile II

is broadened due to interaction on columns 1, 2 and 3. The peaks are

scaled according to area and added to get the overall profile III. After

correction for t_m on the time axis, the peak III may be compared to a

real chromatogram. See Section 2.3.6 for a complete description.

described in Section 2.3.5. consisting of sample eluting in two zones. Each of these zones will enter the next column, Column 2, where they will be modified by slow sorption-desorption kinetics associated with the stationary phases contained therein. The zones exiting Column 2 will then enter Column 1 to be further broadened. Column 1 is taken to be associated with the fastest sorption process and the constants n_1 and k_1. Column 2 is associated with the intermediate process and the constants n_2 and k_2. Each of these two columns would therefore act on injected impulses to give the distributions $P(t_s)_1$ and $P(t_s)_2$. In this case, however, the zones entering in these columns are not impulses, but are sample zones which have already undergone broadening.

In Figure 2.6, distribution I is the output from the series considering only the non-interacting fraction of sample molecules which eluted from the Column 3 as an impulse. Notice that the impulse is, in turn, convolved with the distributions $P(t_s)_2$ and $P(t_s)_1$. Distribution II in the illustration is the output from the series considering the sample zone that was broadened by slow sorption-desorption kinetics in Column 3 as well as in the Columns 1 and 2. After scaling (as described in Section 2.3.5), the overall elution profile is the summation of distributions I and II. Once the overall profile, III, is corrected along the time axis (Section 2.3.3), it is the comparable to the elution profile of the sample from a real chromatographic column containing a stationary phase whose sorption rate curve is modelled by a tri-exponential equation containing one relatively small and two relatively large sorption rate constants.

2.3.7 Description of Elution Chromatographic Peaks by Statistical Moment Analysis

The ideal elution profile in chromatography follows a Gaussian distribution. If a profile is Gaussian, it is symmetrical and the peak is easily described or characterized. The time for elution of the peak maximum is the retention time or centre of gravity of the peak. The variance is related to the peak width and can be easily calculated by

graphical methods [2.30]. These quantities are used to calculate the overall column efficiency (see equation 2.1). Most chromatographic peaks are not described by a Gaussian distribution and various schemes have been developed to adequately measure the peak characteristics mentioned above. Estimates of the characteristics can be obtained using graphical methods (summarized in Reference 2.30). For asymmetric peaks, these have proven to be unreliable. Instead, asymmetric peaks are best characterized by their statistical moments. The zeroth, first and second moments, designated as M_0, M_1, and M_2, are integrals defined by equations 2.26, 2.27 and 2.28 respectively. M_0 is the area under the peak and is used in the calculation of other moments. M_1 is the centre of gravity and M_2 is the variance of the peak [2.31].

$$M_0 = \int_0^x h(t)dt$$

eqn. 2.26

$$M_1 = \frac{\int_0^x t * h(t)dt}{M_0}$$

eqn. 2.27

$$M_2 = \frac{\int_0^x (t-M_1)^2 * h(t)dt}{M_0}$$

eqn. 2.27

In equations 2.26 to 2.28, $h(t)$ is the peak height at time t.

If chromatographic data are collected digitally, the moments can be calculated either using summations as approximations of the integrals or using the computer languages which contain integration functions, such as ASYST (see Section 3.5.1). Results of numerical integration for experimental elution profiles are discussed in Section 4.2.1.1.

An alternate method of characterizing elution profiles which are asymmetric is to fit the profile to an exponentially-modified Gaussian (EMG) function. This fit

simplifies the calculation of the moments which characterize the peak because the moment equations (ie. 2.26, 2.27 and 2.28) can be applied analytically. The EMG function is shown in equation 2.29 [2.32].

$$h_{EMG_i}(t) = A\frac{\sigma_{G_i}}{\tau}\sqrt{2}\exp\left[\frac{1}{2}\left(\frac{\sigma_G}{\tau}\right)^2 - \frac{t - t_{G_i}}{\tau}\right]\int_{-z}^{\prime\,r}\exp(-x^2)dx$$

eqn. 2.29

where
$$Z = \frac{t - t_{G_i}}{\sigma_{G_i}} - \frac{\sigma_{G_i}}{\tau}$$

eqn 2.30

The EMG function is defined by three parameters. The constants t_G and σ_G are the centre of gravity and the variance of the parent Gaussian peak. The parameter τ is the centre of gravity of the modifying exponential function. The factor A in the pre-exponential term determines the amplitude of the function. The function has been shown to be a good approximation of chromatographic peak shapes [2.33].

In order to evaluate the integral contained in the EMG function, the identity shown in equation 2.31 [2.32] is used to take advantage of the built-in error function (erf) routine in the language.

$$\int_{-z}^{\prime}\exp(-y^2)dy = \frac{\sqrt{\pi}}{2}[1 + erf(x)]$$

eqn 2.31

At values of $Z \leq -3$, techniques utilizing the error function have previously been shown to be inaccurate in evaluating the integral in equation 2.29 [2.32].

The moments of an EMG profile can be calculated from the constants of the function as shown in equations 2.32 and 2.33.

$$M_1 = t_{G_i} + \tau$$

eqn. 2.32

$$M_2 = \sigma_{G_i}^2 + \tau^2$$

eqn. 2.33

CHAPTER 3

Experimental Procedures

3.1 Reagents

Naphthalene, supplied by Coleman and Bell (Norwood, OH), was recrystallized from methanol before use as the sample. Phloroglucinol (1,3,5-trihydroxybenzene), obtained form Fisher Scientific Co. (Fairlawn, NJ), was recrystallized from water and was used to determine hold-up volumes and mobile phase linear velocity in the elution experiments on PRP-1. Analytical reagent grade $Ca(NO_3)_2 \cdot 4H_2O$ was used as supplied by BDH Chemicals (Poole, England) in the elution experiments on Partisil-10 ODS-3 to measure the mobile phase linear velocity.

3.2 Solvents and Mobile Phases

Doubly-distilled water was obtained from a Barnstead (Dubuque, IA) Nanopure water filtration/distillation system (part D4741). Reagent grade methanol was obtained from two suppliers, Anachemica Ltd. and Mallinckdrot and was distilled before use. Eluents and solvents were made by measuring appropriate volumes of methanol into a 2L volumetric flask and diluting to volume with doubly distilled water. For all experiments in which the stationary phase was PRP-1, 85% $MeOH/H_2O$ was used as the solvent and eluent. This solvent was made by diluting 1700 mL of MeOH to a volume of 2000 mL. Because Partisil-10 ODS-3 is not as strong a sorbent as PRP-1, 52.5% $MeOH/H_2O$ was used as the solvent and eluent for this packing. This solvent was made by diluting 1050 mL MeOH to 2000 mL. Before use, the mixed solvents were vacuum filtered through Nylon 66 membrane filters of 0.45 μm porosity (part 00140, Schleicher & Schuell, Keene, NH).

3.3   Packings

Two types of stationary phase packings were used in this experiment. PRP-1 (lot 372), a polystyrene-divinylbenzene copolymer, was donated by Hamilton Co. (Reno, NV). The second material was the silica-based Partisil-10 ODS-3 (part 4128-010, Whatman, Clifton, NJ, batch 100763). The characteristics of both packings are shown in Table 3.1.

3.4   Measurement of Sorption Rate using the Shallow Bed Apparatus

3.4.1   Apparatus for Sorption Rate Measurements

Figure 3.1 provides a schematic diagram of the apparatus. The centre of the system is a slider valve V2, illustrated in Figures 3.2.a and 3.2.b. The basic design of the valve follows the design of commercially available slider valves with some important distinctions. The valve is constructed mainly of stainless steel. The valve body, as shown in Figure 3.2.b, is basically a stainless steel box with sides approximately 1/4" thick. The valve body disassembles to allow access to the slider. The slider is a 2 mm thick stainless steel plate with four holes of 3 mm diameter drilled at 3/8" intervals on centres. At the bottom of each of the holes is a stainless steel mesh screen of 2 μm pore size. One of the holes contains the shallow bed, a small "column" of packing material approximately 0.5 mm in height. The bed is held in place on the bottom by the metal screen and on the top by a 3 mm diameter Zitex Teflon porous plug. This material, available in sheets (part K1064-122D, Chemplast, Wayne, NJ), is approximately 0.6 mm thick and of 30-60 μm pore diameter. Typical shallow bed characteristics are shown in Table 3.2.

The slider is mounted in a stainless steel assembly between two Teflon face plates. The Teflon face plates provide low friction for the sliding action. The actual surface area contacting the slider is decreased by milling grooves along the sides of the

Table 3.1   Packing properties of PRP-1 and Partisil-10 ODS-3. Properties of the
Partisil marked with an asterisk (*) are data given by the manufacturer
for the underivatized silica gel. Further information about the pore
volume of the derivatized packing is given in Appendix 2.

Packing Property	PRP-1	Partisil-10 ODS-3
Material	Poly(Styrene Divinylbenzene)	C_{18} groups bonded to Partisil Silica Gel
Particle Shape	spherical	irregular
Particle Size	10 ± 2 µm	10 µm
Packing Density	0.42 g/mL	0.45 g/ml.*
Avg. Pore Diameter	7.5 nm	6.8 nm*
Specific Pore Volume	0.79 mL/g	0.796 ml./g*
Specific Surface Area	415 m2/g	467 m2/g*
% C Loading	N/A	10.5
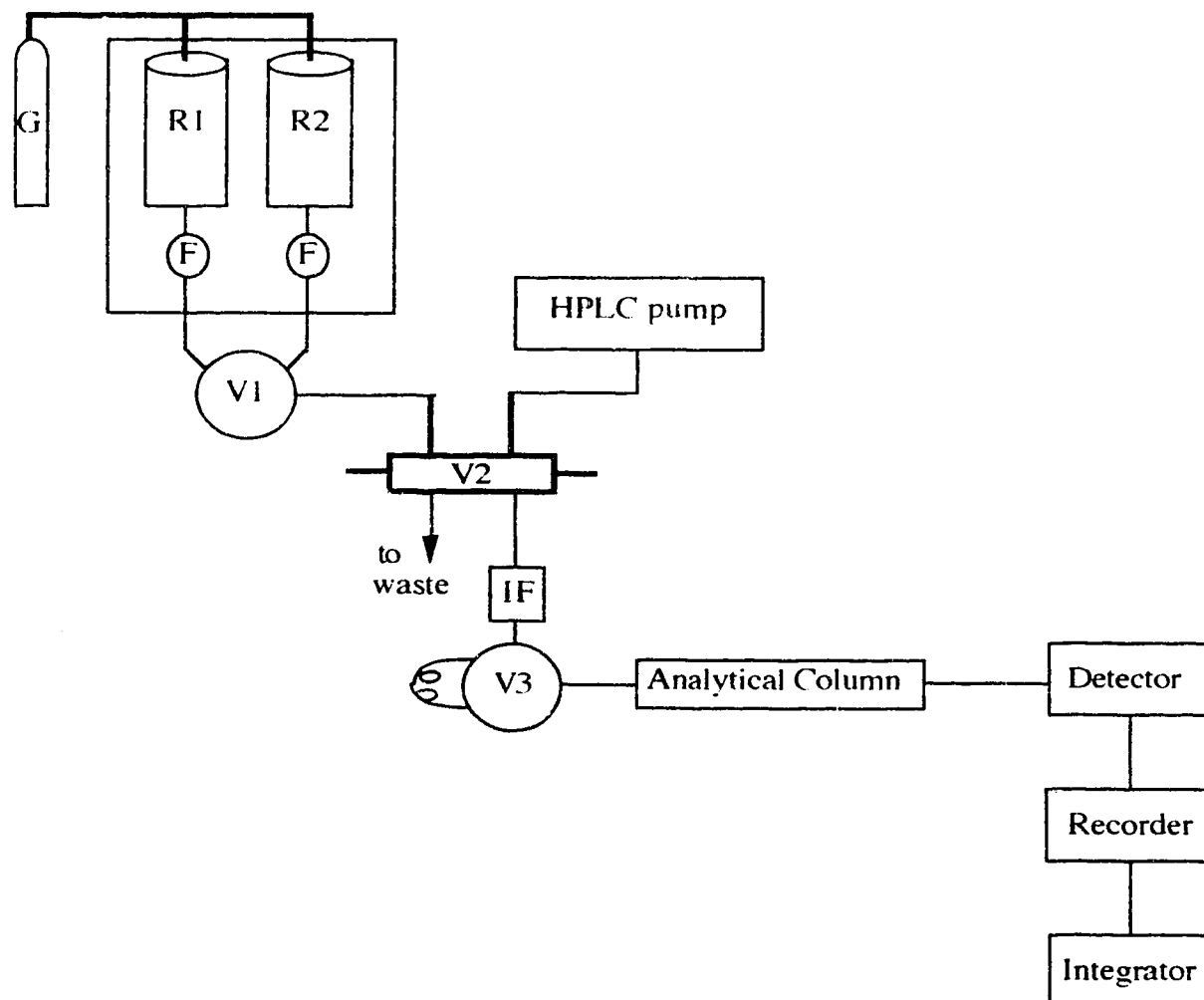
Figure 3.1   Schematic diagram of apparatus used for sorption rate measurements.
G: Gas cylinder (N_2). R1 and R2: solvent and sample solution
reservoirs of constant pressure pumps. F: Millipore solution filter
holders. V1: Rheodyne six-way valve. R1, R2 and the filters F are
immersed in a constant temperature bath. V2: Slider valve. IF:
Rheodyne in-line filter. V3: Rheodyne injection valve. The system is
described in detail in Section 3.4.1.
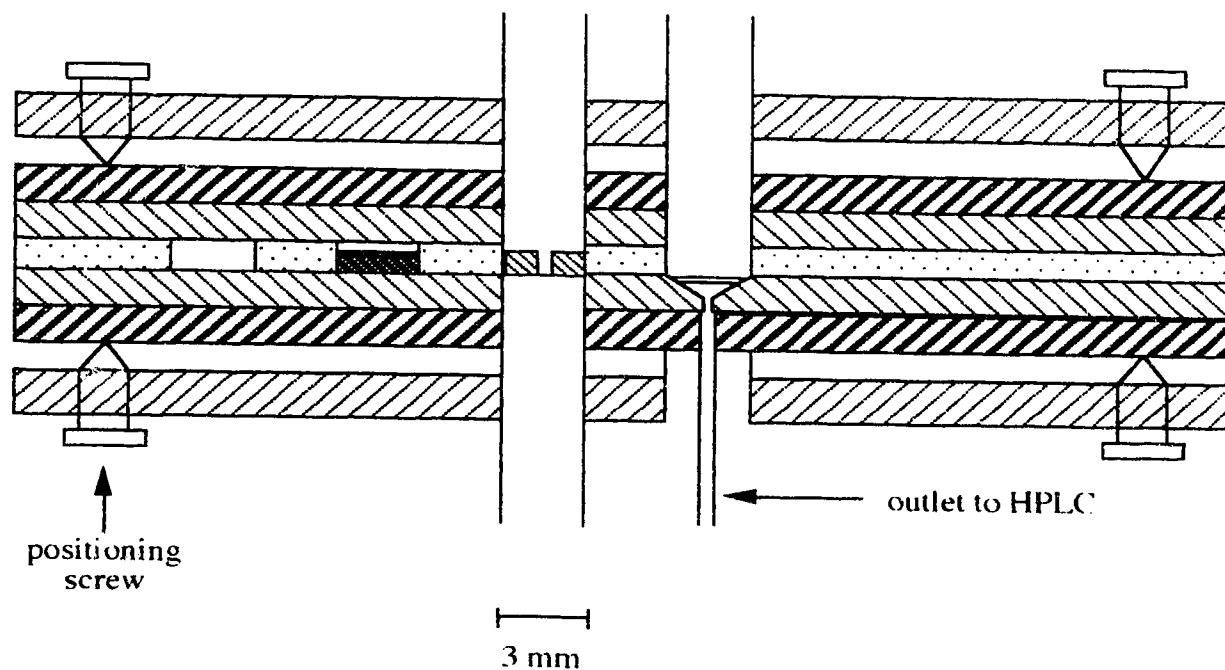
outlet to HPLC

positioning
screen

3 mm

Materials:

Stainless Steel Valve Body

Stainless Steel Face Plates

Teflon Face Plates

Stainless Steel Slider

Shallow Bed of Packing

Teflon Plug for Dummy Hole

Porous Teflon Screen

Figure 3.2.a   Schematic diagram of slider valve (side view). The valve is more fully described in Section 3.4.1.

milled groove

1 cm

sealing screw

Materials:

Stainless Steel Valve Body

Stainless Steel Face Plates

Teflon Face Plates

Stainless Steel Slider

Shallow Bed of Packing

Porous Teflon Screen
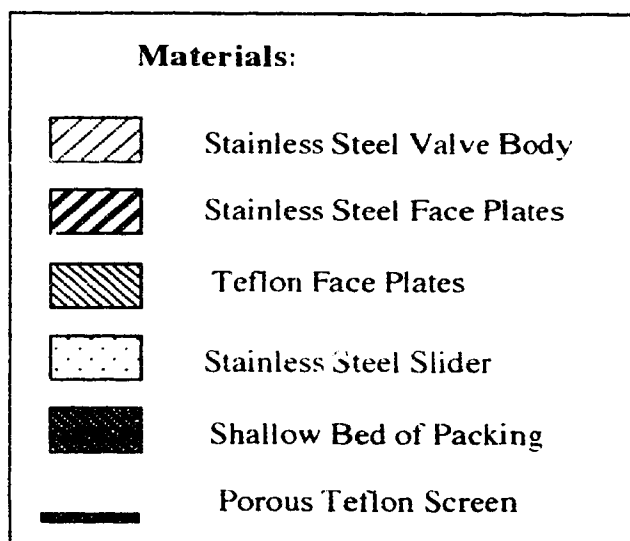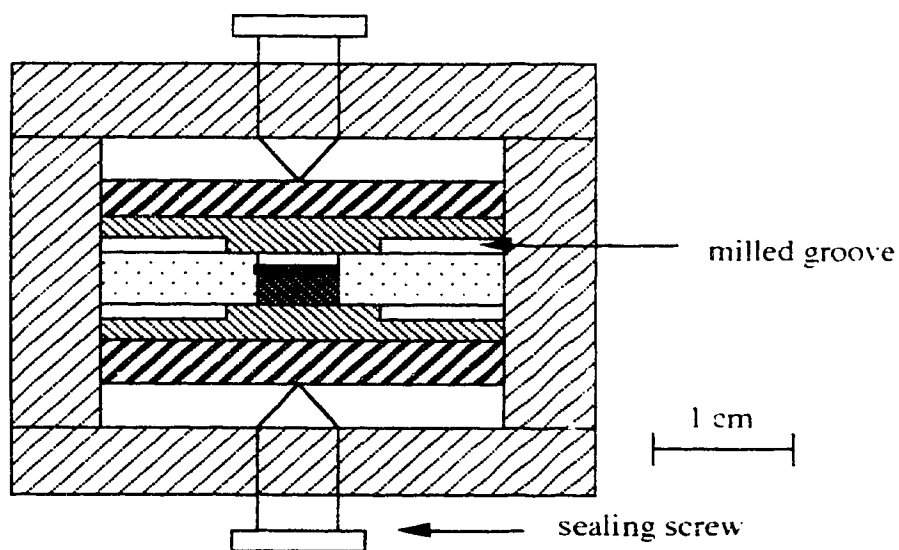
Fig. 3.2.b Schematic diagram of slider valve (end-on view). A complete description of the slider valve is given in Section 3.4.2.

Table 3.2   Properties of shallow beds of PRP-1 and Partisil-10 ODS-3 used in sorption rate experiments. The weight of the shallow beds are measured directly and the error is the absolute error. The $V_{hold-up,T}$ and $V_{hold-up}$ are measured as in Section 3.4.3. The error values are calculated by propagation and are expressed as ± one standard deviation. All other characteristics are estimated from manufacturer's information concerning the packing. The pore volume for the Partisil shallow bed uses the specific pore volume calculated in Appendix 2.

Shallow Bed Property	PRP-1	Partisil-10 ODS-3
weight packing	1.82 ± 0.05 mg	1.06 ± 0.05 mg
bed height	~ 0.6 mm	~ 0.3 mm
packing volume*	~ 4.3 µL*	~ 2.3 µL*
V_{pore}	1.44 ± 0.04 µL	0.64 ± 0.03 µL
$V_{hold-up,T}$	13.88 ± 0.07 µL	15.17 ± 0.44 µL
$V_{hold-up}$	12.44 ± 0.12 µL	14.53 ± 0.46 µL

*Based on bulk density

Teflon face plates as shown in Figure 3.2.b so that only the small area around the holes in the slider are contacted. The decreased area of contact leads to a better seal of the Teflon/stainless steel surfaces.

Screwed to the Teflon plates is a set of stainless steel plates. At four sites, positioning screws through the valve body contact these steel plates. These four positio... screws provide the forces necessary to seal the valve. The steel plates pr...e Teflon plates from being deformed by the sealing screws. Pieces of Teflon tape are placed between the steel and Teflon plates before attachment to assure a good seal between them.

The slider valve has 2 inlets, both of which are stainless steel tubes of 3 mm i.d. which are silver-soldered to the steel plates. The first inlet, shown on the left side of valve V2 in Figures 3.1 and 3.2.a, is connected to a system of constant pressure pumps consisting of two aluminum cylinders, R1 and R2, pressurized by N_2. R1 and R2 contain a solvent and sample solution respectively. The solutions pass through in-line stainless steel filter holders labelled F in Figure 3.1 (part XX44 047 00, Millipore, Mississauga, Ont.) containing Durapore HV membrane filters of 0.45 µm pore diameter (part HVLP 047 00, Millipore, Mississauga, Ont.) before reaching a Cheminert 6-way valve, V1 (part 414 2530, LDC, Riviera Beach, FA). The setting of V1 determines which solution enters the first inlet of the slider valve. R1 and R2 are immersed in a constant temperature bath thermostated by a circulating Haake D3 temperature controller which is set to 25.0 ± 0.1 °C. This left-side inlet of the slider valve has an outlet to waste. Moving the slider to the right, from the position shown in Figure 3.2.a places the shallow bed in the sample flow stream to initiate the timed "exposure step". The exposure time refers to the time the shallow bed spends in the second position, during which the sample stream passes through it.

The second inlet, located on the right side of the slider valve, as shown in Figures 3.1 and 3.2.a is fed by an SP 8000 HPLC pump (Spectra-Physics, Santa

Clara, CA) in constant flow mode. When the bed is moved out of the sample flow stream into this flow stream, any sample which was sorbed in the previous exposure step will be eluted and analyzed using conventional HPLC as follows. The right hand outlet of V2 is directed to narrow-bore (.002" i.d.) stainless steel tubing leading to a Rheodyne in-line filter (part 7315, Rheodyne, Berkeley, CA) and an analytical HPLC column. The analytical column (part 086680, Waters, Mississauga, Ont.) used in the sorption rate experiments is packed with μBondapak Phenyl and is 15 cm in length and 4.6 mm i.d. A Rheodyne injection valve, V3 (part 7010, Rheodyne, Berkeley, CA) with a sample loop of a previously measured volume of 23.88 ± 0.02 μL [3.1] is located upstream of the analytical column and is used to construct a calibration curve, as explained in Section 3.4.2.

The slider can occupy one of three positions which are illustrated in Figure 3.3 and further described in Section 3.4.2. The exposure time (illustrated in Figure 3.3.d) is measured using a small infra-red generator/detector unit which is attached to the lever system. The exposure time is displayed on a modified Hewlett Packard 5321B electronic counter set to display to ± 0.1 msec.

Sample eluted from the shallow bed in the elution step (Figure 3.3.e) passes through the analytical column into a Kratos 757 Variable Wavelength UV detector (λ = 276 nm). The resulting peaks are recorded on a Fisher Recordall Chart Recorder and integrated by an HP 3390A Integrator.

Good temperature control was found to be of some importance for reducing error in the sorption rate measurements. The body of valve V1 and connecting tubing leading from the thermostated reservoirs were both insulated with asbestos tape. Monitoring the temperature of the flowing streams proved to be problematic. Since the slider and slider valve body were for the most part metal, heat conduction between the various valve parts was considered to be good. The temperature of the valve body and of the metal inlet tubing near the slider were monitored with a contact K-type

Solvent   Eluent

Figure 3.3.a Solvent Rinse

Figure 3.3.b Pre-equilibration

Solvent

Figure 3.3.c Sample Rinse

Sample

Figure 3.3.d Sample Exposure

Sample

Figure 3.3.e Elution

Solvent
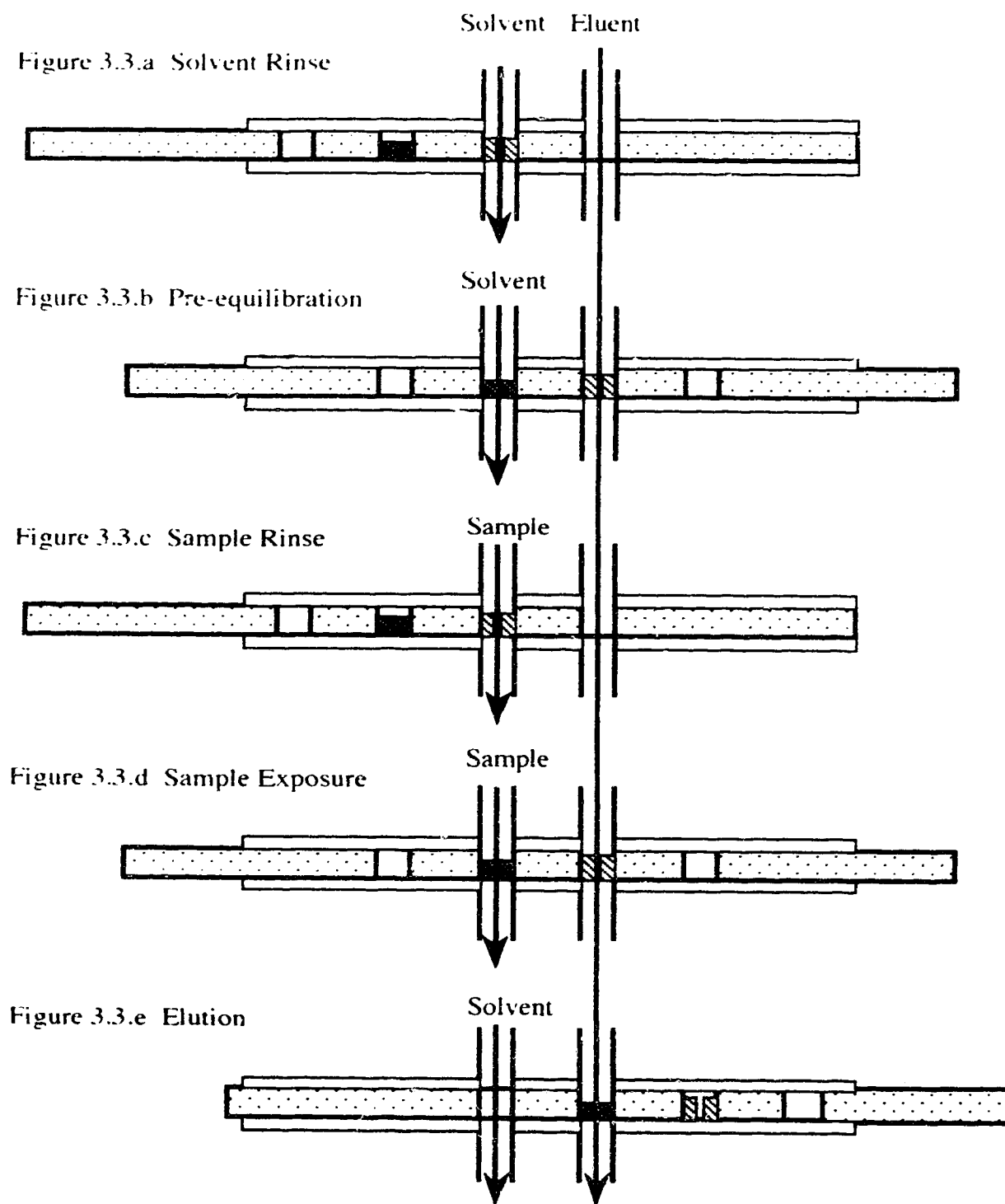
Figure 3.3   The sequence of positions of the slider valve in the sorption rate

experiment as described in Section 3.4.2.

thermocouple and Digi-Sense JTK thermometer readout (part N-08528 20, Cole Parmer) set to read ± 0.1 °C.

The valve is mounted on an aluminum back plate, not shown in the figures, which is mounted on the top of a lab bench. Also mounted on the back plate is a lever assembly which is used to move the slider, as shown in Figure 3.4. The slider is attached at one end to a lever via a brass bar. The lever uses a hinged hook to catch notches in the bar. To change the position of the slider, the lever is pushed forward (to the left in Figure 3.4) until the hook catches the next notch in the bar, then is pulled back until it hits a stop. The stop and the notches in the bar are carefully calibrated so that the slider falls into a position where the holes are aligned directly under the inlet of interest. To return the slider to the original position, it is necessary to pull the slider back manually using a handle (not shown in the schematics) on the left end of the slider. At present, this results in some stress on the slider and a tendency for the slider to twist out of shape. A lever, built on the same principle as the one described above, attached to this end of the slider would be of great help in prolonging the life of the slider.

The valve in its present form provides little back pressure. For example, a flow rate of about 12 mL/min can be achieved in the exposure step with 120 psi for the shallow bed of PRP-1. An HPLC pump is used in the elution step because of the presence of the analytical column which provides most of the back pressure for the system. Relatively low flow rates of the eluent (eg. 0.4 ml/min) are used. The valve seals well up to about 600 psi but is more usually used in the range of 300 psi or less.

The slider is made of stainless steel and should be handled carefully to avoid scratching the polished surface. One persistent problem with the valve is that the sliding action tends to shave off the Teflon surface of the face plate. The sharp edges of the holes in the slider drag across the Teflon surface as the slider moves, planing off flakes of Teflon. The flakes of Teflon become lodged in the empty holes of the slider
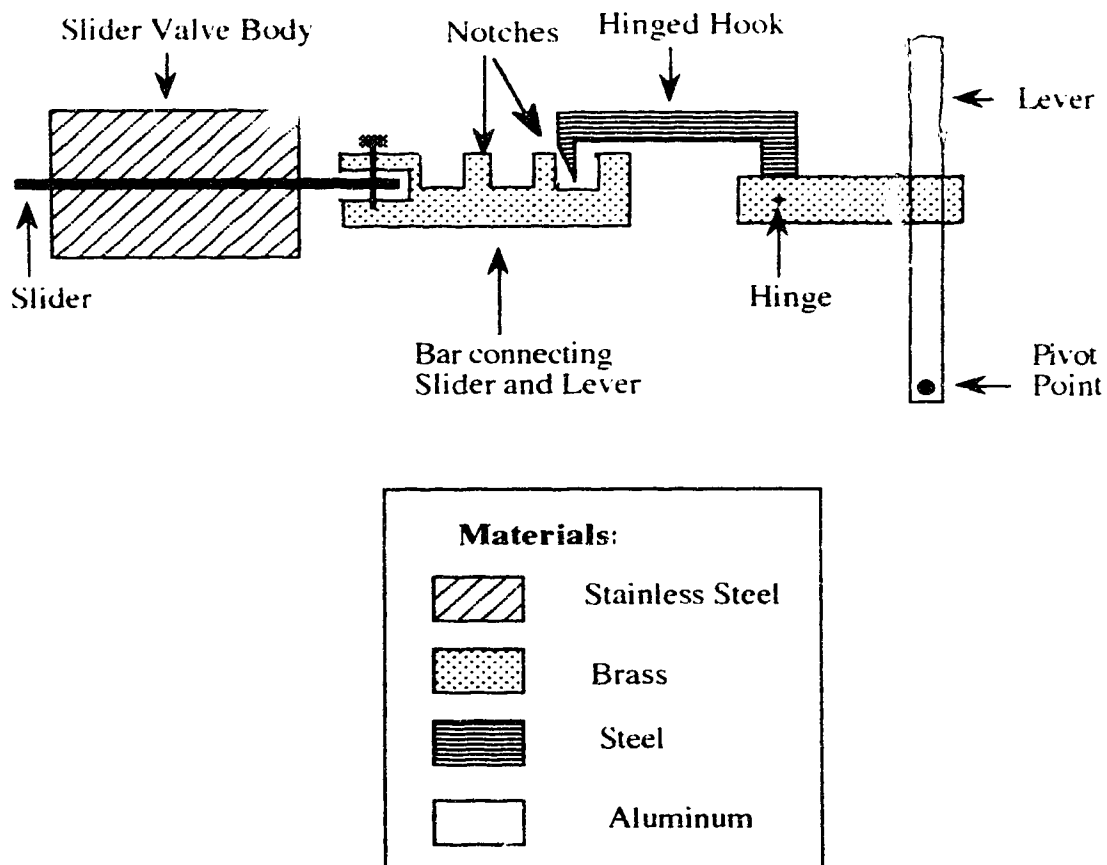
Figure 3.4   Lever System used to move slider in sorption rate experiment. The
lever system is described in detail in Section 3.4.2

and on top of the Zitex retaining screen of the shallow bed. This results in an increase in back pressure. The edges of the holes on the underside of the slider also produce flakes of Teflon which tend to lodge in the inlet to the HPLC. Since the outlet tubing to the HPLC is narrow bore, even a small piece or amount of Teflon can severely increase the system back pressure. This problem is prevented by the use of a stainless steel mesh screen with 2 μm porosity placed over the outlet to the HPLC in the bottom Teflon plate. This is illustrated in Figure 3.2.a. The down stream in-line filter also provides protection against particulate matter but mainly for the analytical column.

The inlets to the slider valve were designed to produce a flow stream having the same 3 mm in diameter as the shallow bed. If the inlet were of a smaller diameter than the shallow bed, a radial flow velocity gradient might be established. The flow through the bed would probably be too fast to allow lateral diffusion to completely relax this gradient. If this were the case, parts of the bed at different radial locations would experience different sample concentrations and the criteria for establishing shallow bed conditions would not be met.

3.4.2 Experimental Procedure

The measurement of the rate of sorption onto a packing involves a series of experiments in which the shallow bed of the packing of interest is exposed to a relatively fast stream of a sample solution for variable amounts of time.

In each run of the series, the bed is initially located in the first position of the slider as illustrated in Figure 3.3.a. The first step in the experiment is the pre-equilibration of the shallow bed with solvent which is being pumped through the left-hand inlet to the slider valve. This solvent is stored in R1 and 25 mL of it is allowed to flow through connecting tubing to adequately rinse the system. Pre-equilibration of the shallow bed begins when the bed is pulled into the solvent stream as shown in Figure 3.3.b. The time needed to collect 10 mL of solvent after it passes through the bed is

measured and recorded. The superficial linear velocity, u, through the bed is calculated from this time. At, using equation 3.1.

$$u = \frac{10 \text{ mL}}{\pi \, r^2 \, \epsilon_{inter} \Delta t}$$

eqn. 3.1

r is the radius of the shallow bed which is 0.15 cm. ϵ_{inter} is the fraction of bed volume contained between the particles. For PRP-1, the quantity was calculated using manufacturer's information concerning the specific interparticle volume and the bed density. For PRP-1, ϵ_{inter} was calculated to be 0.31. For the silica-based packing, similar information was not available and ϵ_{inter} was assumed to be 0.4 [3.2, 3.3].

Once pre-equilibration is complete, the shallow bed is pulled back into its initial position as seen in Figure 3.3.c and the rotary valve V1 is used to change the liquid flowing through the left hand tube from solvent to sample solution. The connecting tubing is flushed with approximately 25 mL of sample solution before the bed is pulled back into the sample stream to initiate the exposure step (Figure 3.3.d). In the exposure step, the bed is left in the flowing stream for the desired amount of time. The slider is then pulled to the third position (Figure 3.3.e) in which the shallow bed is located in the eluent stream fed by the HPLC pump. Once elution is complete, the slider is pulled back to the first position (Figure 3.3.a) and the experiment is repeated with a different exposure time. The minimum exposure time used in this experiment (> 0.3 s) was determined by the minimum time required by the lever and hinged hook assembly to move the slider from the position shown in Figure 3.3.d to that shown in Figure 3.3.e. Each repetition of the sequence shown in Figure 3.3 results in a detected peak with area proportional, after corrections described below, to the number of moles sorbed by the shallow bed.

A calibration curve is constructed by injecting solutions of known concentration into the analytical column using the injection valve V3 (in Figure 3.1) and plotting the integrated area against the number of moles injected. Next, the area of the peak eluted

from the shallow bed is used to calculate the total moles of sample eluted, N_{el}. In order to calculate the number of moles sorbed, N_{sorb}, the number of moles eluted from the shallow bed must be corrected for $N_{hold-up}$, the moles of sample contained in the hold up volume of the shallow bed (see Section 3.4.3) as shown in Equation 3.2.

$$N_{sorb} = N_{el} - N_{hold\ up}$$

eqn. 3.2

For short exposure times, an additional correction is necessary. The 3 mm hole to the right of the shallow bed in the slider (see Figure 3.3) is filled with a Teflon plug with a very small hole (~0.3 mm diameter and volume 0.37 µL) drilled through it. The plug was installed to decrease the volume in this dummy hole. The hole in the centre of it is necessary to allow flow through the valve when the valve is in any of the positions illustrate in Figure 3.3. During the step in which the connecting tubing is rinsed with sample solution (see Figure 3.3.c), this dummy hole is located in the sample stream and is thus filled with sample solution. When the valve is switched into the next position (see Figure 3.3.d), the dummy hole lies in the eluent stream and the sample solution it contains is injected into the analytical column. For very long exposure times, the sample peak resulting from sample solution in the dummy hole will elute from the analytical column well ahead of the sample peak resulting from elution from the shallow bed. However, as the exposure time for the shallow bed is decreased, the two sample peaks are injected closer and closer together. When the eluent flow rate is 0.4 mL/min, the two peaks were found to overlap when the exposure time was less than about 20 sec. In this case, the integrator treats them as one peak. The number of moles of sample contained in the dummy hole, N_{dummy}, must therefore also be subtracted from the number of moles eluted from the shallow bed for these short exposure times.

$$N_{sorb} = N_{el} - N_{hold\ up} - N_{dummy}$$

eqn 3.3

Once N_{sorb} is calculated, the data are normalized to Wt, the weight of packing in the shallow bed.

$$n(t) = \frac{N_{sorb}}{Wt}$$

<div align="right">eqn 3.4</div>

The units of n(t) are mol/g. The quantity n(t) is a function of exposure time, t, so the experiment results in a sorption rate curve which is the plot of n(t) vs exposure time. A typical sorption rate curve is illustrated in Figure 2.3.

3.4.3 Hold-up Volume Measurement

The procedure used for measuring the sorption rate was, with a few modifications, also used to measure the hold-up volume for the shallow bed. The sample for these experiments was phloroglucinol in 85% MeOH/H$_2$O which was shown to be unretained on chromatographic columns of both sorbents. The exposure time was 60 s. The result of this procedure was a peak of area $A_{hold-up}$. For detector calibration, the phloroglucinol solution was then injected onto the analytical column using the injection valve V3 with an injection volume of V_{inj} giving a peak of area A_{inj}. The measured total hold-up volume of the bed, $V_{hold-up,T}$ was calculated by equation 3.5.

$$V_{hold\;up,\;T} = V_{inj} \frac{A_{hold-up}}{A_{inj}}$$

<div align="right">eqn. 3.5</div>

The measured hold-up volume was corrected by subtracting the pore volume, V_p, of the packing in the shallow bed. This correction, shown in equation 3.6, was necessary because diffusion of the sample into the pores of the packing must be considered to be part of the overall time consuming process of sorption.

$$V_{hold\;up} = V_{hold-up,\;T} - V_p$$

<div align="right">eqn. 3.6</div>

The quantity $V_{hold-up}$ is the volume associated with interparticle space as well as space within and below the retaining screen and within and above the porous Teflon plug in the 3 mm hole in the slider containing the shallow bed. The pore volume V_p is calculated by multiplying the specific pore volume of the product by the weight of

packing used in the shallow bed. The specific pore volume, in ml/g, of Hamilton PRP-1 is a packing characteristic listed in Table 3.2 and found in the manufacturer's information accompanying the product. The specific pore volume of Partisil-10 ODS-3 was calculated according to information described in the literature for silica based bonded phase packings [3.4] The authors found that as silica was derivatized, the decrease in the pore volume related only to the carbon loading and not the phase type. Since the specific pore volume for the original silica and the resulting % C loading were available (see Table 3.2), the specific pore volume, v_p, was calculated by using the linear relation described in Reference 3.4, substituting the appropriate value for the specific pore volume of the silica out of which the Partisil-10 ODS-3 was synthesized. Detailed calculations are found in Appendix 2.

Since the concentration of the naphthalene sample solution C_m, is constant in a particular shallow bed experiment, the moles of naphthalene present in the hold-up volume, $N_{hold-up}$, can be calculated according to equation 3.7.

$$N_{hold-up} = V_{hold-up} C_m$$
<div style="text-align: right">eqn 3.7</div>

This quantity is needed for equations 3.2 and 3.3.

As discussed, the hold-up volume of the Partisil-10 ODS-3 shallow bed is determined using phloroglucinol in 85 % MeOH/H_2O and sorption rates are measured with naphthalene in 52.5 % MeOH/H_2O. Ideally, the hold-up volume should be determined in the same eluent as used for a sample. In this case, that was not possible since phloroglucinol was retained on Partisil in 52.5 % MeOH/H_2O. Certain kinds of packings such as ion-exchangers and agarose swell as the water content of the mobile phase increases. Swelling would lead to an increase in the hold-up volume of the packing. Silica-based packings are rigid, however, so the hold-up volume should not vary with water content of the mobile phase. Therefore, the hold-up volume as

determined with phloroglucinol in 85% MeOH should be applicable when the 52.5 % MeOH solvent is used.

3.4.4 Measurement of the Sorption Isotherm

The sorption isotherms for naphthalene on the two packings were studied using the shallow bed apparatus as illustrated in Figure 3.1 in a procedure developed by May, Hux and Cantwell [3.1] called the 'column equilibration method'. In the experiment, the shallow bed is exposed to the sample solution until the stationary and mobile phases are in equilibrium. The exposure time in this experiment was 60 seconds. After this time, the shallow bed is slid under the eluent stream from the HPLC pump and the number of moles eluted is determined as described above. This quantity must be corrected for the sample contained in the hold-up volume. The quantity of interest in this case is the number of moles of sample actually adsorbed on the stationary phase. (In the shallow bed experiment, the quantity of interest is the amount adsorbed as well as the amount located in the pores of the packing.) In this case, therefore, the necessary calculation used the total hold-up volume $V_{hold-up,T}$, not $V_{hold-up}$ which was defined in Section 3.4.3.

$$N_s = N_{el} - C_m V_{hold-up}$$

eqn. 3.8

The quantity N_s differs from N_{sorb} by the number of moles in the pore volume of the packing.

$$N_s = N_{sorb} + C_m V_{pore}$$

eqn. 3.9

The sorption isotherm is a plot of C_s, the concentration in the stationary phase, in mol/g vs C_m, the concentration in the mobile phase. C_s is determined by dividing N_s by the weight of packing in the shallow bed.

$$C_s = \frac{N_s}{Wt}$$

eqn. 3.10

3.5   Elution Chromatography

3.5.1   Experimental Procedure

The purpose of measuring the sorption rate (kinetic) curves for naphthalene on a particular packing by the shallow bed experiment is to allow prediction of the chromatographic peak shape expected when naphthalene is eluted from a long column of the packing. The experimental elution chromatograms needed for comparison with those predicted by the calculations given in Section 2.3.7 were collected using the instrument illustrated in Figure 3.5. The HPLC pump, run in constant flow mode, the in-line filter, the injection valve and the UV detector are the same components mentioned above. The columns used were commercially available HPLC analytical columns. The PRP-1 column (part 79425, Hamilton, Reno, NV) was 4.6 mm i.d. and 15 cm long and packed with 10 μm spherical particles. The Partisil-10 ODS-3 column (part 1P9913, Whatman, Clifton, NJ) was 4.6 mm i.d. and 25 cm long and was packed with 10 μm irregular particles. The absorbance signals of the eluted peaks were fed into an analog-to-digital converter (Lab Master, TM-40-PGL, Tecmar, Cleveland, OH) in an IBM-XT microcomputer. Peak characteristics were calculated using ASYST Version 2.0 (McMillan Software Co., New York, NY). The programs, previously described in detail [3.5] permit the calculation of peak area, peak retention time, t_r, and peak variance, s^2, using statistical moment analysis. The experimental plate height is then determined using equation 2.1. Several problems with the ASYST software had to be overcome. The problems encountered with the moment analysis for naphthalene on PRP-1 are discussed in Section 4.2.1.1.

An alternate method of analysis was developed to compensate for some of the problems encountered in attempting to use numerical methods to calculate the moments of the elution peaks. Data were collected using the above instrument and the digital data
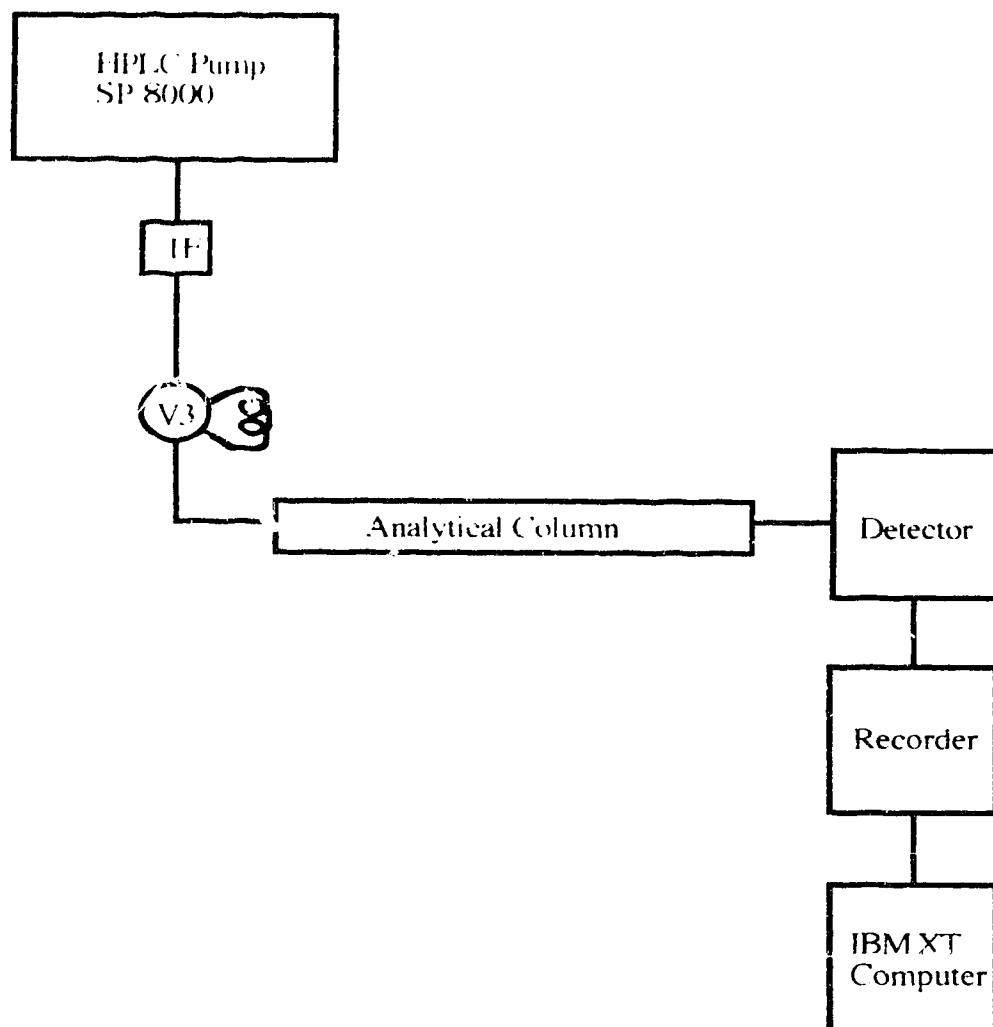
Figure 3.5   Schematic diagram of the apparatus used to collect experimental elution profiles as described in detail in Section 3.5.1. IF: Rheodyne In-line filter. V3: Rheodyne injection valve.

was smoothed using the smoothing function in the ASYST program. The data were saved in a data file which was then converted to MS-DOS format using a routine written in ASYST. This routine can be found in Appendix 3.1. The DOS file was then converted to a MacWrite (Claris Corp., 1988) format using Apple File Exchange software (Apple Computers Inc.. 1990) on a Macintosh IIsi. The data were then copied to an Excel (Microsoft. 1991) data file. The data was easy to manipulate and view in this format. A data subset was chosen from each data file with limits as discussed in Section 4.2.1.2 and the subset transferred to a home-grown non-linear least squares fit program called EXPGAUSS written in Matlab (MathWorks. Inc.. Natik. MA.). The program EXPGAUSS then chooses a user specified number of equally spaced data points within the subset which are used to fit the elution profile to an exponentially modified Gaussian (EMG) function. Statistical moments were then calculated analytically for the EMG function. as discussed in Section 2.3.7. Discussions of the limitations of this program including the effect of the number of data points chosen and the effect of uncertainty in the location of the baseline are discussed in Section 4.2.1.2.

On PRP-1, the linear velocity of the mobile phase, u_o, in the elution chromatography was measured by injecting a 10^{-3} M solution of phloroglucinol and calculating the first moment of the eluted peak. The first moment was corrected for extra-column effects as described in Section 3.5.2. The corrected first moment, t_m, is the time to elute the void volume of the chromatographic column. The linear velocity can be calculated from equation 3.11, where L is the column length.

$$u_o = \frac{L}{t_m}$$

eqn. 3.11

On Partisil-10 ODS-3, the phloroglucinol proved to be retained in 52.5 % MeOH which was the eluent for this packing. Therefore. a 10^{-3} M solution of

$Ca(NO_3)_2$ was used as the unretained compound to measure the linear velocity in this solvent system.

3.5.2   Correction for Extra-Column Bandbroadening

The contribution to the centre of gravity and the variance of elution profiles is evaluated using the instrument illustrated in Figure 3.5 with the chromatographic column removed. Broadening of the sample zone can occur due to effects in the injector, detector and connecting tubing [3.6]. The extra-column contributions were evaluated using approximately 10^{-5} M naphthalene in 85 % MeOH and collecting data as described in section 3.5.1. The elution profiles were then analyzed using the ASYST program previously discussed and the averages of the first and second moments were calculated to estimate the extra-column effects. At the four flow rates studied, the contribution was relatively small, as shown in Table 3.3. These corrections have been subtracted in all values of the first and second moments as reported in this thesis, no matter what method was used to calculate the moments.

The same data were used to correct for extra-column effects in 52.5 % MeOH. Some error would be involved in this since the effects are dependent on the diffusion properties of the sample in the mobile phase. 52.5 % MeOH has a higher viscosity and the diffusion coefficient will be less. The extra-column effects would therefore be expected to be lower in this second solvent system. Since the corrections are small in relation the peak profile characteristics, the error associated with the change in solvent is expected to be small.

Table 3.3   Corrections for extra-column bandbroadening at four different flow rates. The extra-column contributions are first moments (retention times) and second moments (variances) that are present due to components of the chromatographic system like the injector, detector and connective tubing. The experimental details can be found in Section 3.5.2. The confidence limits shown are at the 95 % level.

Flow rate (mL/min)	M_1 (s)	M_1 (s^2)
2.0	2.15 ± 0.05	0.349 ± 0.011
1.5	2.56 ± 0.07	0.459 ± 0.023
1.0	3.88 ± 0.10	1.81 ± 0.29
0.5	7.35 ± .07	10.3 ± 0.8

CHAPTER 4

Results and Discussion

4.1 Introduction

In this chapter, the sorption characteristics of two HPLC packings, the polymeric PRP-1 and the silica-based bonded phase Partisil-10 ODS-3, are measured and discussed. In Section 4.2, the sorption characteristics of PRP-1 are considered, including: the problems involved in characterizing the broadened elution profiles of naphthalene: the measurement of k' by two separate methods: the rate of sorption of naphthalene onto PRP-1: the relationship between the measured sorption rate and elution profiles: and comparison to observed chromatographic elution peaks. A similar series of investigations is discussed in Section 4.3 for the sorption of naphthalene on Partisil-10 ODS-3. Finally, in Section 4.4, the major differences between the sorption characteristics of naphthalene on PRP-1 and on Partisil-10 ODS-3 as found in this investigation are summarized.

4.2 Hamilton PRP-1 as a Sorbent

4.2.1 Characterization of Experimental Elution Profiles On PRP-1

The characterization of elution profiles (ie. elution chromatographic peaks) was discussed in Section 2.3.7. The details of obtaining the data and analyzing it according to two methods were described in Section 3.5.1. The following discussion presents the results of using these two methods of describing elution profiles collected from PRP-1.

4.2.1.1 Numerical Integration

The first method was that of numerical integration using the digitally recorded data and a program written in ASYST. The program uses Simpson's rule [4.1] to numerically integrate a data set between chosen limits. The program performs well for peaks which are relatively noise-free (some smoothing capability is built in). For example. phloroglucinol is the unretained compound and elutes very quickly from the column. Its chromatogram. an example of which is shown in Figure 4.1. is fronting and elutes over a short period of time. The signal to noise ratio of phloroglucinol at the peak maximum is approximately 20 and there was no difficulty in collecting sufficient data to adequately define both the starting and the ending limits of the peak. Consequently. no difficulties were encountered in using the ASYST program to numerically integrate the phloroglucinol peaks. The first moments or centres of gravity for loroglucinol peaks obtained at four different linear velocities of the mobile phase are shown in Table 4.1. The first moment is used to calculate the linear velocity of the mobile phase using equation 3.11. Good precision is obtained using these values and no other method was used to characterize phloroglucinol peaks.

The numerical integration method proved less successful for characterizing the elution peaks of naphthalene. a compound which is retained on PRP-1. Naphthalene peaks were difficult to characterize for a variety of reasons Because the compound is highly retained and the resulting peaks are tailed. as shown in Figure 4.2. data had to be collected over a long period of time so that the signal was affected by baseline drift. Data sets were plagued by an uncertainty in the location of the baseline in the tailing portion of the peak because of problems with premature termination of data collection and because of the presence of noise, especially for low concentrations. For the profile shown in Figure 4.2. the signal to noise ratio is 10 at the peak maximum, which is only a factor of 2 below the S/N ratio of the phloroglucinol peak. Nevertheless, there were major difficulties in using the ASYST program, with less than half of the collected profiles leading to successful moment analysis. It was difficult by visual inspection to
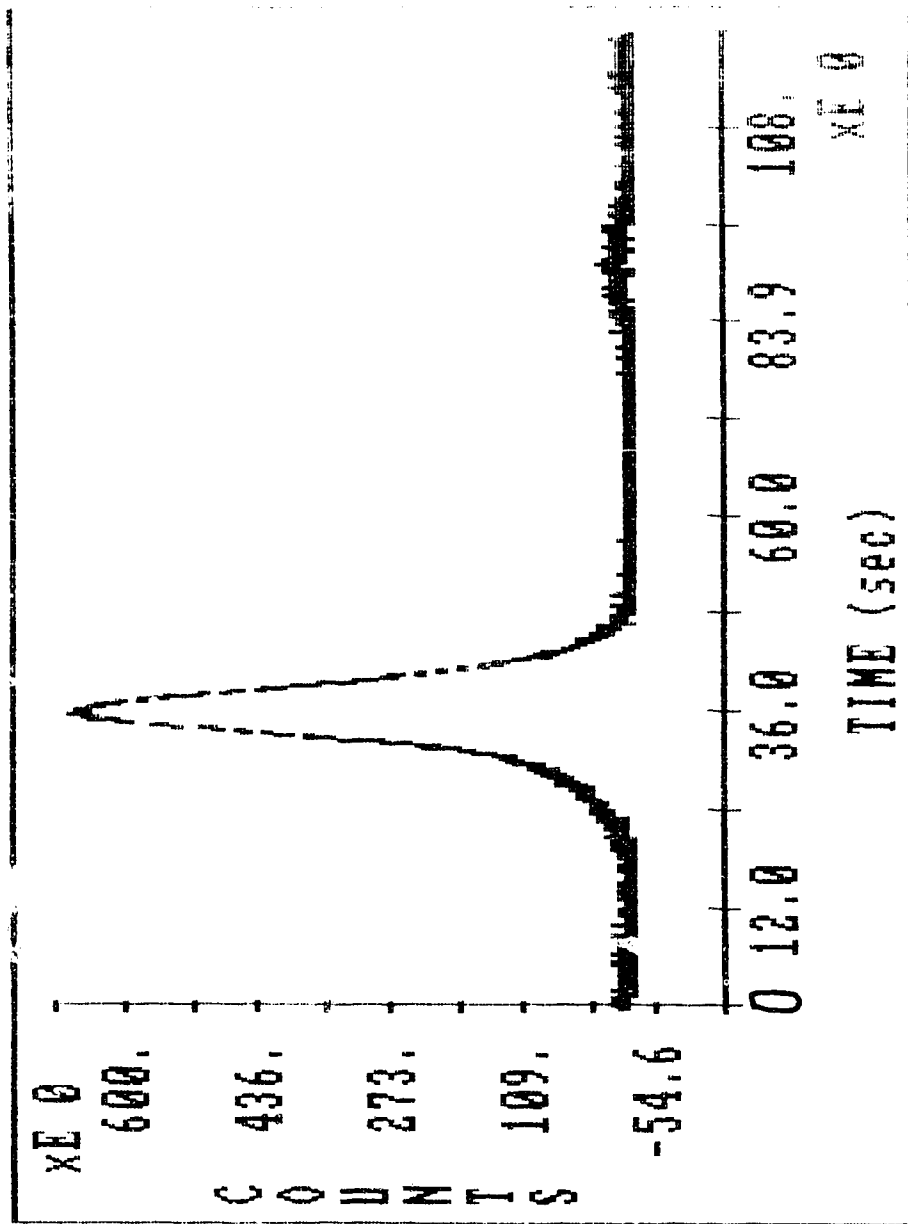
Figure 4.1   Chromatogram of $5.92 \pm 0.12 \times 10^{-6}$ M phloroglucinol in 85 % MeOH on PRP-1 with a mobile phase flow rate of 0.5 mL/min. The chromatogram in shown as the unsmoothed output from the data collection program written in ASYST. The zero mark on the time axis corresponds to a time of 2 minutes after injection. The u_0 in this case is 0.10 cm/s.

Table 4.1   First moments of phloroglucinol elution profiles on PRP-1 and calculation of linear velocity of the mobile phase, u_o. The sample concentration was $5.92 \pm 0.12 \times 10^{-5}$ M in 85% MeOH. Other conditions are described in Section 3.5.1. The confidence limits shown for the first moment values are calculated at the 95 % confidence level. The variable s is the standard deviation in the linear velocity, calculated by propagation of error.

Flow Rate (± 0.1 mL/min)	number of repetitions	$M_1(s)$	u_o (cm/s)	s (cm/s)
2.0	5	37.32 ± 0.92	0.40	0.03
1.5	4	49.08 ± 0.40	0.30	0.02
1.0	4	74.56 ± 0.86	0.20	0.01
0.5	5	148.2 ± 1.1	0.101	0.006
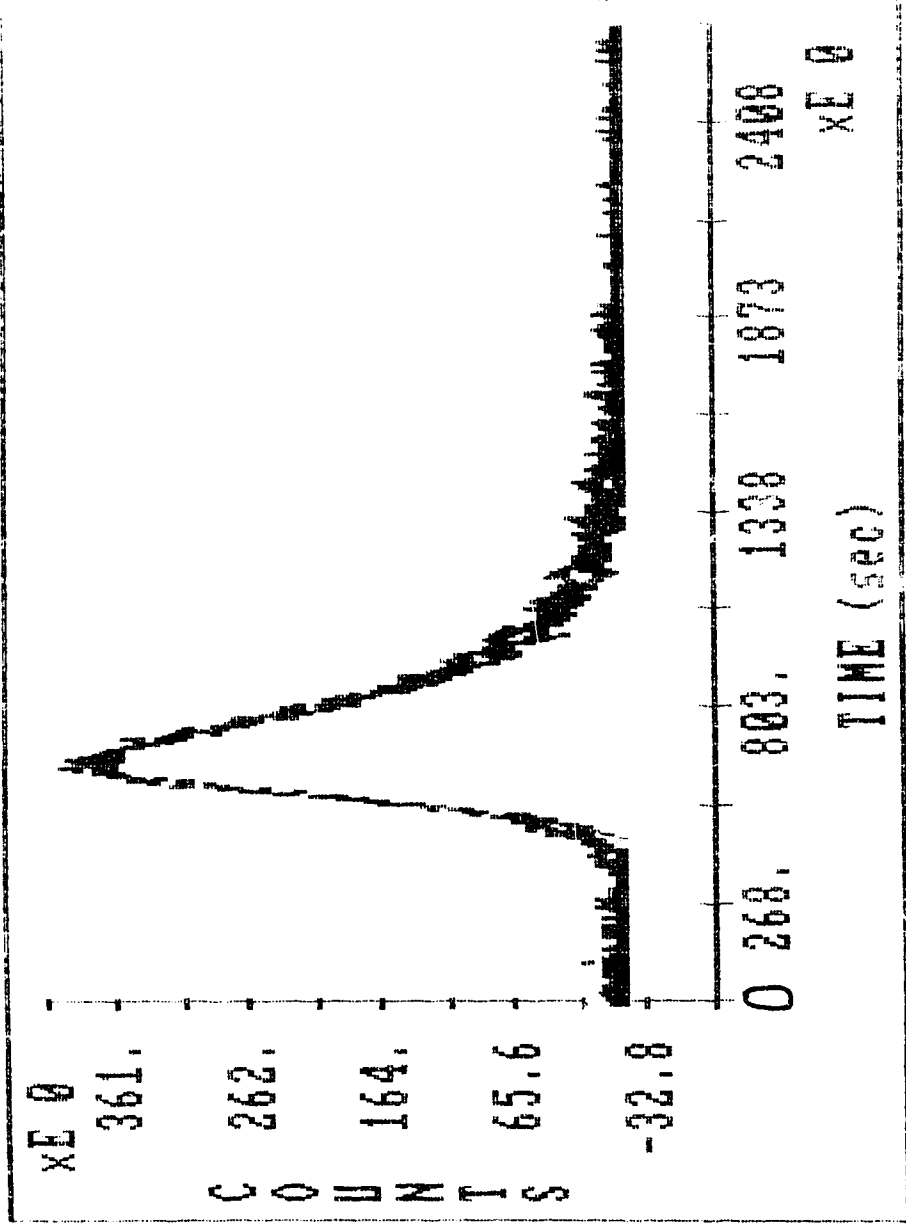
Figure 4.2   Chromatogram of $2.504 \pm 0.099 \times 10^{-6}$ M naphthalene in 85 % MeOH on PRP-1 with a mobile phase flow rate of 0.5 mL/min. The chromatogram in shown as the unsmoothed output from the data collection program written in ASYST. The zero mark on the time axis corresponds to the initiation of data collection. This zero is actually 60 minutes after injection. The u_0 in this case is 0.10 cm/s.

predict which data sets could be successfully analyzed. These problems were not unexpected. Numerical integration methods have been shown to be sensitive to noise [4.2 to 4.4], baseline drift [4.2], premature termination of data collection [4.2 to 4.6] and number of data points [4.5]. The higher moments are most sensitive to problems with data in the tailing portion of the peak [4.2]. A more reliable method of peak characterization was sought.

4.2.1.2   Non-linear Least Squares Curve Fitting

The second method described in Section 3.5.1 to characterize chromatograms involved first using a non-linear least squares program to fit the experimental elution profiles to an exponentially-modi..ed Gaussian (EMG) function (equation 2.30). An example of the result of using such an approach is shown in Figure 4.3. The EMG curve gives a good fit for the tailing portion of the peak. The very early data in the rising part of the peak are not very well fit by the EMG function. There are two possible reasons for this. First, the elution peaks may not have a truly Gaussian parent profile. In fact, the phloroglucinol peak in Figure 4.1 shows that fronting profiles may be expected. Alternatively, the reason for the poor fit in the rising part of the peak may lie in the use of the identity given in equation 2.31. Use of an error function in EMG curve fitting has been shown to lead to inaccuracies when $Z \leq -3$ [2.32]. To test this possibility, the Z values were calculated for the subsets of data used for the curve fit. The results of this calculation are shown in Table 4.2. The values of Z_i, early in the peak, are, indeed, less than the prescribed value of -3.

Regardless of its origin, the poor fit in the early portion of the curve is not much of a concern since the peaks are so asymmetrical that the variance is due mainly to the broad tailing portion and the EMG function seems to adequately describe the peaks in this region.

The EMG curve-fitting program was evaluated for sensitivity to various user
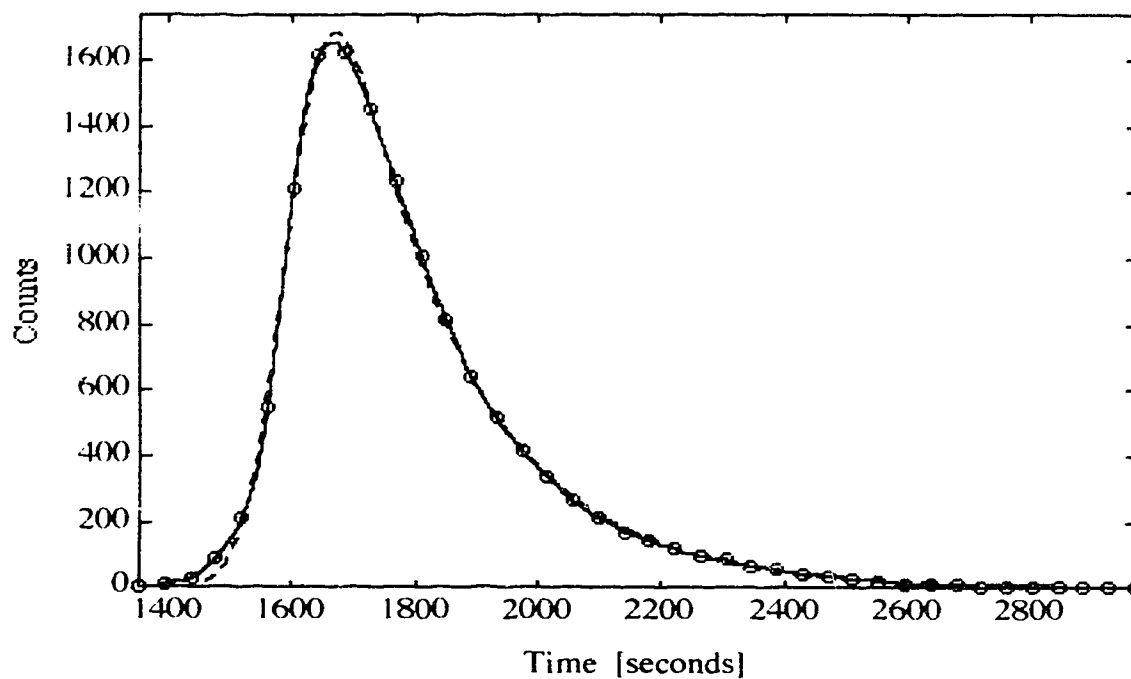
Figure 4.3　　Elution profile of 1.002 x 10⁻³ M Naphthalene in 85 % MeOH on PRP-
1 at u_o = 0.30 cm/s. The solid line shows the experimental data points.
The open circles illustrate the data points chosen by the EXPGAUSS
program to fit to an EMG function. The dashed line is the resulting
EMG function. The EMG constants for this function are shown in
Table 4.5 where the number of data points is 40.

Table 4.2   Calculated Z values at the beginning and end of the subset used for fitting experimental elution profiles of naphthalene in 85 % MeOH on PRP-1. t_i is the time of the first data point included in the subset and Z_i is the value of Z at this time as calculated from equation 2.30 using the EMG constant t_G, σ_G, and τ which are defined in Section 2.3.7. Z_f is the Z value calculated from equation 2.30 at time t_f, the time of the last data point included in the data subset. Results for two concentrations C, of naphthalene are shown. The standard deviation of the concentration is given in brackets following the concentration values. Other information regarding the chromatographic experiment is given in Section 3.5.1.

Run no.	C (s.)	t_i (±1.05 s)	t_f (±1.05 s)	t_G (s)	σ_G (s)	τ (s)	Z_i	Z_f
1	1.002 (.003)	964.20	2013.15	1157	42.01	143.8	-4.9	20
2	1.002 (.003)	987.83	2050.43	1154	41.92	141.5	-4.3	21
3	1.002 (.003)	988.52	2066.87	1176	43.06	141.2	-4.7	20
1	2.504 (.099)	1051.65	1921.05	1258	57.98	128.7	-4.0	11
2	2.504 (.099)	1077.97	1890.97	1248	52.16	144.5	-3.6	12
3	2.504 (.099)	1088.29	1912.54	1248	50.89	132.5	-3.5	13

input parameters. Two key parameters are of interest. First of all, the raw data collected by the ASYST program described in Section 3.5.1 must somehow be truncated into a data subset. The criteria for choosing points for this subset are examined below. Secondly, the user specifies the number of equally-spaced data points within the subset which the program will use to fit the EMG curve. The sensitivity of the goodness of fit to the number of these data points is also discussed.

The elution data were collected for each peak over a relatively long period of time so some of the data points at the beginning and end of the raw data set lie on the baseline. In transferring the data from the raw set into a subset to be used in the the curve-fitting program, a decision about the initial and final points of the subset had to be made. The fit was shown to be greatly affected if a very large number of data points in the tailing portion of the profile were included in the subset. For instance, Figure 4.4 shows the results of the analysis of the same raw data using two subsets which differ in the times chosen to limit the set. The peak shown is for the elution of naphthalene from PRP-1 at a linear velocity of 0.40 cm/s. Curve A is the EMG curve fit when the 40 data points are chosen from a subset which begins at 987.83 s and ends at 2050.43 s. The curve is well fit except for the beginning of the peak; the portion of the peak of greatest interest in this discussion, the tailing portion, is well-fit. The constants of the fit curve are shown in Table 4.3. Curve B in Figure 4.4 is the result of the EMG curve fit when the 40 data points are chosen by the routine from a subset which begins at 987.83 s and ending at 2363 s. The fit is very poor and the constants in Table 4.3 are radically different from results of the first analysis. The EMG constants were originally defined in Section 2.3.7. The fit is therefore sensitive to employing data points that lie too far out along the baseline on the tailing edge of the peak.

Some criteria must therefore be established for choosing points to include in the subset. If including too many points in the tailing portion results in a poor fit, is
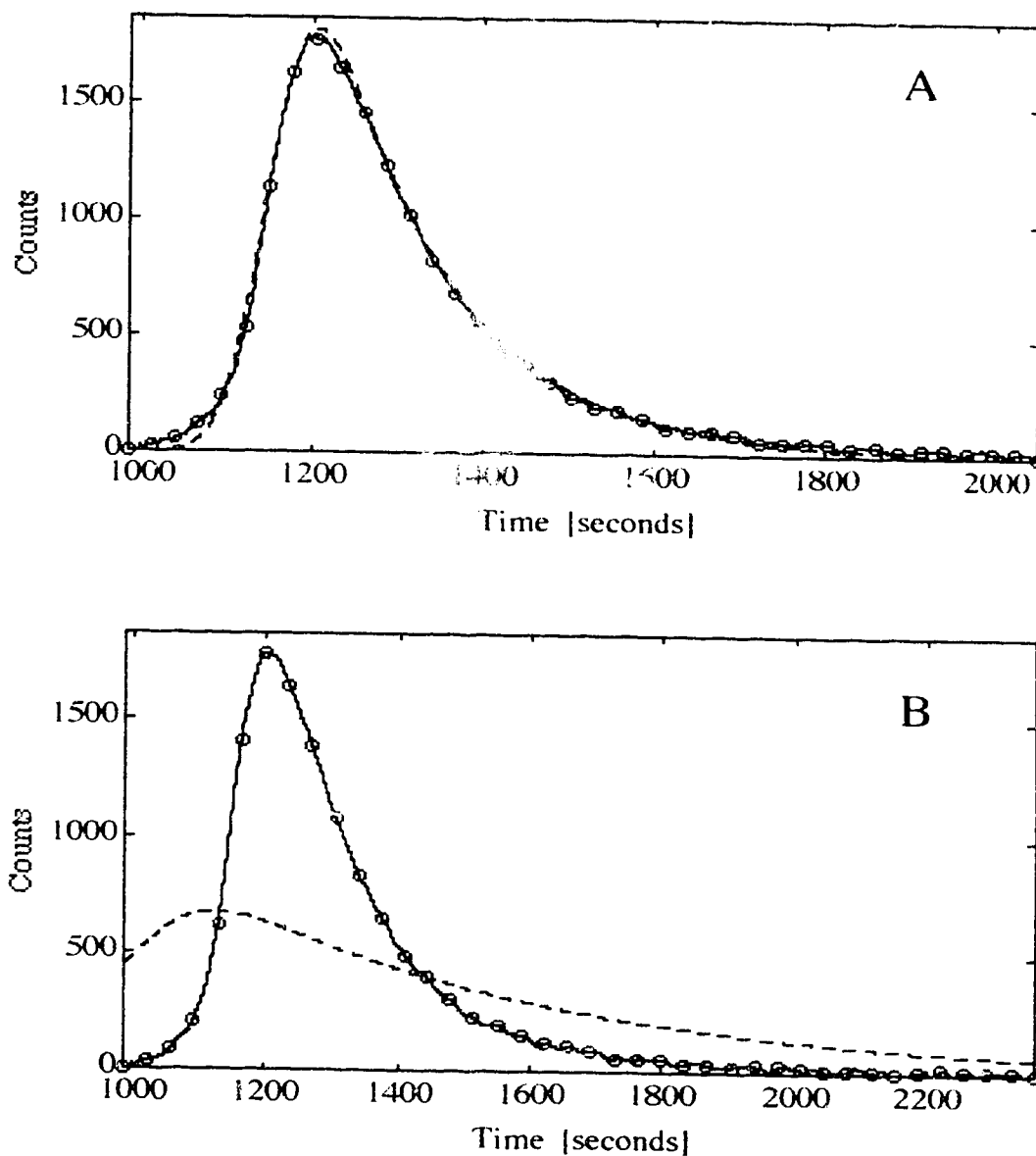
Figure 4.4   EMG fit of an elution profile of 1.002 x 10-3 M Naphthalene on PRP-1
at 0.40 cm/s. The solid line represents the experimental profile while
the dashed line is the EMG function fit to the chosen data points (o).
Figure A and B are the same peak except that fewer data points in the
tailing section of the profile are included in the data set in Curve A.

Table 4.3   Effect of incorporating a large number of data points in the subset used
for EMG curve-fitting from the tailing portion of the elution profile.
The fit profiles are shown in Figures 4.4.a and 4.4.b. The subsets are
taken from the same elution profile of 1.002×10^{-5} M naphthalene in 85
% MeOH on PRP-1 with a linear velocity of 0.40 cm/s. The variables
$ht(t_i)$ and $ht(t_f)$ are the signal values at times t_i and t_f respectively. Other
variables are defined in the Section 2.3.8.

Figure	4.4.a	4.4.b
t_i ($\pm$ 1.050 s)	987.83	987.83
$ht(t_i)$	0	0
t_f ($\pm$ 1.050 s)	2050.43	2363.00
$ht(t_f)$	5.4874	0.024
t_G (s)	1154	1029
σ_G (s)	41.92	5.24×10^{-15}
τ (s)	141.5	513.3
M_1 (s)	1296	1542
M_2 (x 10^5 s)	2.178	2.634

possible that using too few data points in the subset will also result in a poor fit. The effect of choosing different limiting times for the subset was evaluated for the elution curve shown in Figure 4.3, obtained at a linear velocity of 0.30 cm/s. The data forming the profile in Figure 4.3 were chosen from the raw data set as being bounded by the last occurrence of zero signal before the peak maximum and the first occurrence of zero signal after the peak maximum. This corresponded to all data between times 1353.97 s and 2968.34 s inclusive. It should also be noted that the original raw data were gathered between times 1130.3 s and 3492.8 s inclusive. The fit was also conducted on subsets with limits of 0.1 %, 1%, and 5% of the peak maximum signal. The results of these analyses are shown in Table 4.4. The parameter τ, which is the characteristic time of the exponential function that modifies the parent Gaussian peak, is most sensitive to the limits but not by much. The signal chosen for this exercise was a data set with little noise and with no evidence of baseline drift. In general, subsets were chosen with limits as close to the zero signal values as possible. The presence of noise and baseline drift complicated this choice and therefore the first data point in the subset was chosen usually taken to be the first point before the peak maximum after which the signal only increased with increasing time. The last data point included in the set was a little more difficult, but not impossible to choose. If zero signal was found in the data in the tailing portion, the first occurrence of zero signal after peak maximum was taken as initial estimate of the last data point. However, as poor fits often resulted in these cases, the data set was truncated by steps until a good fit was produced. In this case, a "good fit" means that the EMG function visually overlapped with the observed peak. The above exercise demonstrates that the choice of data points to limit the subset is not crucial for a good fit except in the case of including too many data points from the tailing portion of the profile in the subset. Comparison of values in the horizontal rows in Table 4.4 for the parameters t_G, σ_G, τ, M_1 and M_2 reveals that, within reason, premature truncation of the data subset at the tailing end of the peak produces minimal

Table 4.4   Effect of decreasing size of subset with times defining the subset chosen according to as a % of peak maximum. The elution profile is that of 1.002×10^{-5} M naphthalene in 85 % MeOH on PRP-1 at a linear velocity of 0.30 cm/s. The $ht(t_i)$ and $ht(t_f)$ are the signal values at times t_i and t_f respectively. These times are the first and last times included in the data subset. The raw data set originally consists of data collect from 1130.3 s to 3492.8 s after injection.

% peak max.	0	0.1	1	5
t_i (± 1.575)	1353.97	1388.74	1427.995	1475.245
$ht(t_i)$	0	1.781	17.4057	83.8444
t_f (± 1.575)	2968.34	2721.07	2568.295	2292.67
$ht(t_f)$	0	1.9304	17.5843	83.0824
t_G (s)	1597	1597	1597	1597
σ_G (s)	55.64	55.86	55.45	55.64
τ (s)	195.8	196.2	196.7	196.4
M_1 (s)	1793	1793	1794	1793
M_2 (x 10^4 s)	4.14	4.16	4.18	4.17

scatter compared with other problems which introduce scatter.

Once the truncated data subset has been chosen, the user specifies the number of equally-spaced data points within the subset to which to the program will perform the curve fitting procedure. The sensitivity of the resulting fit to the number of points chosen was examined for the data shown in Figure 4.3. The number of data points chosen from the subset was varied between 10 and 200. The constants generated by the curve-fitting routine are shown in Table 4.5 with all other parameters remaining the same. The table shows that t_G, the centre of gravity of the parent Gaussian peak, reaches a constant value when 30 or more data points are chosen. Both σ_G and τ show some variability but reach relatively constant values when 30 or more data points are used. For all subsequent curve fitting, 40 data points were chosen. The curve fit in Figure 4.3 employed 40 data points in the calculation which are shown as open circles superimposed on the data set.

The precision of the curve fitting procedure was evaluated using three replicate injections of sample at each of four linear velocities. First, however, the effect of sample concentration was studied at one of the linear velocities (0.40 cm/s or 2.0 ml/min). The results are shown in Table 4.6. For the higher concentration, the values of the constants calculated by the curve-fitting routine show good precision, with RSD values of about 1% for each parameter. For the lower concentration the calculated values show poorer precision, with the exception of the parameters t_G and M_1, which have about the same uncertainty as the same parameters for the higher concentration. For the lower concentration, the RSD values of σ_G and τ are relatively high. This could be due to the lower signal to noise ratios obtained for these profiles which could complicate the curve fitting procedure. These large uncertainties are reflected in the large RSD value for M_2 which depends on the square of these two EMG constants.

Table 4.7 shows the results of the evaluation of elution profiles of naphthalene in 85 % MeOH injected at the lower concentration, for all four linear velocities,

Table 4.5   Effect of number of data points used by the EXPGAUSS routine from the data subset to be used in the curve-fitting procedure. Data shown in the table is from the elution profile of 1.002×10^{-4} M naphthalene in 85 % MeOH on PRP-1 at a linear velocity of 0.30 cm/s. The data subset is bounded by data points acquired at times 1353.97 s and 2968.34 s after injection. The signal at each of these times is 0. Chromatographic conditions are discussed in Section 3.5.1. Unfortunately, as the program is written, no error estimates for the EMG parameters are available.

# data points from subset	t_G (s)	σ_G (s)	τ (s)	M_1 (s)	M_2 ($\times 10^4$ s^2)
10	1606	62.79	188.5	1669	3.947
20	1594	56.22	199.1	1650	4.280
30	1597	55.96	195.8	1653	1.147
40	1597	55.64	195.8	1653	4.143
50	1597	55.79	195.9	1653	4.149
60	1597	55.74	196.5	1653	4.172
70	1597	55.73	196.4	1653	4.168
80	1597	55.78	196.2	1653	4.160
160	1597	55.72	196.2	1653	4.160

Table 4.6   EMG characteristics of elution profiles of naphthalene in 85 % MeOH
on PRP-1 at a mobile phase velocity of 0.40 cm/s for two
concentrations.

Run no.	Conc. (x10^{-3}M)	t$_G$ (s)	σ$_G$ (s)	τ (s)	M$_1$ (s)	M$_2$ (x 10^4 s^2)
1	1.002	1176	43.1	141	1315	2.18
2	"	1157	42.0	144	1299	2.24
3	"	1154	42.0	142	1293	2.18
avg	1.002	1162	42.3	142	1302	2.20
RSD (%)	-	1.0	1.5	1.0	0.887	1.7
1	0.2504	1258	58.0	129	1384	1.99
2	"	1248	52.2	144	1390	2.42
3	"	1248	50.5	132	1378	2.01
avg	0.2504	1254	53.5	135	1384	2.14
RSD (%)	-	0.46	7.3	6.1	0.43	11.4

Table 4.7   EMG characteristics of elution profiles of 2.504×10^{-4} M naphthalene in 85 % MeOH on PRP-1 at four mobile phase linear velocities, u_0. The data for $u_0 = 0.40$ cm/s was presented in the Table 4.6.

u_0 (cm/s)	0.40	0.30	0.20	0.10
t_G (s)	1251	1704	2564	5197
RSD t_G (%)	0.46	0.64	1.4	1.2
σ_G (s)	43.5	69.1	93.6	169
RSD σ_G (%)	7.3	7.4	1.4	5.9
τ (s)	135	190	273	530.1
RSD τ (%)	6.1	7.7	7.6	8.7
M_1 (s)	1384	1892	2833	5697
RSD M_1 (%)	0.43	1.3	1.7	0.24
M_2 ($\times 10^4$ s^2)	2.14	4.09	8.35	3.11
RSD M_2 (%)	11	13	13	15

including the one discussed above and described in detail in Table 4.6. In most cases, the RSD values for τ are greater than those for the other EMG constants in the fit equation. This is not unexpected: the τ parameter represents the exponential modification of the Gaussian peak. It is this function that describes the tailing portion of the peak and as such is most sensitive to errors such as baseline drift, noise and uncertainty in baseline location. The relatively large RSD figures for the variance (M_2) reflects the higher uncertainty in the τ parameter.

From the detailed evaluation revealed in Table 4.1 through 4.7, it can be concluded that the Exponentially Modified Gaussian function gives an acceptable fit to experimental data, with RSD values of all fit parameters better than 15% even at the lower concentrations. The EMG function (equation 2.30) obtained by non-linear least squares curve fit is an analytical function which gives a much more accurate and precise representation of the experimentally observed elution peak than does the alternative "numerical integration" approach. For this reason, all future discussions of peak shape in this thesis will employ the appropriate EMG equation as a representation of the experimentally observed peak.

4.2.1.3 Efficiency of PRP-1 HPLC Columns

A measure of efficiency of a chromatographic column is the height equivalent of a theoretical plate, H, which is defined by equation 2.1. The plate height is related to the central statistical moments of a chromatographic peak by equation 4.1 [4.7].

$$H = L \frac{M_2}{M_1^2}$$

eqn. 4.1

M_1 and M_2 are the first and second statistical moments of the peak. L is the length of the chromatographic column. For the profiles fit to an EMG function, the EMG constants are used to calculate the moments.

$$H = L \frac{(\sigma_G^2 + \tau^2)}{(t_i + \tau)^2}$$

<div align="right">eqn. 4.2</div>

For the chromatograms of naphthalene at the lower concentration which were previously fit to EMG functions, the plate height was calculated and the results plotted against mobile phase linear velocity in Figure 4.5. There is, unfortunately, a large amount of scatter and the shape of the curve is indeterminate. However, unambiguously, it should be noted that the plate height associated with this particular column is exceptionally large. Hamilton includes a brochure with the column in question citing the plate height as being 0.003 cm. This is measured with monoaromatic compounds such as phenol, benzene and cumene in an unspecified solvent and at an unspecified mobile phase linear velocity and so the efficiencies may not be directly comparable. It is obvious, however, that the measured efficiency for the polyaromatic compound on the column is much less than expected for a microparticulate packing.

A plot of the plate height against linear velocity is often termed a "Van Deemter" plot. Because of the large amount of scatter in the data in Figure 4.5, any conclusions on the shape of the graph are questionable. The dependence of the plate height on the linear velocity is generally expressed in terms of an empirical equation originally proposed by Van Deemter [4.8] and modified by several researchers. Thorough discussions of the form of this relationship may be found elsewhere [for example, 4.9]. The plate heights are approximately two orders of magnitude higher than more typical results for HPLC columns [4.10].

The calculated RSD values for both the number of theoretical plates and the plate height are in the range from 10 to 16 %. This is similar to the RSD range observed for M_2 values calculated from the EMG characteristics of the elution profiles. The major source of error can therefore be assumed to be problems in the EMG curve fitting process.
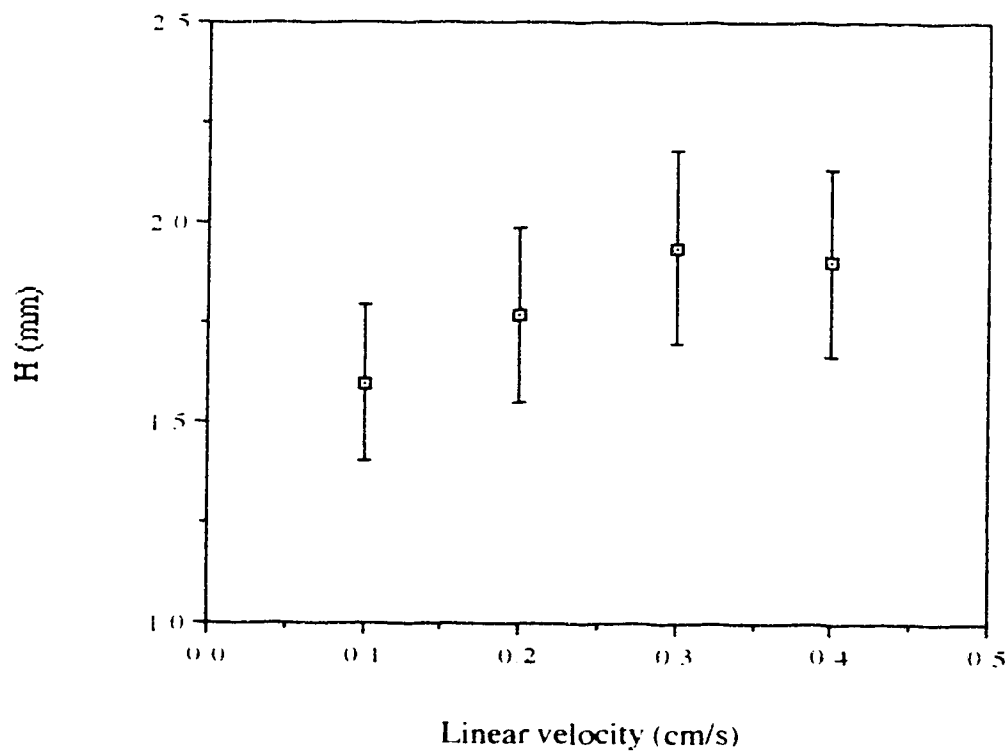
Figure 4.5   Plot of height equivalent of a theoretical plate against mobile phase linear
velocity for naphthalene on PRP-1 in 85 % MeOH. The plate height.
H, is calculated from equation 4.2. The data shown represent the
averages of three injections at each linear velocity. The error bars are
12.3 % of the average plate height at each linear velocity.

4.2.2   Equilibrium Sorption of Naphthalene on PRP-1

4.2.2.1   Measurement of the Sorption Isotherm of Naphthalene on PRP-1

The isotherm for the sorption of naphthalene on PRP-1 from 85 % MeOH was measured by the so-called column equilibration method described in Section 3.4.4. Figure 4.6 illustrates the sorption isotherm for naphthalene on PRP-1 in the concentration range from 0 to approximately 1×10^{-4} M. The isotherm is not linear over the entire concentration range and is concave at the higher concentrations. Figure 4.7 shows only the linear portion of the isotherm, in the concentration range 0 to approximately 2×10^{-5} M. The linear regression constants for this portion of the curve are shown in the caption to Figure 4.7 including the confidence limits. Note that for the shallow bed kinetics experiment, naphthalene solutions having concentrations about 5×10^{-6} M were used. Since this concentration is well within the linear portion of the isotherm, the concentration is expected to have little effect on the measured sorption kinetics.

The slope of the linear region of the isotherm, D, in L/g, is related to the capacity factor of a compound on an HPLC column, k', by the phase ratio of the column, which is the ratio of the weight of the stationary phase in the column, W, in grams, to the hold up volume of the column, V_m, in litres. The latter includes the interparticle and pore volumes.

$$k' = D \frac{W}{V_m}$$

eqn. 4.3

The value of D obtained from the column equilibration experiment was used to predict the capacity factor for the HPLC column used in subsequent elution experiments. A nominal hold-up volume of 1.30 mL is included in the manufacturer's information. The actual value of V_m for this column was measured by injecting the unretained compound, phloroglucinol (Table 4.1). The value of V_m is the product of
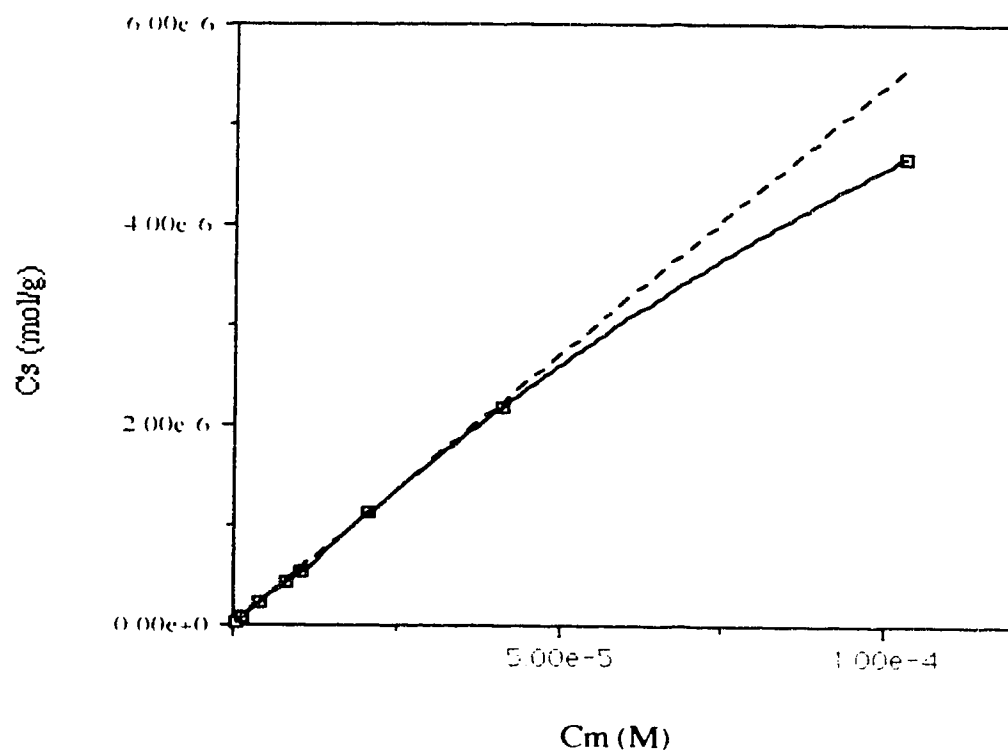
Figure 4.6   Sorption isotherm for naphthalene on PRP-1 in 85 % MeOH.
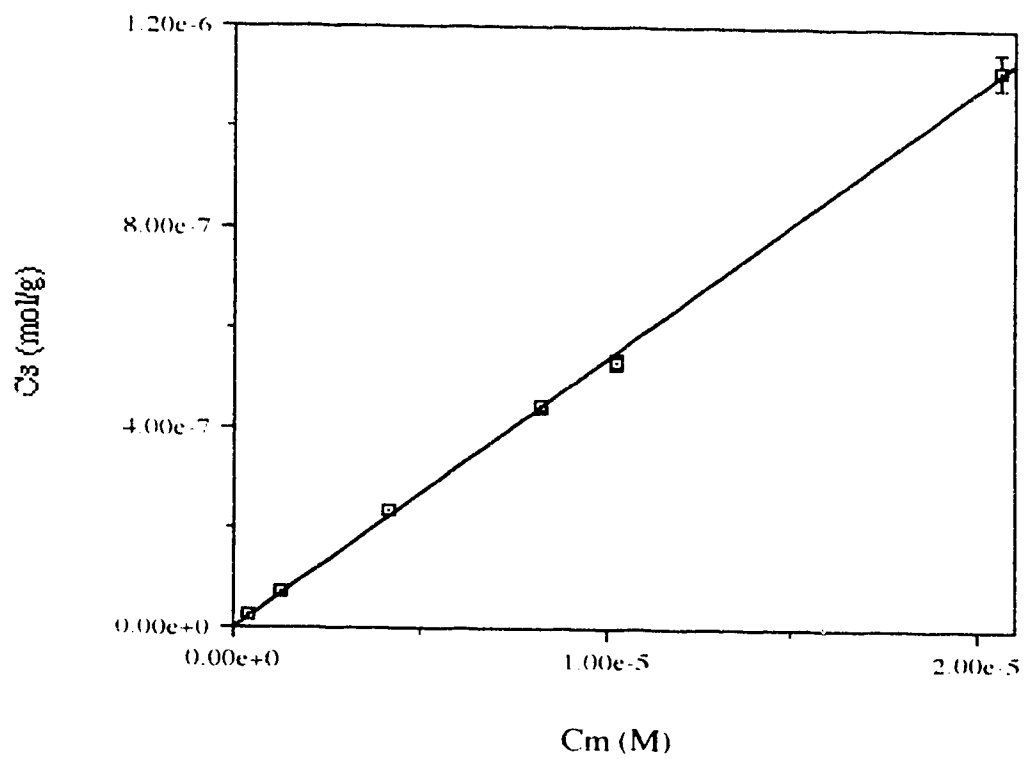
Figure 4.7   Linear region of the sorption isotherm from Figure 4.6 for naphthalene
on PRP-1 in 85 % MeOH. The linear region has an intercept of 2.223 ±
8.543 x 10^{-9} mol/g and a slope of 5.36 ± 0.20 x 10^{-2} L/g.

the flow rate (mL/min) times M_1 in minutes. The average V_m from the flow rates in Table 4.1 is 1.24 mL with an error of 0.06 mL . The weight of stationary phase is determined from the manufacturer's information concerning the pore volume of the column and the specific pore volume. The amount of packing, W, in the column is 0.835 g with an error of ± 0.016 g. The error in the weight is calculated by propagation of errors, assuming that both the pore volume and the specific pore volume have errors of ± 1 in the last quoted decimal place. This is probably an underestimation of the errors in these quantities.

The slope of the isotherm, D, has a value of $5.36 \pm 0.20 \times 10^{-2}$ L/g. Therefore, the capacity factor calculated from equation 4.3 is 36.0 ± 4.3 at the 95 % confidence level. In the following section, this value is compared to the k' measured from a second method of determination, using the EMG characteristics of elution profiles.

4.2.2.2 Calculation of k' from Elution Profiles of Naphthalene on PRP-1

The capacity factor, k', can also be determined from the experimentally measured chromatographic elution profiles. As previously indicated, the elution profile will be represented by its EMG function. The first moment, M_1, of the elution profile, is calculated using equation 2.27 and is the centre of gravity of the peak, once it is corrected for extra-column effects as described in Section 3.5.2. The capacity factor can be calculated from equation 4.4.

$$k' = \frac{M_1 - t_m}{t_m}$$

<div align="right">eqn. 4.4</div>

The quantity t_m, is the time that the unretained compound, phloroglucinol, takes to elute from the column, also corrected for extra-column effects. The extra-column effects were measured as described in Section 3.5.2.

Results for the elution profiles discussed in Section 4.2.1 are shown in Table 4.8. For peaks injected at the lower concentration, there is good agreement in k'

Table 4.8   Values of k' calculated from the EMG characteristics of elution
profiles of naphthalene in 85 % MeOH from PRP-1 at two different
concentrations. Data is given for four mobile phase linear velocities, u_0,
and is based on three injections at each linear velocity. The quantity s is
the standard deviation for k' at that linear velocity.

Conc (x 10^{-3} M)	u_0 (cm/s)	k'	s
0.2504	0.10	37.3	0.3
"	0.20	37.0	0.6
"	0.30	37.5	0.5
"	0.40	35.8	0.4
1.002	0.10	36.1	0.8
"	0.20	34.1	0.3
"	0.30	35.7	0.4
"	0.40	33.9	0.3

among all flow rates except for $u_x = 0.40$ cm/s. A t-test of the k' obtained at this linear velocity shows that it is significantly different than the k' obtained at other velocities. When the mean k' at 0.40 cm/s is t-tested against the mean values measured at 0.10, 0.20 and 0.30 cm/s, the t statistic is 7.22, 2.93, and 4.78 respectively. All of these values are larger than the tabulated value of t at the 95 % level, which is 2.78. Considering the data from the three lowest linear velocities for the 0.2504×10^{-3} M injected naphthalene, the capacity factor of naphthalene in 85 % MeOH on PRP-1 is calculated to be 37.3 $\pm$ 0.4 at the 95 % confidence level. If data at all four linear velocities are considered, the measured k' is 37.0 $\pm$ 0.6 at the 95 % confidence level so the inclusion of the data at the highest linear velocity makes little difference to the k' value measured by this method.

Table 4.8 also shows the k' values calculated from the EMG characteristics of the elution profiles obtained by injection of 1.002×10^{-3} M naphthalene at four different linear velocities. There is greater scatter among these k' values. However, if all data are used, the k' for naphthalene at this concentration is calculated to be 34.9 $\pm$ 0.8 at the 95 % confidence level. The apparent difference in the k' value measured at the two concentrations may be associated with the non-linearity of the sorption isotherm. Because of the large degree of bandbroadening observed on this particular packing, relatively high concentrations, in the range of 10^{-4} to 10^{-3} M, must be injected to be detected at the other end of the column. When a sample is injected onto a column, the sample is immediately diluted by the mobile phase and its dilution becomes greater as it progresses down the column. At the top of the column, therefore, the sample is present in the mobile phase with a concentration outside the linear region of the isotherm. Because the sorption isotherm is concave at higher concentrations, the distribution coefficient and therefore the capacity factor are expected to be smaller.

The k' values evaluated by the two different experimental methods agree within experimental error. The k' of 37.0 $\pm$ 0.6 measured from the elution

chromatograms at the lower concentration, at which more of the sample migration would have occurred at concentrations in the linear par of the isotherm, is not significantly different than the value of 36.0 ± 4.3 calculated from the sorption isotherm.

4.2.3   Sorption Rate of Naphthalene on PRP-1

Figure 4.8 shows results of the shallow bed experiment for the measurement of the rate of sorption of naphthalene on PRP-1 from a 5.225 x 10-6 M solution in 85 % MeOH on PRP-1. The linear velocity of the sample solution through the shallow bed was measured to be about 15 cm/s, calculated according to equation 3.1. The shallow bed used in this experiment is described in Table 3.2. The experimental data points are overlaid by the solid curve that is the result of a non-linear least squares fit in the form of a tri-exponential, previously described in equation 2.25.

$$n(t) = n_o - n_1 e^{-k_1 t} - n_2 e^{-k_2 t} - n_3 e^{-k_3 t}$$

eqn. 2.25

The constants generated by this curve fit are shown in Table 4.9 along with the standard deviation computed by the least squares program. Notice that the term showing the smallest rate constant is associated with the largest RSD.

Figure 4.9 illustrates the relative contributions of each of the three terms of the exponential to the overall sorption rate curve. The term with the largest rate constant, k_1, defines the steeply rising portion of the curve. This curve reaches 1/e of its limiting value in less than 0.4 s. The second term of the exponential contributes to the less steeply rising portion of the overall curve. This curve reaches 1/e of its limiting value in less than 2 s. The remainder of the sorption curve is a slowly rising portion defined by the term containing the smallest rate constant, k_3. This curve reaches 1/e of its limiting values in approximately 17 s.

The sorption rate curve was characterized by calculating the first three statistical
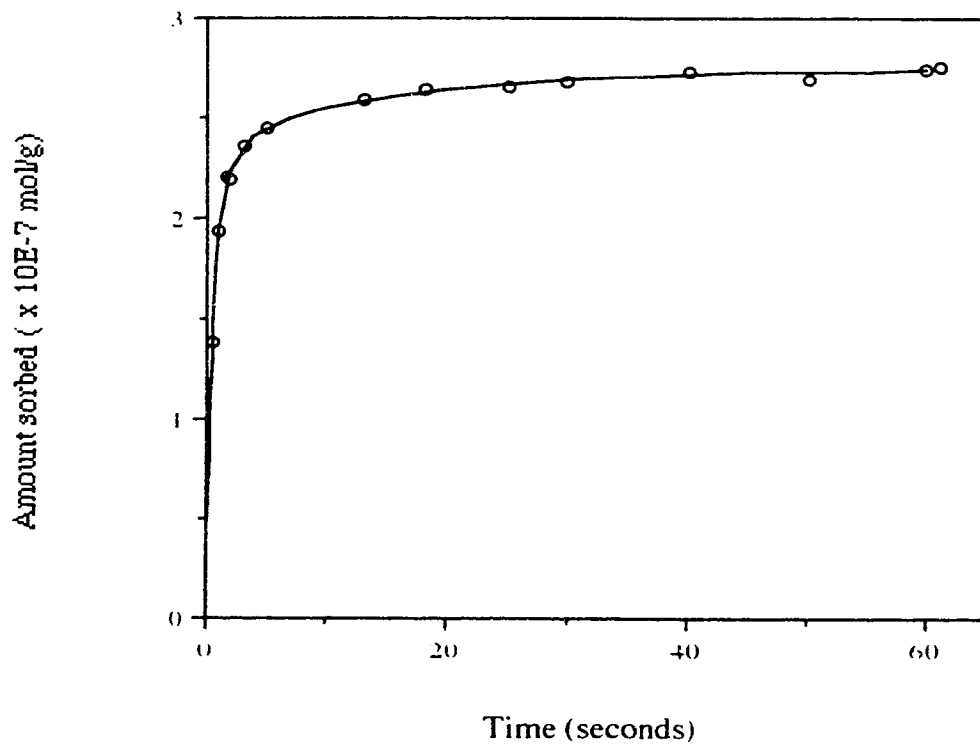
Figure 4.8   Sorption rate curve for Naphthalene on PRP-1 in 85 % MeOH. The experimental data point (o) are overlaid by a solid line representing the tri-exponential function that fits them. The tri-exponential constants for this sorption rate curve are shown in Table 4.9.

Table 4.9   Tri-exponential constants describing the Replicate 1 sorption rate curve
              of 4.716×10^{-6} M naphthalene in 85 % MeOH on PRP-1. The
              constants shown are for the curve which fits the experimental data in
              Figure 4.8. The standard deviation for the constants is calculated by the
              curve fitting routine. The relative standard deviation (RSD) is expressed
              in terms of percent and is calculated by dividing the standard deviation
              by the value of the constant of interest.

constant	value	standard deviation	relative standard deviation (%)
n_0 (x 10^{-7} mol/g)	2.75	0.017	0.62
n_1 (x 10^{-7} mol/g)	1.70	0.26	15.6
n_2 (x 10^{-8} mol/g)	0.697	0.217	31.1
n_3 (x 10^{-8} mol/g)*	0.353	0.49	139
k_1 (s^{-1})	2.79	0.38	13.6
k_2 (s^{-1})	0.642	0.270	41.9
k_3 (s^{-1})	0.0572	0.0166	28.0

* n_3 is determined by difference where $n_3 = n_0 - n_1 - n_2$.
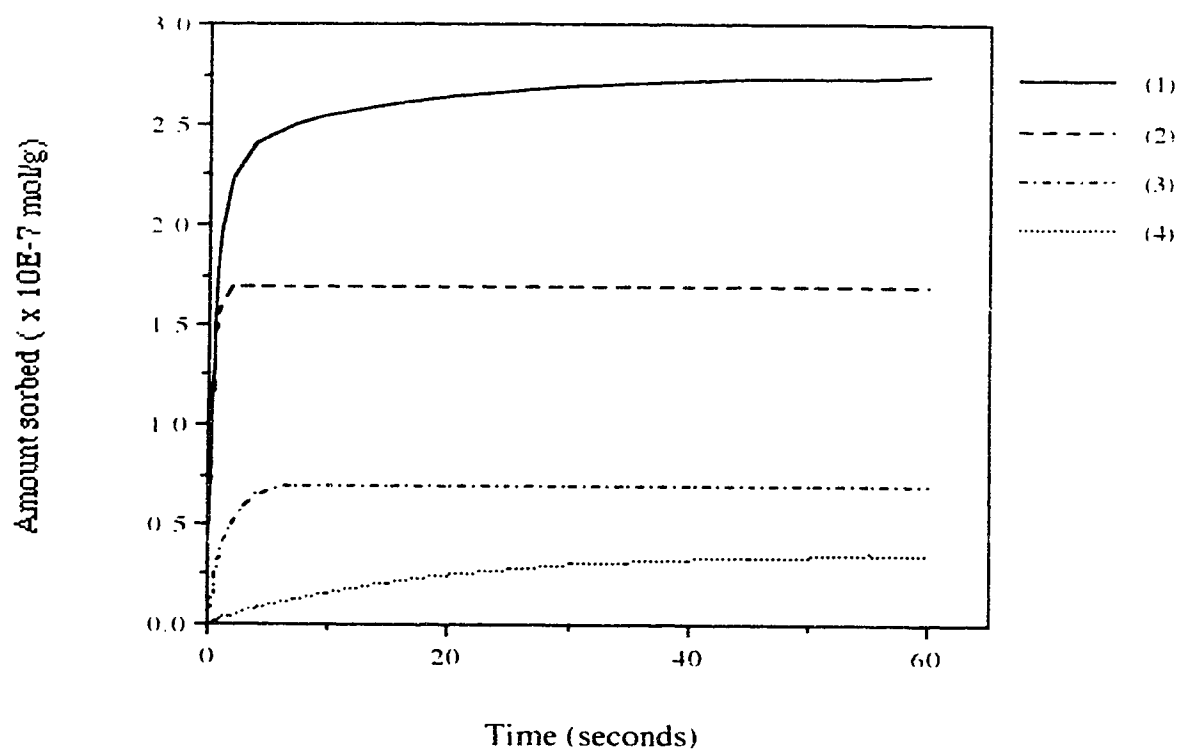
Figure 4.9   Contributions of the three exponential terms to the overall sorption rate curve of naphthalene on PRP-1 in 85 % MeOH. The curves are labelled as follows: (1) the overall tri-exponential curve; (2) the contribution to the curve from the first term in the tri-exponential; (3) the contribution to the curve from the second term in the tri-exponential; (4) the contribution to the curve from the third term in the tri-exponential.

moments. The moments are used to compare results of replicate experiments. Because the sorption rate curve is fit to a tri-exponential equation in this case, the moments can be solved analytically as shown in equations 4.5 to 4.7.

$$M_0 = \frac{n_1}{k_1} + \frac{n_2}{k_2} + \frac{n_3}{k_3}$$

eqn. 4.5

$$M_1 = \frac{n_1/k_1^2 + n_2/k_2^2 + n_3/k_3^2}{M_0}$$

eqn. 4.6

$$M_2 = \frac{2n_1/k_1^3 + 2n_2/k_2^3 + 2n_3/k_3^3}{M_0} - M_1^2$$

eqn. 4.7

The rate measurement experiment was repeated four times under identical conditions and the results were fit to the tri-exponential equations. The analytical moment analysis of these equations yielded results shown in Table 4.10. The moments of the curve obtained in Replicate 4 were discarded as they fail the Q test. The average of the moments for the remaining repetitions are shown in the last row of the table along with the RSD obtained for each moment. The RSD values for the zeroth and first moments are relatively low, having values less than 5 %. The RSD value for the second moment is largest . The reason for this is discussed below.

This method of characterizing the sorption rate curves was found to be of limited value for reasons shown in Table 4.11. If the sorption rate curve shown in Figure 4.8 is broken down into the component curves, as in Figure 4.9, the statistical moments of the overall curve is related to the statistical moments of the constituent curves. Each of the three terms in the tri-exponential contribute to the overall statistical moments. The contribution from the ith term of the tri-exponential to the moments can be described in terms of the moments associated with the individual constituent curves. The moments for the ith constituent curve determined by the ith exponential term are calculated from equations 4.8 to 4.10.

$$M_{0,i} = \frac{n_i}{k_i}$$

eqn 4.8

Table 4.10   Results of statistical moment analysis of the sorption rate curves from four replicates of the experiment to measure the sorption rate of naphthalene in 85 % MeOH on PRP-1. The average of the moments and the relative standard deviation (RSD) is shown for Replicates 1, 2, and 3. The results of the statistical moment analysis for Replicate 4 are rejected on the basis of the Q test. The experimental conditions for the measurements are described in the text.

replicate number	M_0 (x 10^{-7} s x mol/g)	M_1 (s)	M_2 (s^2)
1	7.92	14.0	285
2	7.94	14.5	318
3	7.79	13.2	248
4*	20.6*	42.6*	2250*
avg.	7.88	13.9	35.3
RSD (%)	1.0	4.5	12.5

*rejected on basis of Q-test

Table 4.11   The contributions of each ith term of the multi-exponential to the statistical moments of the overall sorption curve. The analysis is shown for the curve fit shown in Figure 4.8 and previously termed Replicate 1; these constants are shown in Table 4.9 along with the standard deviation associated with each constant. The variable i is the number of the exponential term in the multi-exponential equation. The contributions are calculated according to equations 4.8 to 4.10. The last row shows the summation of the terms $M_{0,i}$, $M_{1,i}$, and $M_{2,i}$. The sums are equal to the statistical moments for the overall sorption rate curve as shown in Table 4.10 for experiment Replicate 1.

i	$M_{0,i}$ (x 10^{-7} mol/g)	$M_{1,i}$ (s)	$M_{2,i}$ (s^2)
1	0.61	0.028	.019
2	1.09	0.213	0.70
3	6.22	13.7	285
Σ	7.92	14.0	286

$$M_{1,i} = \frac{n_i/k_i^2}{M_0}$$

<div align="right">eqn 4.9</div>

$$M_{2,i} = \frac{2n_i/k_i^3}{M_0} - \left(\frac{n_i/k_i^2}{M_0}\right)^2$$

<div align="right">eqn 4.10</div>

The moments for the overall rate curve are given by the sum of the individual moments. For instance,

$$M_0 = M_{0,1} + M_{0,2} + M_{0,3}$$

<div align="right">eqn. 4.11</div>

Here, M_0 is the zeroth moment of the overall sorption rate curve and $M_{0,1}$, $M_{0,2}$, and $M_{0,3}$, are the zeroth moments of the curves determined by the first, second and third exponential terms in the equation. These are determined by equation 4.8. By inspection, the sum of the individual first and second moments equal the first and second moments of the overall sorption rate curve, defined by equation 4.6 and 4.7.

Table 4.11 shows the individual contributions of each term ($i = 1$ to 3) in the tri-exponential equation that describes the sorption rate curve in Replicate 1 (constants are shown in Table 4.9). The results in Table 4.11 show that the statistical moments of the sorption rate curve are determined mainly by the smallest rate constant, that is, by the very slowly rising portion of the curve at relatively long times. Statistical moment analysis gives little information about the more steeply rising portions of the curve and is therefore of limited value. The results from Table 4.11 also show why the RSD values increase with the number of moment under consideration. A large standard error is attributed to the smallest rate constant and the second moment is almost entirely due to the cube of that rate constant. Any error associated with the smallest rate constant will therefore result in large uncertainties in the second moment. Since the smallest rate constant has the greatest uncertainty in the experiment (Table 4.9), characterization of the sorption rate curve by statistical moments is virtually useless.

For this reason, moment analysis was abandoned and, instead, the constants describing the sorption rate curves for replicate experiments were considered on an

Table 4.12   A comparison tri-exponential constants of four replicate runs of the measurement of the sorption rate of naphthalene on PRP-1 from 85 % MeOH. The relative standard deviation, as a percentage, is shown in brackets below the value of the constant. Column 2 (the data for Replicate 1) contains the same information as found in Table 4.9).

Replicate	1	2	3	4
n_0 (x 10^{-7} mol/g)	2.75 (0.62 %)	2.72 (0.60 %)	2.77 (0.70 %)	2.85 (3.9 %)
n_1 (x 10^{-7} mol/g)	1.70 (15.6 %)	1.75 (7.7 %)	1.26 (24.0 %)	1.81 (5.3 %)
n_2 (x 10^{-7} mol/g)	0.697 (31.1 %)	0.652 (15.3 %)	1.12 (22.9 %)	0.682 (11.6 %)
n_3 (x 10^{-7} mol/g)*	0.353* (139 %)	0.318* (79.3 %)	0.390* (148 %)	0.358* (80.9 %)
k_1 (s^{-1})	2.79 (13.6 %)	2.65 (7.4 %)	6.05 (51.7 %)	2.43 (6.3 %)
k_2 (s^{-1})	0.642 (41.9 %)	0.525 (29.3 %)	0.846 (31.4 %)	0.413 (21.5 %)
k_3 (s^{-1})	0.0572 (28.0 %)	0.0560 (29.5 %)	0.0617 (26.7 %)	0.0209 (64.6 %)

*n_3 is determined by difference where $n_3 = n_0 - n_1 - n_2$.

individual basis. The results of the replicate experiments are shown in Table 4.12. In this table, the relative standard deviation of each constant, calculated by dividing the standard deviation (as calculated by the curve fitting program) by the value of that constant, is shown in brackets below the value for each constant. The sorption rate experiment appears to be reproducible in that the four replicate experiments all fit tri-exponential functions and the constants are of the same orders of magnitude in all four experiments. The constants in and of themselves probably have no physical significance. The differences in the values of the constants between the three replicates may be due to irreproducibility of the experiment or to the curve fitting procedure. Note that because the constants are not independent of each other, they cannot be independently averaged. At present, there is no real direct method for evaluating the robustness of this experiment.

The reproducibility of the shallow bed method can be further evaluated once the results are used to predict elution profiles as discussed in Section 2.3.6 and in Section 4.2.5.

The sorption rate measurement also provides a method of measuring k'. At long exposure times, the shallow bed experiment basically becomes a modification of the column equilibration method because the amount of sample sorbed approaches that sorbed at equilibrium. The amount adsorbed at equilibrium can therefore be derived from the value n_0 in the multi-exponential equation that fits the sorption rate curve. This value can be used to calculate $D = C_s/C_m$. Note that the quantity C_s deals only with the amount actually adsorbed (the sample located only in the stationary phase). The quantity n_0 describes the equilibrium amount of sample in the stationary phase and the amount of sample in the pores of the packing. In order to get the quantity D (and derive k' from equation 4.3 for the HPLC column of interest), the quantity n_0 must be corrected for the number of moles of sample in the pores at equilibrium. This can be

done by assuming that, at equilibrium, the pores are filled with a solution of concentration equal to C_m, which is the concentration in the mobile phase.

$$C_s = n_0 - \frac{v_p C_m}{1000}$$

eqn. 4.12

The units of C_s and n_0 are in mol/g. The variable v_p is the specific pore volume (0.79 mL/g for PRP-1) and the factor 1000 converts the units to L/g to agree with the units of C_m.

From the average of the four replicate sorption rate experiments discussed above, $n_0 = 2.77 \pm 0.09 \times 10^{-7}$ mol/g at the 95 % confidence level. In this case, $C_m = 4.716 \times 10^{-6}$ M and D calculated by this method is 5.80×10^{-2} L/g. For the HPLC column discussed above, the k' calculated by equation 4.3 is therefore 38.9 with an error of 2.2. At the 95 % confidence level, the value for k' is therefore 38.9 ± 3.6. The large error is due primarily to propagation of the uncertainties in the packing and column properties.

This quantity compares well to the values of k' measured by the other two methods. The k' measured from the sorption isotherm was 36.0 ± 4.3, while that measured from the elution peaks was 37.0 ± 0.6. Measuring the capacity factor from chromatographic data gives the best precision. The other two methods give comparable precision, due mostly to the propagation of error from packing characteristics used in the calculations. But for packings which show very slow sorption, the method that uses the data from the shallow bed experiment could save a considerable amount of time if the sorption rate curve can be relatively accurate defined using only data points at short exposure times.

4.2.4   Sources of Error

Shallow bed conditions were previously defined as the conditions under which the concentration of the sample solution in the bed was constant at all times including an

exposure time of zero. There are two possible problems in meeting these conditions. which would be sources of error in the rate measurement, both of which are discussed below.

First, even when no sorption occurs, there should be a physical limitation in rinsing out the hold-up volume of the shallow bed in a finite time. The hold-up volume of the shallow bed, including the space in the top and bottom retaining screens, and in the area above the top screen takes a finite time to rinse with sample solution. The overall hold-up volume of the shallow bed, including the spaces described above, is on the order of 15 μL. For a volumetric flow rate of 0.3 mL/s through the bed, which was a typical volumetric flow rate in the exposure steps, approximately 800 hold-up volumes pass through the shallow bed in 0.4 seconds, which is close to the shortest exposure time employed. There is therefore a rather large quantity of sample solution passing through the shallow bed in a very short time, enough to adequately rinse the void volume.

A second, more probable source of error in the rate measurement method occurs when the sample is sorbed. Sorption will decrease the concentration of the sample in the mobile phase in the shallow bed. In order to maintain a constant sample solution concentration at all times and locations throughout the bed, a fast solution flow rate and a very short bed of packing are used in the experiment. If the flow rate through the shallow bed is not fast enough to instantaneously rinse the solution of decreased concentration from the bed, a concentration gradient would be established in the bed along the axis of flow. Particles located farther along in the bed would be in contact with a solution of lower concentration of naphthalene.

One way to determine if the constant concentration condition is being maintained is to measure the effect on the sorption rate curve of changing the solution flow rate through the shallow bed. At low flow rates, the sample stream flow will be insufficient to "instantly" sweep out the solution in which the concentration has

decreased by the process of sorption . The effect on the sorption rate curve will be greatest at the low exposure times where the initial slope of the curve will be erroneously low. If the flow rate of the sample solution through the bed is increased. the initial slope of the sorption rate curve will increase until the flow rate is "fast enough" to maintain the constant concentration. If the flow rate of the sample solution is increased beyond this point. the sorption rate curve should not vary with flow rate.

Figure 4.10 shows the effect on the sorption rate curve of changing the superficial linear velocity of the sample solution through the shallow bed. The sorption data are normalized to the value of n_o for each rate curve. The linear velocity is calculated using equation 3.1. As the linear velocity increases, the initial slope of the curve also increases. It is important to note that the rate curves in Figure 4.10 show only sorption data for exposure times up to 2 s. After about 8 s however, the curves become indistinguishable: at the high exposure times. even at slower flow rate. the flow is fast enough to sweep out the bed with a sufficient volume to maintain a constant concentration.

Figure 4.11 shows the slope of the initial part of the sorption rate curve for four different flow rates through the shallow bed. In order to calculate the initial slope. the functions fitting the sorption rate curves were used to generate data at exposure times between 0 and 0.5 s at intervals of 0.05 s. Data which fit a straight line with a correlation coefficient of 0.999 were used. The steeply rising portion of the four curves shown in Figure 4.10 are plotted in Figure 4.12 along with the linear regression lines that fit them. Notice that the sorption rate curve rises in a straight line only for a very short time. For the fastest linear velocity through the bed, the sorption rate curve starts to deviate perceptibly from linearity after only 0.10 s.

A plot such as Figure 4.11, which displays the initial slope of the sorption rate curves collected at four different linear velocities, would be expected to flatten at high linear velocities where shallow bed conditions are met. Also, when shallow bed
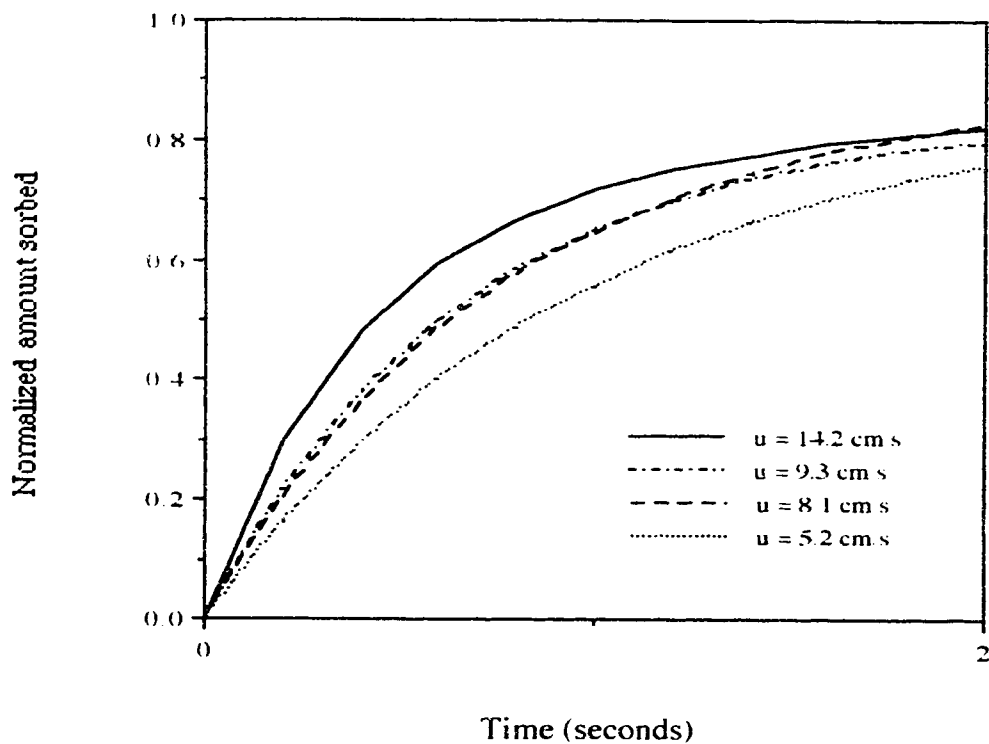
Figure 4.10   Sorption rate curves for naphthalene on PRP-1 in 85 % MeOH as a
function of superficial linear velocity of sample solution through the
shallow bed. Three curves are shown; each curve is the tri-exponential
curve describing experimental data (not shown) at each linear velocity.
The curves have been normalized to their value at infinite exposure time.
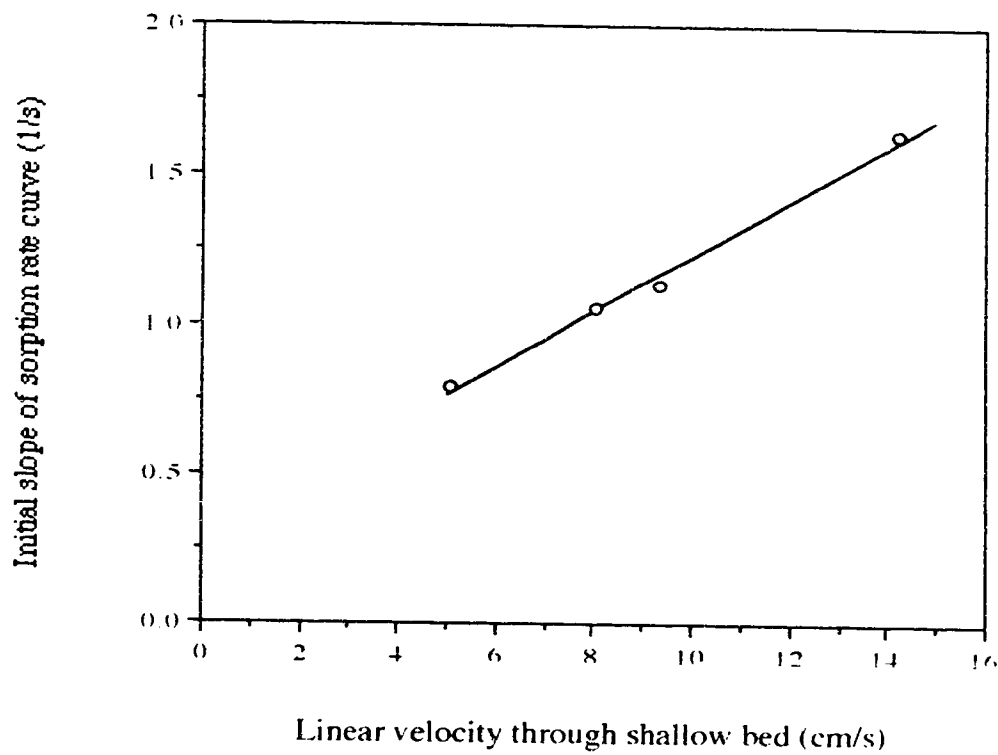
Figure 4.11   Initial slope of the sorption rate curve at four different superficial linear velocities through the shallow bed. The slopes are calculated from the plots shown in Figure 4.10.
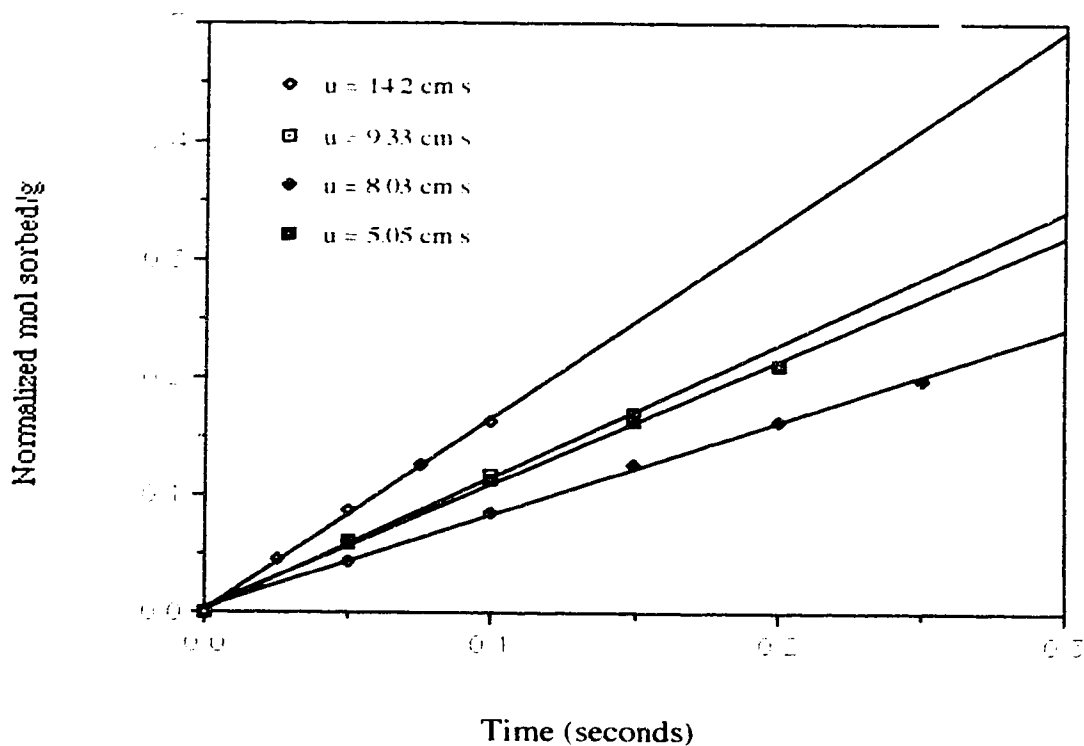
Figure 4.12 Plot of linear region of sorption rate curves for naphthalene on PRP-1 in 85 % MeOH at four different superficial linear velocities through the shallow bed. Notice the very small exposure times shown in this plot. The data points are generated from the multi-exponential equations that fit the sorption rate curve at each linear velocity and the line shown is the result of a linear regression on data which fits the straight line with a correlation coefficient of 0.999.

conditions have been established. the initial slope is expected to become independent of the linear velocity. However, it is observed that the initial slope plotted in Figure 4.11 continues to increase with linear velocity through the shallow bed rather than flattening out. This indicates that while we may be approaching shallow bed conditions, they are not met for data obtained early in the rate experiment. The linear velocity through the shallow bed was the fastest possible in the apparatus used (approximately 14 cm/s). This is limited by the relatively high viscosity of the solvent system and the upper limit of the gas regulator on the constant pressure system.

Because shallow bed conditions were not met, the slope of the initial portion of the sorption rate curve is presumably erroneously low. This results in an underestimation of the rate constant, k_1, in the first term of the tri-exponential. There is also the possibility of underestimation of the rate constant for the second term of the multi-exponential, since the curve may not solely be defined in this region by the fastest sorption term. Also subject to error will be the multipliers n_1 and n_2 in the tri-exponential equation. When the sorption rate data are used to predict elution profiles, an underestimation of rate constants would result in anomalously wide distributions predicted by these rate constants. This possibility is explored further in Section 4.2.6.

4.2.5 Prediction of Elution Profiles from Sorption Rate Curve of Naphthalene on PRP-1

A method for predicting the elution profile of a sample from its sorption rate curve was discussed in Chapter 2. Under the experimental conditions described here, the sorption rate curve for naphthalene fits a tri-exponential equation and the method described in Section 2.3.6 can be used to predict its elution profile on PRP-1, as discussed below.

The four replicate sets of constants describing the replicate sorption rate curves (shown in Table 4.12) were used separately to predict four replicate elution profiles.

The chromatographic column was assumed to be 15 cm long and packed with PRP-1 stationary phase identical to the material used in the shallow bed for the sorption rate measurements. The constants of the tri-exponential equation were used to calculate the probability distributions according to equation 2.15 for each rate constant and the overall elution profile was calculated in the manner described in Section 2.3.6. The following discussion describes the modelling process using the tri-exponential curve fit data from Replicate 1 (the constants are shown in Table 4.9 and in column 1 of Table 4.12). Results from the other replicates will be discussed later.

Briefly, the elution column is modelled by three hypothetical columns, each associated with only one of the three types of sorption processes. In the first hypothetical column the fastest sorption process, associated with k_1 occurs while in the second, the process associated with k_2 occurs and in the third, only the slowest sorption process, associated with k_3 occurs. The fractions Φ_i of the sample which will pass through each of the hypothetical columns without being sorbed are presented in Table 4.13. Note that the subscripts indicate the term of the tri-exponential used to calculate the fraction. For example, Φ_1 is the non-interacting fraction in a hypothetical column which models the sorption described by the first term of the tri-exponential equation. In general the non-interacting fraction decreases with linear velocity. It can be seen that only Φ_3 is significantly greater than zero at the linear velocities of interest. The data treatment is described in Section 2.3.6 is therefore appropriate.

It should be noted at this point that one source of error in the data treatment is the assumption that both Φ_1 and Φ_2 are essentially zero. As the linear velocity increases, these fractions increase (since there is less time for the sample to interact with the stationary phase). Even at the highest linear velocity studied the values for these fraction remain very small. As seen in Table 4.13, even in the worst case, Φ_2 is only about 0.3 % which is expected to add little error to the data treatment. In terms of other experimental errors, the error due to this factor is negligible.

Table 4.13   The non-interacting fractions, Φ_i, for the three hypothetical columns
which are predicted by the sorption rate data from Replicate 1 (see Table
4.9). The three fractions are calculated at four different mobile phase
linear velocities according to equation 2.24. The subscripts indicate the
term of the tri-exponential equation.

u_o (cm/s)	0.40	0.30	0.20	0.10
Φ_1	6.10×10^{-28}	1.62×10^{-36}	4.25×10^{-55}	~ 0
Φ_2	2.70×10^{-3}	4.19×10^{-4}	7.40×10^{-6}	6.34×10^{-7}
Φ_3	0.764	0.702	0.584	0.344

The distributions associated with the broadening occurring in each hypothetical column, designated P1, P2 and P3, can be calculated from the tri-exponential constants. An injection of a sample will elute from the series of columns in two zones. The first, consisting of sample which passes through the series of column after undergoing sorption only in hypothetical columns 1 and 2 but not undergoing the slowest sorption in column 3, will have a distribution designated P1/2. The second zone consists of sample which passes through the series of columns after undergoing all three types of sorption. This zone is designated P1/2/3. In each case, the profiles result from convolution of the individual distributions from the columns in which sorption actually occurs. In order to get the final elution profile, the two peaks are scaled on the basis of area. The ratio of the area of the distribution P1/2 to that of the total area under the two curves will be the same as Φ_3, the fraction of sample which does not interact with the third column. The scaled peaks are then added. To compare to real chromatograms, the predicted peak is then corrected along the time axis by adding t_m for the original column.

The data treatment described in brief above and in detail in Section 2.3.6 was performed using the tri-exponential constants describing the sorption rate curve for Replicate 1 and assuming a linear velocity of 0.10 cm/s. The value of t_m was taken to be 148.2 s and the k', as determined from elution experiments, was 37.3. Figure 4.13 illustrates the predicted profile. The discussion in this section of the thesis will be restricted to how well the EMG function describes the predicted profiles and how the elution profiles predicted by the replicate experiments compare among themselves.

The three-column model was used to predict the elution profiles for the remaining sets of tri-exponential constants shown in Table 4.12. The resulting profiles are illustrated in Figure 4.14 where Curve A is the profile predicted from Replicate 1 and Curves B, C, and D are the profiles predicted from Replicates 2, 3 and 4 respectively. All of the predicted profiles were subject to an EMG curve fit. The EMG

Figure 4.13   The predicted elution profile for naphthalene on PRP-1 at a mobile
phase linear velocity of 0.10 cm/s. The profile is predicted using the tri-
exponential constants that describe the sorption rate curve for Replicate
1 (see Table 4.9).

Figure 4.14   The predicted profiles from the four replicate sorption rate

measurements (Table 4.12) for naphthalene on PRP-1 at $u_o = 0.10$

cm/s. The curve A is the predicted profile using the tri-exponential rate

constants for Replicate 1 and has already been illustrated in Figure 4.13.

Curves B, C, and D are the profiles predicted by the constants for

Replicates 2, 3, and 4 respectively.

characteristics for the predicted profiles are shown in Table 4.14. Since the constants associated with Replicates 1 and 2 are so similar, the peaks predicted by the model have a similar shape and similar EMG characteristics. Note that the data treatment for Replicates 1, 2, and 4 was based on predicting the probability distribution for each hypothetical column using equation 2.15. Because the k_1 value for the Replicate 3 experiment was so large the distribution associated with this process, P1, was calculated using equation 4.13 an approximation of the equation which is discussed in more detail in the next section.

In general, the EMG characteristics for the elution profiles are highly reproducible, despite some values which seem extreme. For instance, while the relatively small value of k_3 for Replicate 4 is, as expected, reflected in the longer tail in Curve D, it is not reflected in the value of τ. One would expect to see a larger value of τ for Replicate 4. This discrepancy results because the EMG function gives a rather poor fit to the predicted profile. For all other profiles, the fit was satisfactory. The contrast is clear in Figure 4.15 which shows the EMG fit to the predicted profiles as dashed lines. In graph A, which is the peak predicted by Replicate 1, the dashed line overlaps the predicted profile so well it is visually indistinguishable. In graph B, however, the EMG function (the dashed line) is visible and does not visually give a good fit to the profile, predicted, in this case, from Replicate 4.

The RSD values shown in Table 4.14 are an expression of the precision of the overall experiment, including contributions from the sorption rate measurement experiment, contributions from the routine used to predict the elution profile and contributions from the EMG curve fitting routine. Overall, the precision is surprisingly good, better than 10 % for all of the constants. Considering the number of steps in the data processing that is used to convert the raw experimental sorption data into a predicted elution profile, this relatively low uncertainty in the peak characteristics is encouraging.

Table 4.14   The EMG characteristics of the profiles predicted by the Replicate measurements of the sorption rate of naphthalene on PRP-1 at a mobile phase linear velocity of 0.10 cm/s. The observed values are for the elution profiles resulting from injection of 2.504×10^{-4} M naphthalene in 85 % MeOH on a 15 cm column of PRP-1.

Replicate	t_G (s)	σ_G (s)	τ (s)
1	4667	426.7	1048
2	4700	448.2	1008
3	5473	448.5	1094
4	4485	459.1	883.9
avg.	4831	445.6	1008
RSD (%)	9.1	3.0	8.9
Observed	5133	157.4	581.3
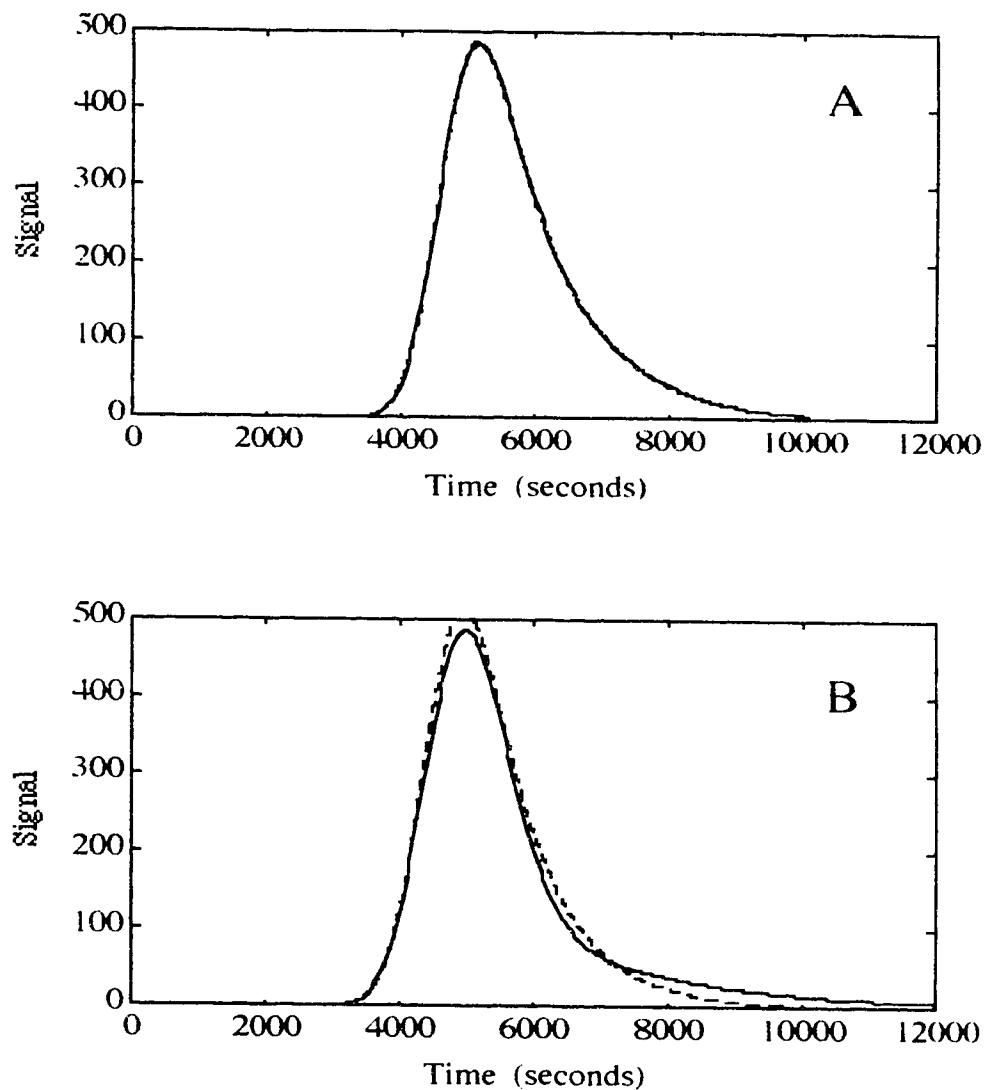
Figure 4.15   The EMG fits to predicted elution profiles at 0.10 cm/s of the tri-
exponential constants of Replicates 1(Curve A) and 4 (Curve B). The
predicted peaks are represented by the solid line while the EMG fits are
represented by the dashed lines. For Curve A, the EMG fit is so good
that the dashed line is impossible to distinguish from the curve predicted
by the data treatment.

4.2.6　Comparison of Predicted and Observed Elution Profiles on PRP-1

In the previous section, the reproducibility of the shallow bed experiment was evaluated in terms of how the profiles predicted by replicates of the experiment compared with each other. This section examines how the predicted profiles compare with actual elution profiles. We begin by using one set of sorption rate data (Replicate 1) and one set of elution conditions ($u_0 = 0.10$ cm/s). The effect of the uncertainty in the tri-exponential constants is examined in order to try to predict the effect of the sources of error in the shallow bed experiment on the predicted profile. The profiles predicted by Replicate 1 at other elution conditions and those predicted by the other Replicate sorption rate experiments are also examined.

Figure 4.16 shows the profile that is predicted by the sorption rate experiment for elution conditions of $u_0 = 0.10$ cm/s as well as an actual experimentally observed elution profile. The observed elution profile was collected under conditions described above by injection of 2.504×10^{-4} M naphthalene in 85 % MeOH. The predicted peak is much wider than the observed peak, which may mean that the effect of the sorption-desorption kinetics is overestimated by this data treatment. The times of the peak maxima are relatively close but are not coincident. The shape of the tailing portion of the observed profile is not well matched by the shape predicted from the rate constants.

In order to better understand the origin of the predicted peak shape, each of the distributions predicted for the three hypothetical columns which were used to model the overall elution column were investigated. The tri-exponential constants used in this calculation were previously shown in Table 4.9.

Figure 4.17 shows the distributions, P1, P2 and P3, calculated from the three terms of the tri-exponential. The first term, P1, which is associated with the largest rate constant and the greatest number of sorbing "sites" generates a profile which is the narrowest of the three and, due primarily to the larger number of sites, located the farthest down the time axis. As the number of sites associated with a term decreases,
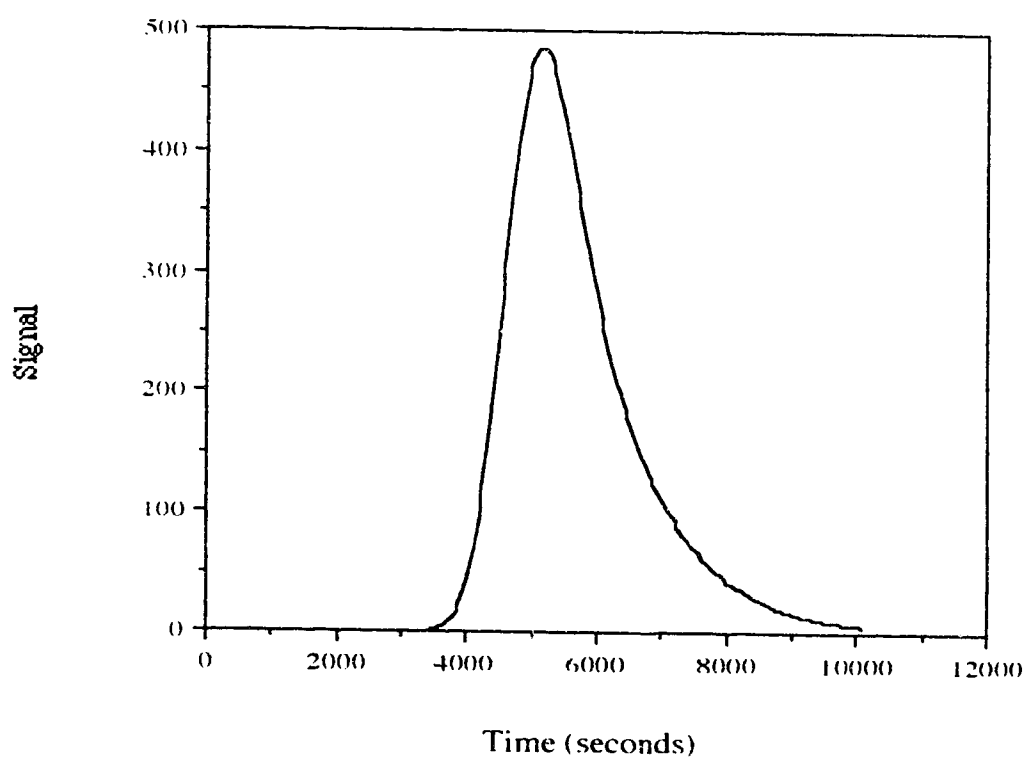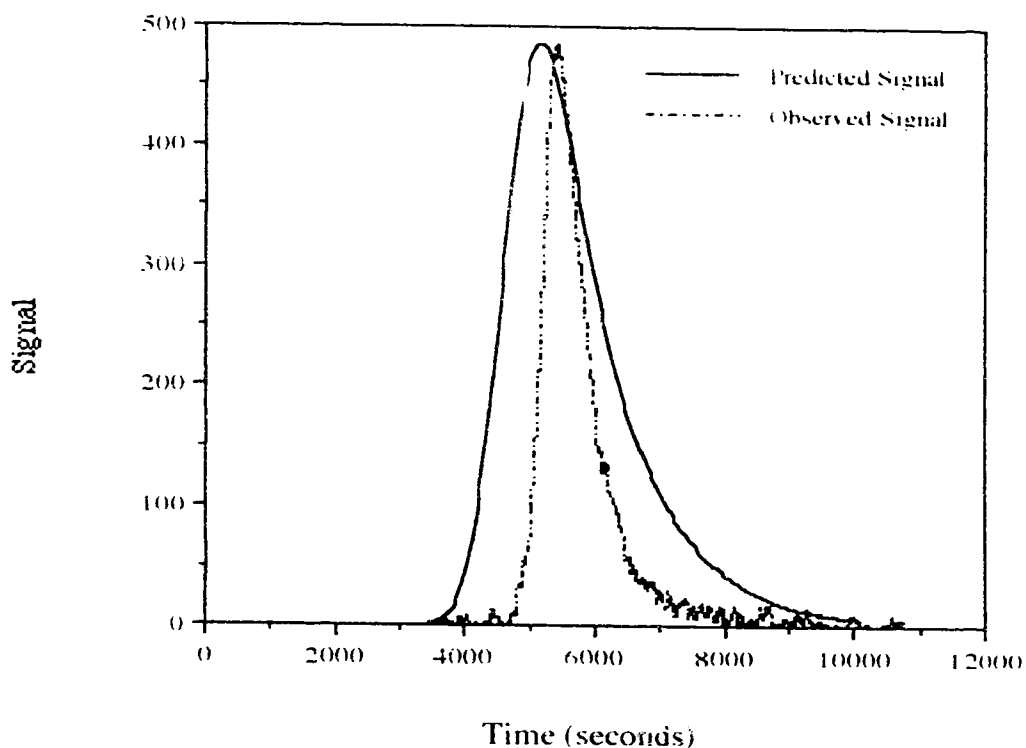
Figure 4.16   The predicted elution profile for naphthalene on PRP-1 at a mobile
phase linear velocity of 0.10 cm/s compared to the observed peak.
which is obtained by injection of 2.504 x 10⁻⁴ M napthalene on PRP-1
in 85 % MeOH.   The predicted profile (previously seen in Figure 4.13)
is predicted using the tri-exponential constants that describe the sorption
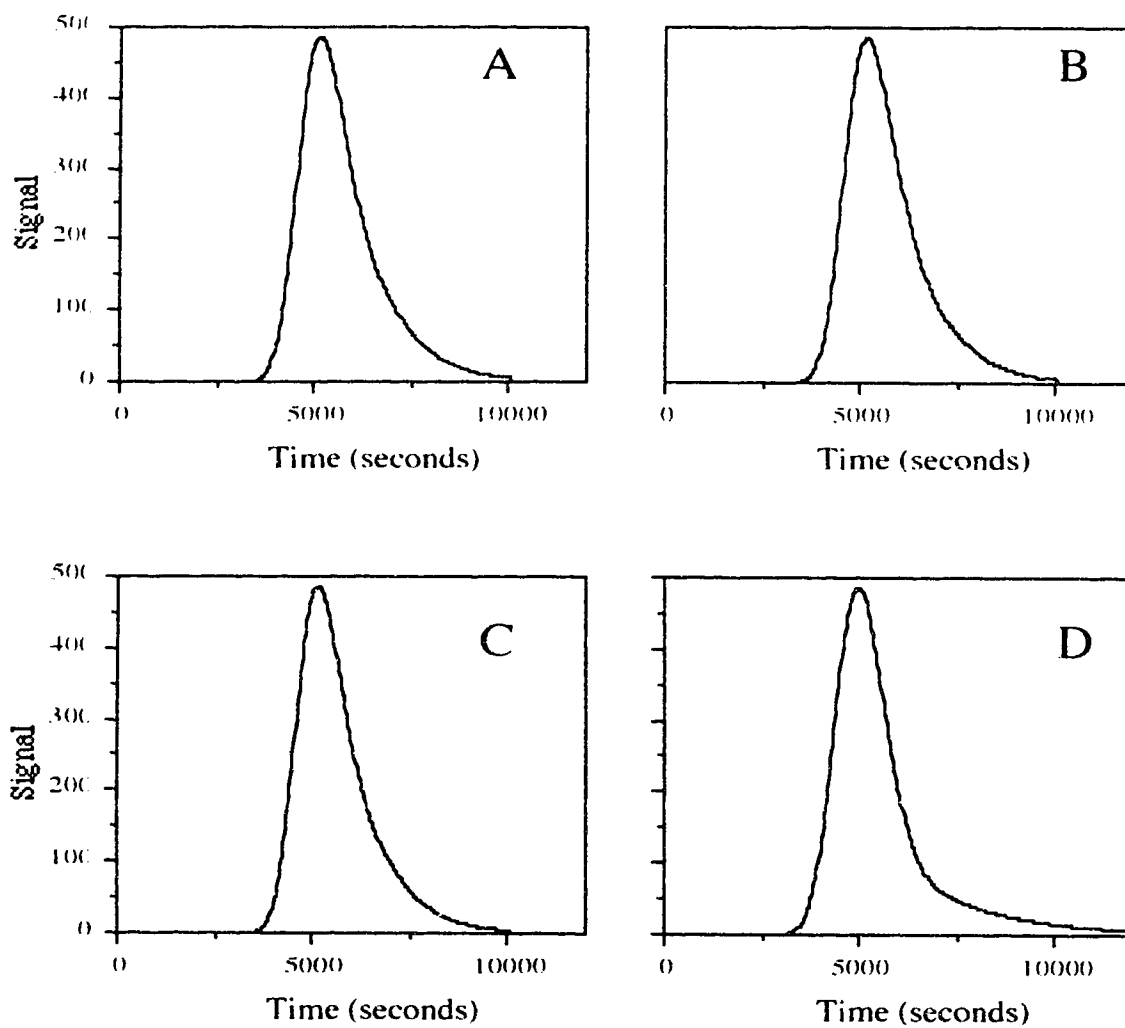rate curve for Replicate 1 (see Table 4.9).
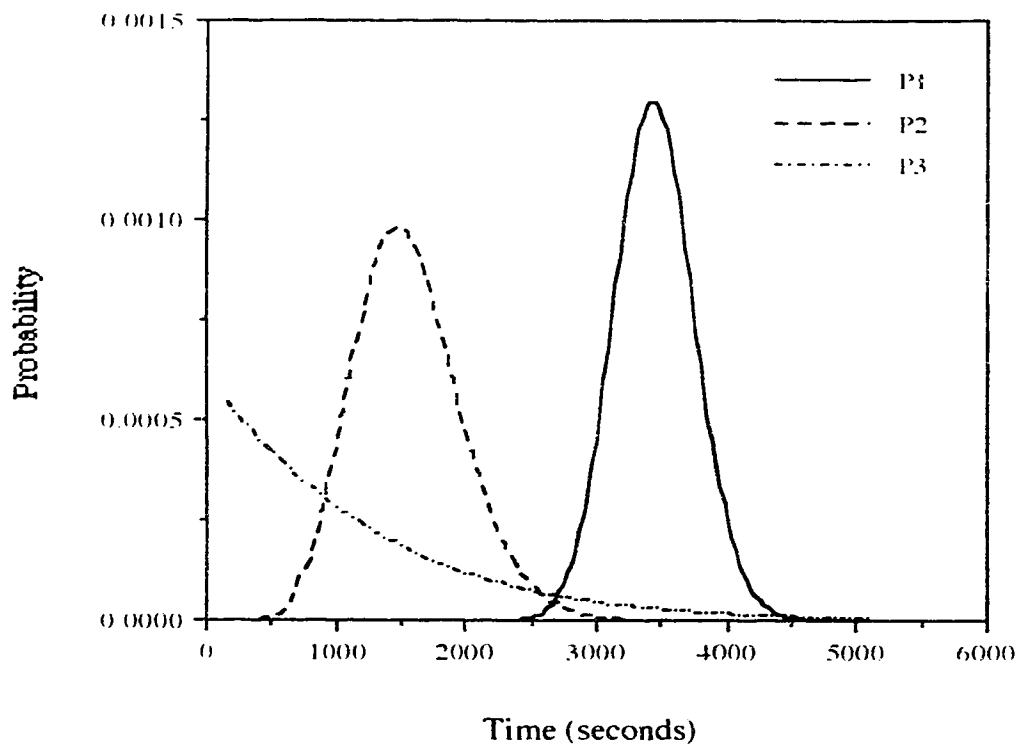
Figure 4.17   The probability distributions P1, P2 and P3 which are calculated from
equation 2.15 using the tri-exponential constants for Replicate 1 (see
Table 4.9) and $u_0 = 0.10$ cm/s. The distribution P1 is associated with
the hypothetical column in which only the rate processes described by
the first term in the tri-exponential equation describing the sorption rate
curve occurs. The distributions P2 and P3 are associated with columns
in which processes described by the second and third terms occur.

the distribution associated with that process also shifts farther left on the time axis. Thus, the distribution decreases in width for a decrease in n_1 and an increase in k_1. The shape of P3, predicted by the third term, is mainly exponential as a result of the small rate constant associated with this term. Because n_3 is so small, the distribution P3 has a centre of gravity which is smaller than those associated with P1 and P2.

As previously discussed, further manipulation of the distributions is necessary to predict the elution profile from a chromatographic column. All three distributions, P1, P2 and P3, must be convolved to form P1/2/3, one of the distributions shown in Figure 4.18. This is the distribution due to sample molecules in a band which elute from the hypothetical columns after interacting at least once with each type of site. In addition, P1 and P2 are convolved to give P1/2, which is also shown in Figure 4.18. This is the distribution due to the sample molecules which elute from the hypothetical columns after interacting after undergoing only the fastest and intermediate sorption processes. The two peaks shown in Figure 4.18 are added to get the final predicted elution profile shown in Figure 4.16. Note that P1/2 and P1/2/3, as illustrated, have already been scaled, as described in Section 2.3.4, as is required before addition. The ratio of the area of P1/2 to the total area under the two curves is Φ_3, which, in this case, was calculated to be 0.34. Inspection of Figure 4.18 shows that indeed 34 % of the total area under the curves is contained beneath P1/2 which represents the distribution of the fraction that does not interact with Column 3.

The profiles in Figure 4.17 are interesting in terms of their contributions to the shape of the final profile. The major source of the tailing shape of the profile is the contribution from the probability distribution due to the slowest process, P3. The distribution due to the intermediate process, P2, is likely to be the major source of the width of the profile, assuming that the fastest process, P1, predicts a very narrow, nearly Gaussian profile. The distribution P2 is shown, along with the observed profile, in Figure 4.19. The distribution has been artificially shifted down the time axis

Time (seconds)
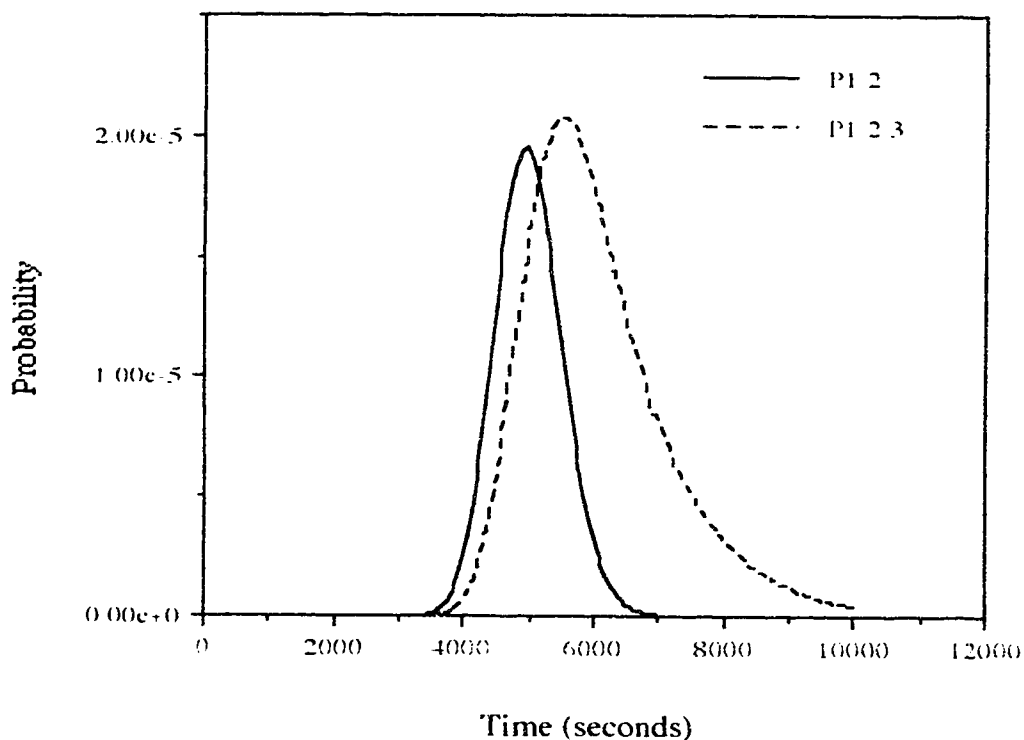
Figure 4.18   . probability distributions P1/2 and P1/2/3 calculated from the tri-
exponential constants of Replicate 1. The distribution P1/2 is the
convolution of P1 and P2 (see Figure 4.17) and represents the
distribution of sample which passes through the series of three
hypothetical columns undergoing only the fastest and intermediate
sorption processes. The distribution P1/2/3 is the convolution of P1,
P2 and P3 and represents the distribution of sample which passes
through the hypothetical columns after undergoing all three sorption
processes. To get the overall elution profile (as shown in Figure
4.13), P1/2 and P1/2/3 are scaled and added together.

so that the times of peak maxima coincide. The distribution P2 matches the main part of the observed peak fairly well although the observed width is still slightly overestimated by P2. The shapes of the tailing part of the profiles don't match since the distribution P2 is fairly symmetrical. This implies that "kinetic tailing" [2.29], although overestimated by the inclusion of P3 (see below), is not entirely absent.

Figure 4.20 shows P1/2, the distribution predicted by the convolution of P1 and P2, the distributions for the fastest and for the intermediate processes. This peak represents the fraction of the sample molecules that pass through all three hypothetical columns without interacting with any sites associated with the slowest process. The distribution P1/2 shown in Figure 4.20, which, again, has been artificially shifted down the time axis so that the time of its maximum coincides with that of the observed peak, is wider than the observed peak. Since the addition of P1/2/3 to P1/2 to get the overall profile, which was seen in Figure 4.16, contributes primarily to the tailing portion to the overall predicted profile, sources of errors in the experiment which lead to the anomalously wide distribution in P1/2 probably contribute most to the predicted profile that is wider than observed experimentally.

The sources of error in the shallow bed experiment were discussed in Section 4.2.4. One possible source of error was the fact that shallow bed conditions were not established. Not meeting shallow bed conditions is expected to have the largest effect on the first part of the sorption rate curve, where the curve is steeply rising. Errors in the exposure time for this region would likely lead to an underestimation of k_1, the rate constant associated with the fastest sorption process. It may also lead to an underestimation in n_1, although that effect is less obvious. (It is probably not entirely correct to discuss the rate constants and number of sites associated with each term in isolation of each other since the six variables calculated by the non-linear least squares fit are probably dependent on each other to some extent.) For a larger k_1, P1 is expected to narrow; the limit of P1 is a spike of infinitely narrow width which occurs at
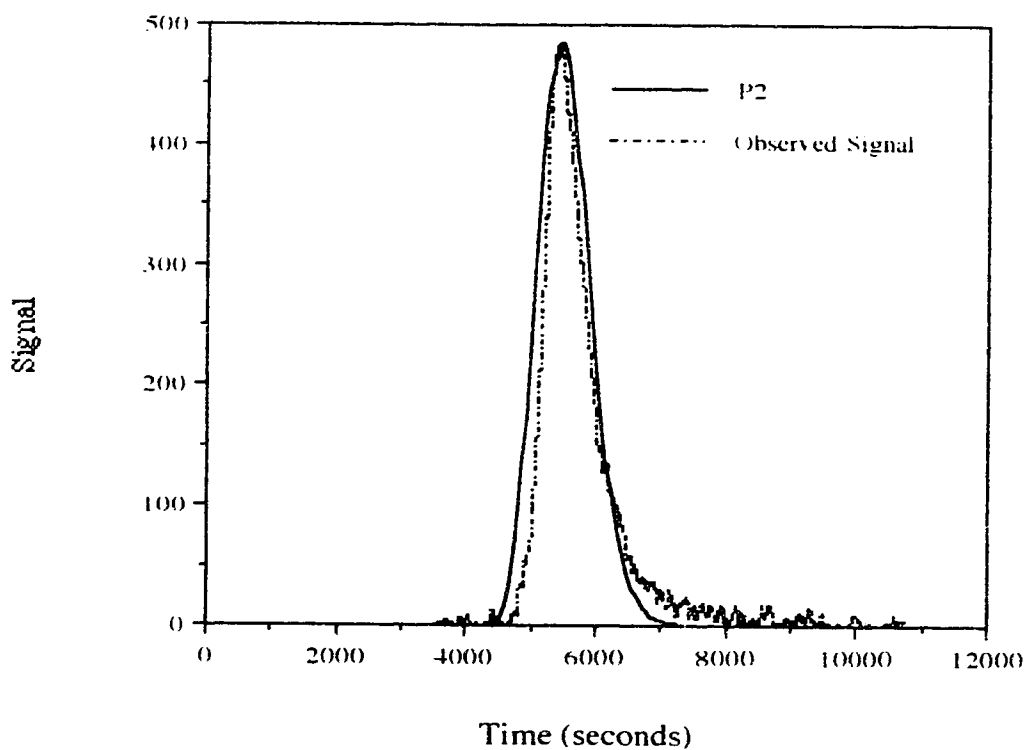
Figure 4.19   The probability distribution P2 shifted along the time axis so that the peak maximum overlaps with that of the observed elution signal. P2 is calculated by equation 2.15 using the tri-exponential constants of Replicate 1. The observed elution signal is the result of injection of 2.504×10^{-4} M naphthalene in 85 % MeOH on PRP-1 at a mobile phase linear velocity of 0.10 cm/s.
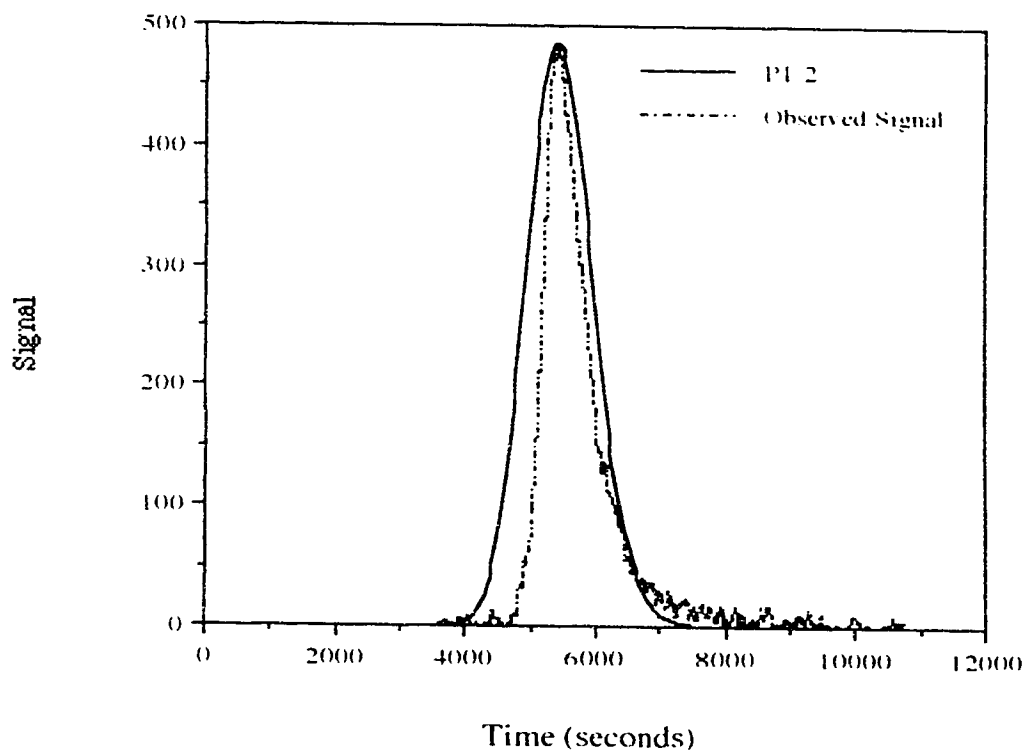
Figure 4.20   The distribution P1/2 shifted along the time axis so that the peak
maximum overlaps with that of the observed elution signal. P1/2 is the
convolution of P1 and P2 which are calculated using the tri-exponential
constants of Replicate 1. The observed elution signal is the result of
injection of 2.504×10^{-4} M naphthalene in 85 % MeOH on PRP-1 at a
mobile phase linear velocity of 0.10 cm/s.

a retention time appropriate to the k' and tm_1 value (determined by the value of n_1; see equation 2.21) of the hypothetical column. In this limiting case for P1, the convolution of P1 with P2 would add no width of the distribution predicted by the intermediate process, but would only shift the centre of the peak.

Figure 4.21 shows how P1 changes with increases in k_1. The distributions in this figure are calculated from an approximation of equation 2.15. This approximation, shown in equation 4.13, uses the first term of the asymptotic expansion of the Bessel function and is valid under the same conditions as when Φ is negligibly small [4.11].

$$P(t_s) = \frac{(k_f \ k_r \ t_m)^{1/4}}{2\sqrt{\pi}} \ \frac{e^{-\left(\sqrt{k_r t_s} - \sqrt{k_f t_m}\right)^2}}{t_s^2}$$

eqn. 4.13

The profiles predicted by equation 4.13 are well fit by EMG functions. The variables. σ_G, the square root of the variance of the parent Gaussian function and τ, the characteristic time of the exponential modifying function. are plotted in Figure 4.22 as a function of k_1. The width characteristics of the predicted profiles decrease at an exponential rate with increasing k_1. After the rate constant reaches a value of 10 s^{-1}, the rate of change in the width characteristics is small. Notice that τ in this case is small compared to σ_G. an indication that the profile is relatively Gaussian.

From the above discussion it follows that if there is a systematic (determinate) error in the measurement of k_1, so that k_1 is, in fact, considerably larger than would be allowed by the random (indeterminate) error of $\pm$ 13.6 %, then the profile P1 will be significantly narrower than predicted. Since it is likely that shallow bed conditions were not met in these sorption rate experiments (see Figure 4.11 and the discussion in Section 4.2.4), it is reasonable to assume there is some underestimation of k_1, although the magnitude of this systematic error is difficult to assess. A rate of sorption of 48 s^{-1}, the highest rate constant for which a distribution was calculated. may not be unreasonable. Marshall et.al. [2.22] measured the rate of sorption on silica-based
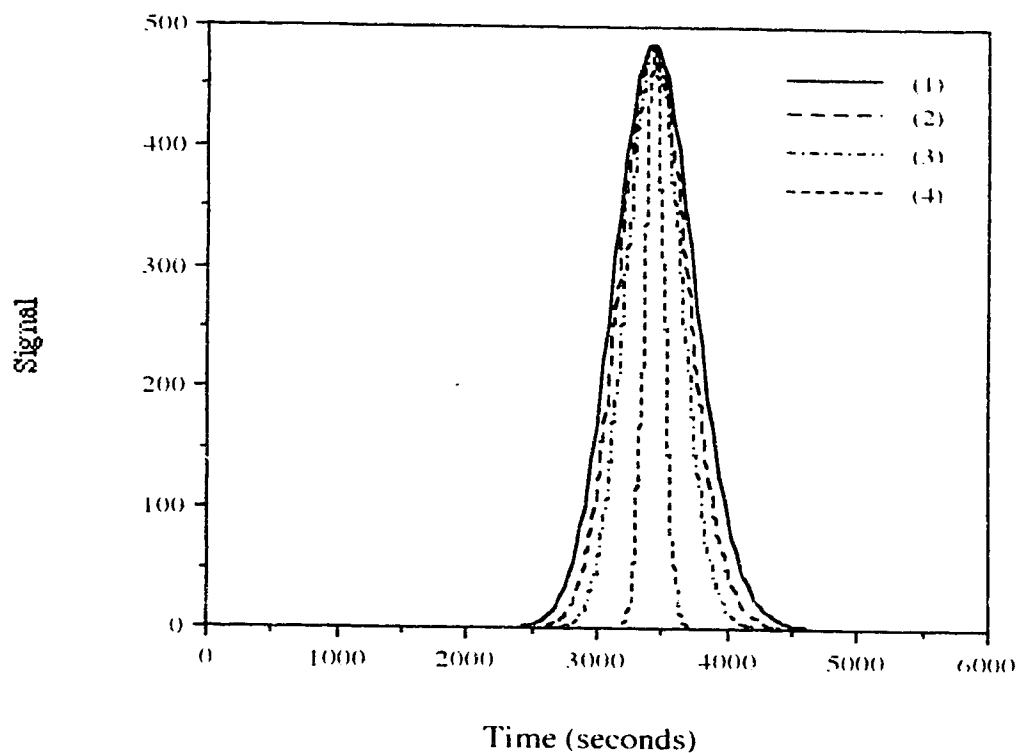
Figure 4.21   The probability distribution. P1, as a function of n_1 as calculated using equation 4.13. The values of k_1 for the four distributions are as follows: (1) $k_1 = 2.79\ s^{-1}$. (2) $k_1 = 3.93\ s^{-1}$. (3) $k_1 = 6.0\ s^{-1}$. (4) $k_1 = 48\ s^{-1}$. The value of n_1 used in these calculation was $1.70 \times 10^{-7}\ mol/g$. The EMG characteristics associated with the width of the distributions are plotted in Figure 4.22.
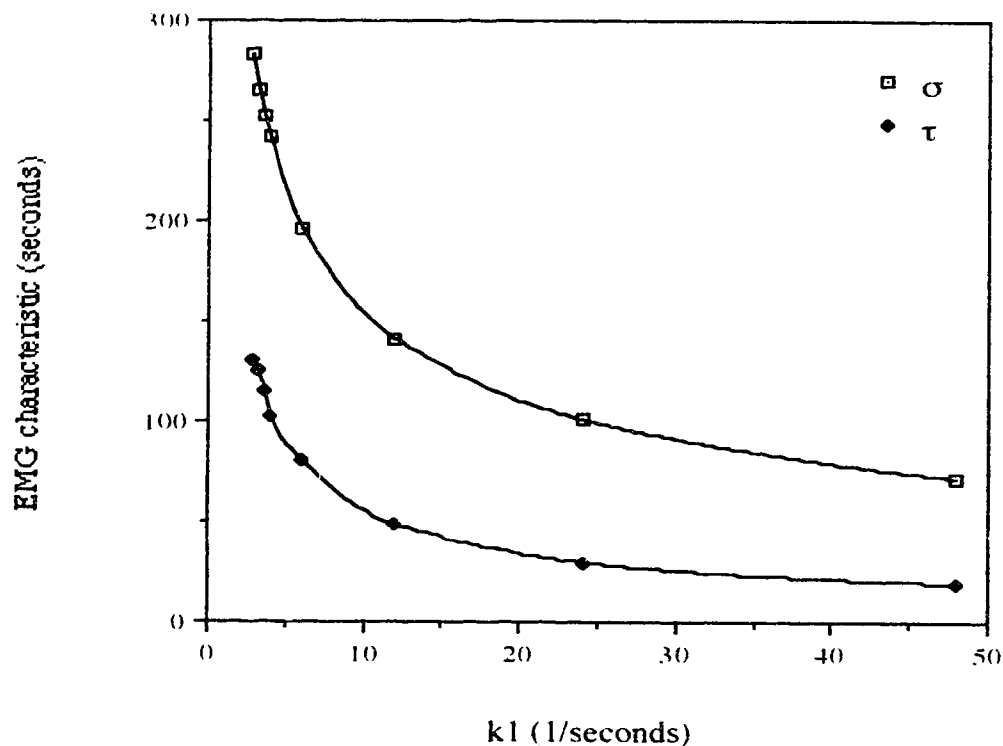
Figure 4.22   EMG characteristics of the probability distribution P1, which is due to the fastest sorption term in the multiexponential equation describing the sorption rate curve, as a function of the rate constant, k_1. The EMG characteristics shown are those related to the square root of the width, namely, σ, which is the standard deviation of the parent Gaussian peak and τ, which is the characteristic time of the exponential modifiying function. The first point in both sets of data are the characteristics of the distribution as predicted by experimental values of k_1. For the observed elution peak, $\sigma = 157.4$ s and $\tau = 581.3$ s.

reverse phases as having inverse characteristics time of 500 s^{-1} or larger. It may be that the mechanism of sorption on the two phases is similar in some respects and that the rather large value of k_1 that appears to be necessary to obtain a sufficiently narrow profile is not outrageous.

The effect of changing n_1, the number of sites attributed to the process is illustrated in Figure 4.23, where the P1 is plotted at three different values of n_1. As n_1 increases, the profile shifts along the time axis to longer times, since $t_{m,1}$, the retention time of an unretained compound in the hypothetical column associated with this process, also increases. It should be noted that the effect of changing n_1 on the peak shape is not necessarily less drastic than the effect of changing k_1. The range over which n_1 is varied is smaller than the range over which k_1 was varied in the previous discussion. The range of reasonable errors for n_1 is smaller than the same range for k_1. From Figure 4.23, the small changes in n_1 do not profoundly affect the peak width. This is supported by data in Figure 4.24 showing the EMG width characteristics for P1 as a function of n_1. The graphs show that any reasonable error, as expressed by the standard deviation in the non-linear least squares fit of the sorption rate curve, results in a relatively small change in the width characteristics.

Figures 4.25 and 4.26 show the width characteristics of distribution P2 as functions of k_2 and n_2, respectively. The distributions P2 were calculated from equation 2.15. The variables in these figures, k_2 and n_2, re changed by multiples of their standard deviations as reported in Table 4.9. The way the shape of the distribution P2 changes with increasing k_2 (Figure 4.25) is similar to the way the shape of P1 changes with increasing k_1 values (Figure 4.22). That is, the peak gets narrower but has the same peak maximum. The range of k_2 values studied was smaller than for P1 because the determinate error in k_2 is probably smaller. The error in the value of k_2 may reasonably be expected to be on the order of magnitude calculated for the uncertainty by the non-linear least squares program. Points corresponding to the
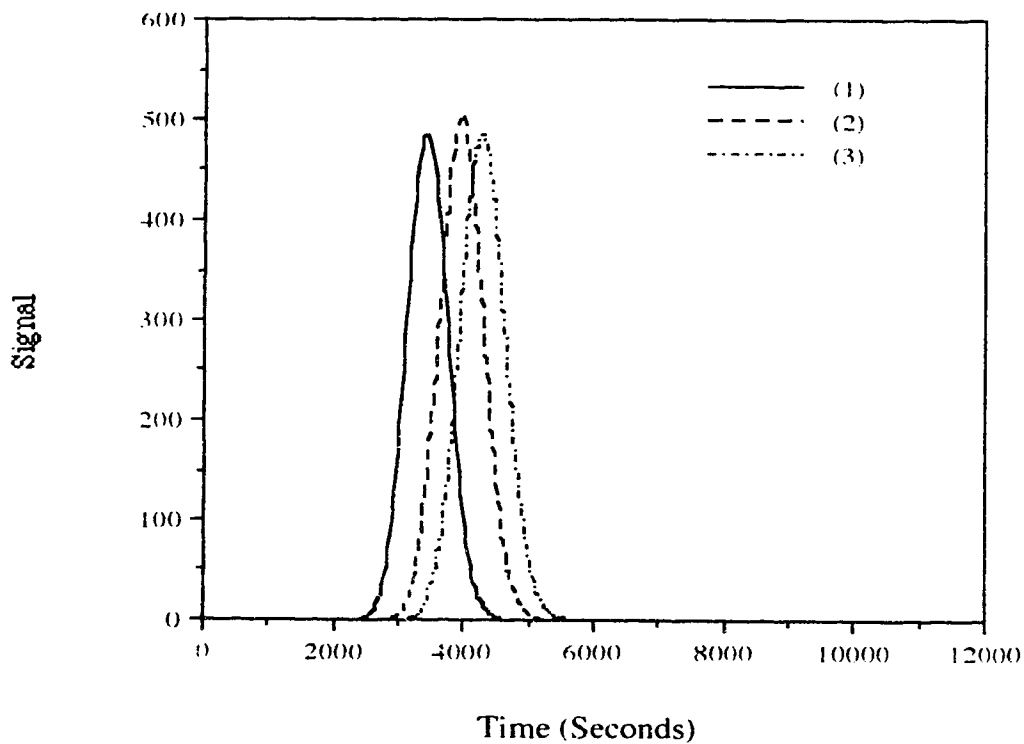
Figure 4.23   The probability distribution, P1 as a function of n_1. The values of n_1
for the three distributions are as follows: (1) $n_1 = 1.70 \times 10^{-7}$ mol/g.
(2) $n_3 = 1.96 \times 10^{-7}$ mol/g. (2) $n_1 = 2.12 \times 10^{-7}$ mol/g. These
distributions were calculated using $k_1 = 2.79$ s^{-1} using the approximate
equation 4.13. The EMG characteristics of the profiles are plotted in
Figure 4.24.
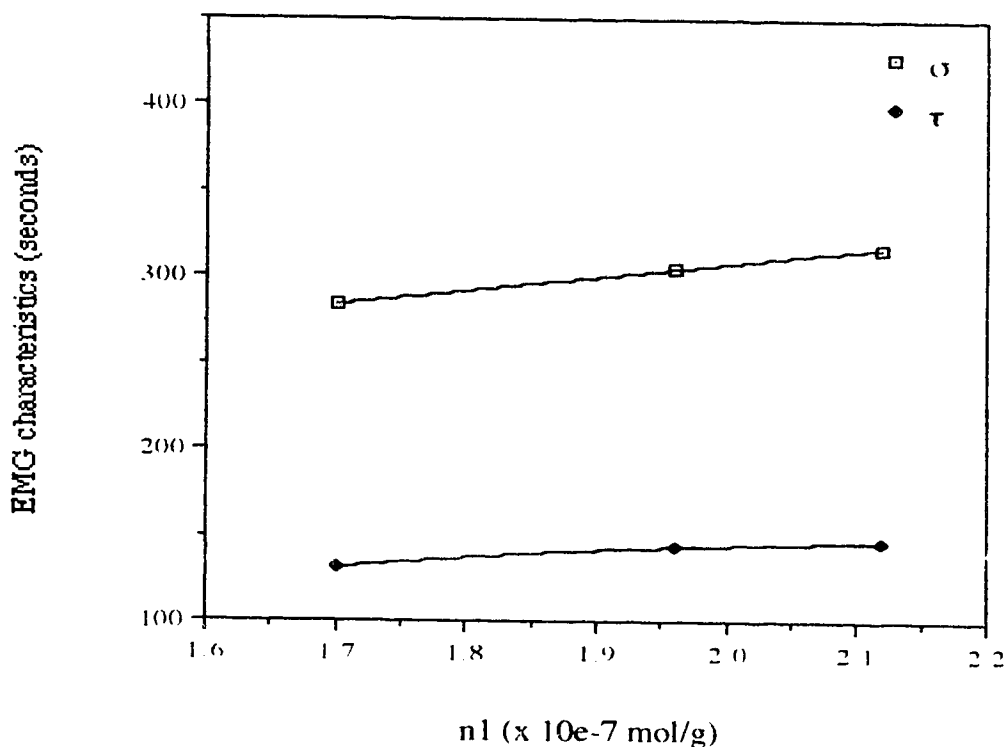
Figure 4.24 EMG characteristics of the probability distribution P1, which is due to the fastest sorption term in the multiexponential equation describing the sorption rate curve, as a function of n_1, the number of sites associated with the process. The EMG characteristics shown are those related to the square root of the width, namely, σ, which is the standard deviation of the parent Gaussian peak and τ, which is the characteristic time of the exponential modifying function. The first point in both sets of data are the characteristics of the distribution as predicted by experimental values of n_1. For the observed elution peak, $\sigma = 157.4$ s and $\tau = 581.3$ s.
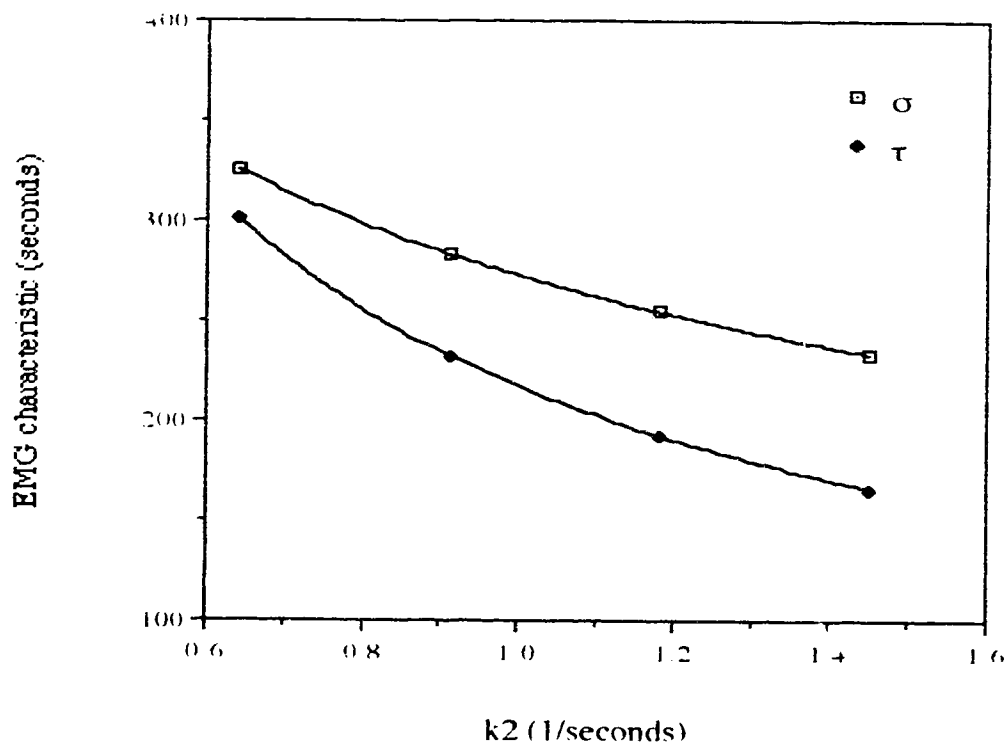
Figure 4.25   EMG characteristics of P2, which is due to the sorption term of intermediate speed in the multiexponential equation describing the sorption rate curve, as a function of the rate constant, k_2. The EMG characteristics shown are those related to the square root of the width, namely, σ, which is the standard deviation of the parent Gaussian peak and τ, which is the characteristic time of the exponential modifiying function. The first point in both sets of data are the characteristics of the distribution as predicted by experimental values of k_2. For the observed elution peak, $\sigma = 157.4$ s and $\tau = 581.3$ s.
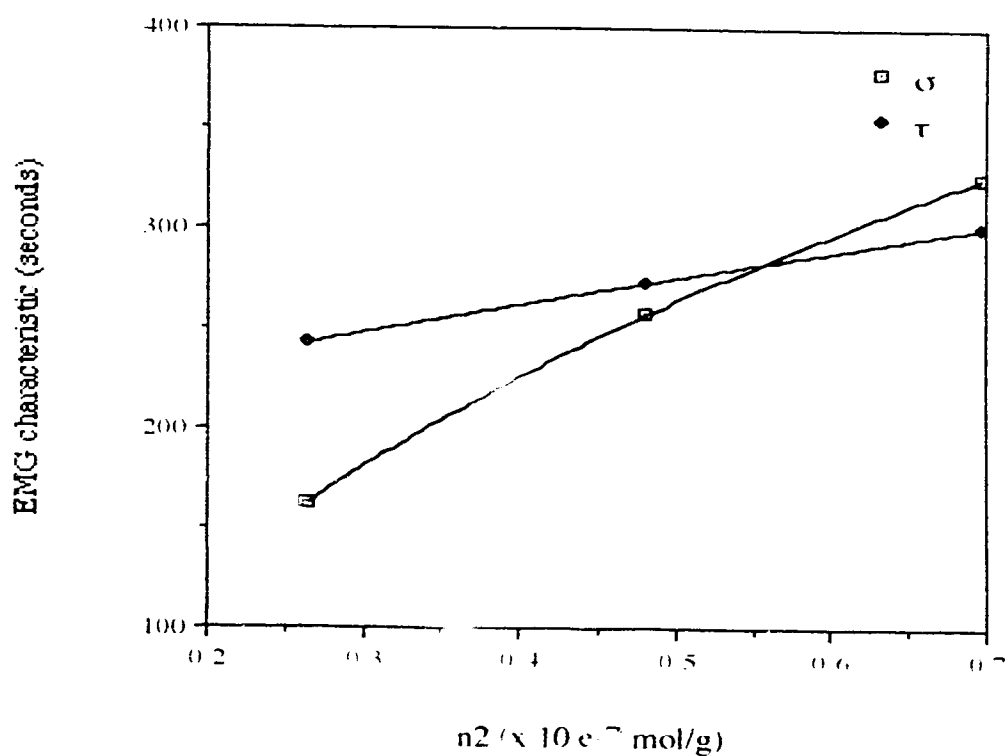
Figure 4.26   EMG characteristics of the probability distribution P2. which is due to the sorption term of intermediate speed in the multiexponential equation describing the sorption rate curve, as a function of the number of sites associated with the process, n_2. The EMG characteristics shown are those related to the square root of the width, namely, σ, which is the standard deviation of the parent Gaussian peak and τ, which is the characteristic time of the exponential modifying function. The last point in both sets of data are the characteristics of the distribution as predicted by experimental values of k_1. For the observed elution peak, $\sigma = 157.4$ s and $\tau = 581.3$ s.

observed values of σ and τ from Table 4.14 (row 1) are located on the far left in this figure. The decrease in the width parameters is again noted. The decrease in width parameters is, however, not very large within the standard deviation calculated by the least squares program.

The effect of increasing n_2 on the width characteristics of the predicted profile is shown in Figure 4.26. The σ parameter increases with increasing n_2 at a faster rate than does the tailing component τ. Points corresponding to the observed values of σ and τ from Table 4.14. (row 1) are located on the far right in this figure. This figure shows the quantitative effect of changing n_2 from the experimental values.

These studies give ballpark estimates of what the values of the four parameters under study here should have in order to predict the shape of the observed elution profile. These studies were primarily done because the effect of four variables on the characteristics of the convolved profile P1/2, which is probably primarily responsible for the width of the main part of the overall predicted peak, is difficult to imagine intuitively.

In all subsequent simulations, if the coefficients n_2 or n_3 are decreased, the number of sites associated with the first process, n_1 is increased to keep the total number of sites constant.

The profile P1/2 that is predicted using the experimentally determined values of k_1, k_2, n_1 and n_2 was previously shown in Figure 4.20. The profile shown in Figure 4.27 is the convolution of a distribution P1, which was calculated using equation 4.13 with the constants $n_1 = 1.917 \times 10^{-7}$ mol/g and $k_1 = 48$ s^{-1}, with the distribution P2 using the constants, $n_2 = 0.480 \times 10^{-7}$ mol/g and $k_2 = 0.642$ s^{-1}. This value of k_2 is the experimentally determined value (shown in Table 4.9) while this value of n_2 is the experimentally determined value minus one standard deviation. The value of n_1 is therefore the experimentally determined value plus one standard deviation of n_2, in order to maintain a constant number of sites. The choice of the value of k_1 was
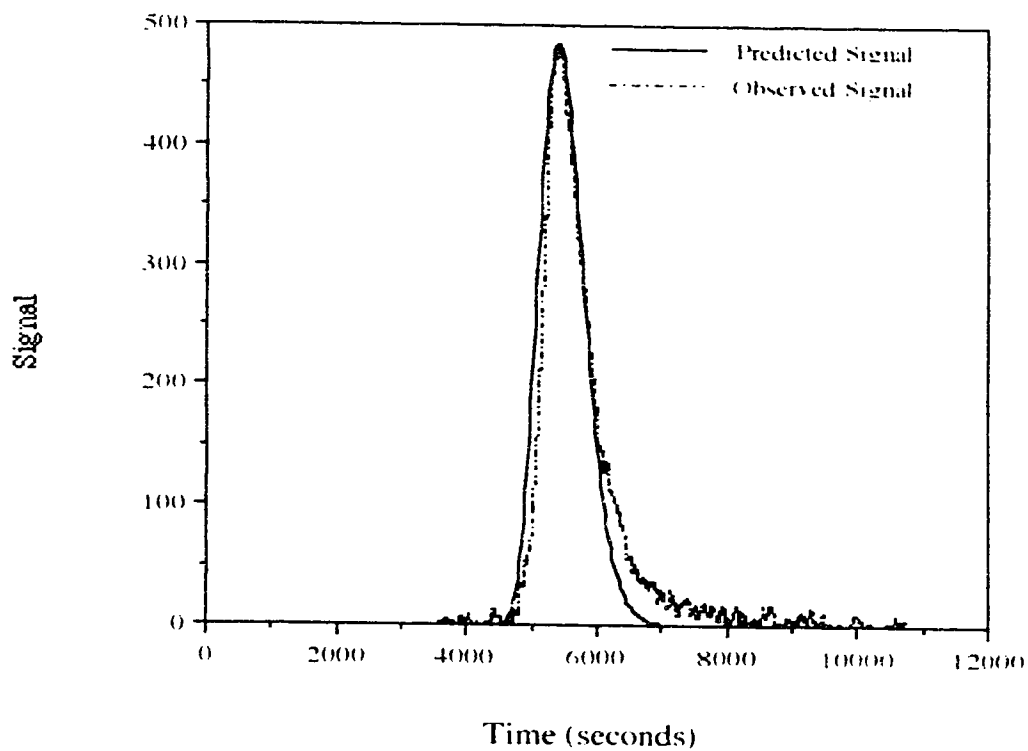
Figure 4.27   The distribution P1/2 which is the convolution of P1 and P2 ... ... ed
using modified values of the constants k_1, n_1 and n_2. P1 is calc ila.ed
by equation 4.13 with $k_1 = 48$ s^{-1} and $n_1 = 1.917 \times 10^{-7}$ mol/g. P2 is
calculated by equation 2.15 with $k_2 = 0.642$ s^{-1} and $n_2 = 0.48 \times 10^{-7}$
mol/g. The distribution P1/2 has been shifted along the time axis to
show the overlap with the observed signal.

discussed above.

The EMG characteristics of the predicted distribution P1/2, based on modified constants and shown in Figure 4.27, and of the predicted distribution P1/2, based on the unmodified constants from the rate curve of Replicate 1 and shown in Figure 4.20, are found in Table 4.15. These can be compared to the same features for the observed elution profile, found in Table 4.16. The term σ_G obtained from the modified constants is closer to that of the observed peak but it is still larger by nearly 71 %. The parameter τ, which represents the exponential modifying function and is representative of the amount of tailing is much less for P1/2 under these conditions than for the observed peak. This is not surprising since the slowest sorption-desorption process has been omitted in the data treatment to this point.

At this point, it might be useful to consider the chromatographic peak as consisting of two sections, the main portion, and the tail. This division is based on observation and is mainly for simplification in the following discussion. The divisions are defined mainly by their extremes. For example, in Figure 4.27, the predicted profile P1/2 consists of a slightly asymmetric main portion with little or no tail. The observed signal, however, consists of a slightly asymmetric main portion with a pronounced tail.

With this distinction in mind, it can be concluded that the main portion of the elution peak can be approximated by P1/2, which results from the two fastest sorption processes. The following discussion will probe the contribution of the slowest process, associated with the third term in the rate equation, to both the main portion and to the tail of the predicted profile.

The effect of the slowest process is accounted for by inclusion of the distribution P3 in the data treatment. The term is incorporated into the process by convolving the distributions P1, P2 and P3 together to form P1/2/3 and adding the result, after scaling, to the distribution P1/2. It is, however, useful to first look at how

Table 4.15   The EMG characteristics of the probability distribution P1/2 predicted from a set of tri-exponential constants that has been modified. The values used in this calculation are as follows: $n_1 = 1.917 \times 10^{-7}$ mol/g; $k_1 = 48$ s^{-1}; $n_2 = 0.480 \times 10^{-7}$ mol/g; $k_2 = 0.642$ s^{-1}. Also shown in this table are the EMG characteristics of the distribution P1/2 calculated from the unmodified tri-exponential constants found for Replicate 1. These can be compared to the same features observed for the real elution profile at a mobile phase linear velocity of 0.10 cm/s which can be found in Table 4.16.

Profile characteristic	modified constants	Replicate 1
t_G (s)	4741	4711
σ_G (s)	268.8	443.5
τ_G (s)	269.5	295.6
M_1 (s)	5010	5154.5
M_2 ($\times 10^5$ s^2)	1.45	2.84

Table 4.16   The EMG characteristics and confidence limits for the elution of naphthalene on PRP-1 from 85 % MeOH at $u_0 = 0.10$ cm/s. The confidence limits are based on three replicate injections and are calculated at the 95 % level. The information in this table can be compared to data found in Tables 4.15 and 4.17.

Profile Characteristic	Avg. ± 95 % confidence limit
t_G (s)	5500 ± 162
σ_G (s)	169 ± 25
τ (s)	530 ± 116
M_1 (s)	5697 ± 34
M_2 (x 10^5 s^2)	3.11 ± 1.17

the uncertainties in the tri-exponential constants k_3 and n_3 affect the distribution, P3.

Figure 4.28 is an illustration of the effect of the value of n_3 on the shape of the distribution P3 predicted by equation 2.15. The solid line corresponds to the experimentally measured value of n_3 (for Replicate 1). It should be noted that in Table 4.9, the error associated with the term n_3 is very large because n_3 is determined by difference. This large degree of uncertainty leaves a great deal of freedom in attempting to find values of the constants, within experimental error, that will adequately described the observed elution profile. To a first approximation, P3 is an exponential function in k_3 only. (This is not strictly true because the variable $t_{m,3}$, which is a function of n_3, appears in the exponential term of equation 2.15, which describes P3). The curves in Figure 4.28 show that as n_3 is decreased the urve decreases in height but the basic exponential shape of the curve is not changed much, even if n_3 is decreased by as much as 75 %.

This type of behaviour contrasts sharply with the effect that changing k_3 has on P3, which is shown in Figure 4.29. As k_3 decreases, the signal predicted by this term at early times decreases but, at later times, the signal in the tail actually increases. The tail also extends to longer and longer times. From Curve (6) in Figure 4.29B, it can be seen that, in the extreme, an almost horizontal tail is predicted if k_3 is very small.

From these two figures, it is not difficult to imagine the effect of uncertainties in n_3 and k_3 on the overall predicted distribution. Because P3 is not added directly to the distribution due to the other processes but is convolved with P1/2, decreasing the value of n_3 within experimental error will have two effects. First, the influence of P3 will decrease in the main portion of the peak (especially in its rear half), resulting in a narrower and more symmetric main portion. Second, the influence of P3 in the tail will also decrease and the tail will extend to smaller times. Likewise, decreasing the value of k_3 will also have two effects. First, decreasing k_3 within experimental error will result in a decrease in the effect of P3 on the main portion of the peak analogous to the
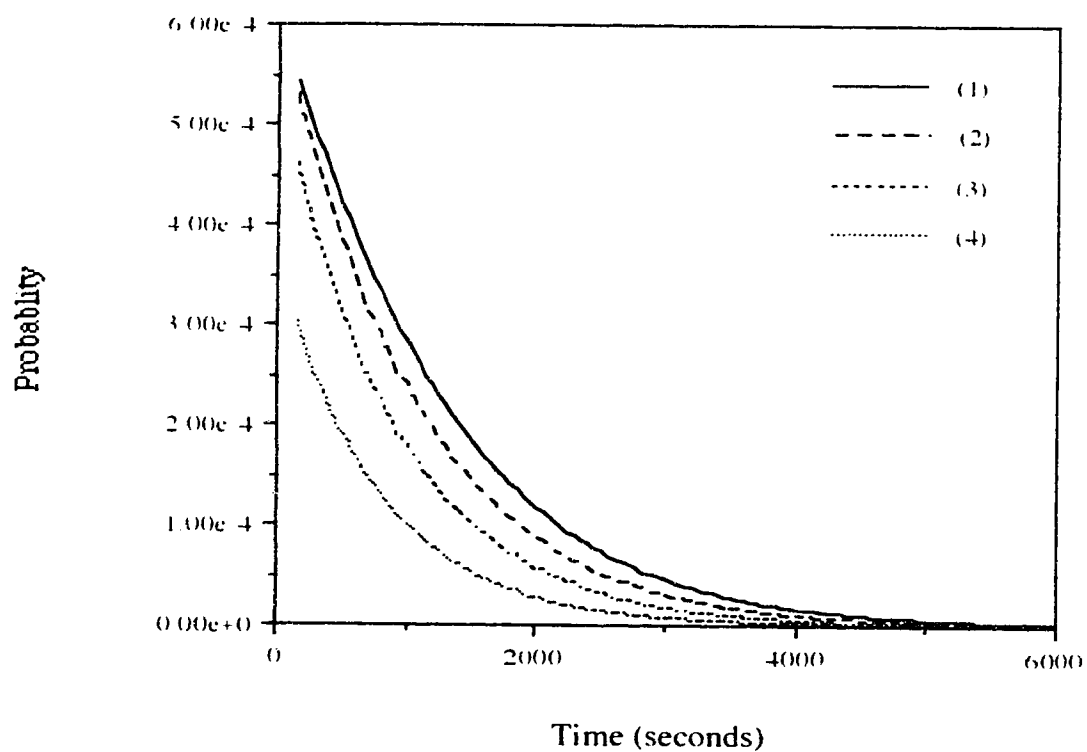
Figure 4.28   The probability distribution. P3 as a function of n_3. The values of n_3 for the three distributions are as follows: (1) $n_3 = 0.353 \times 10^{-7}$ mol/g. (2) $n_3 = 0.265 \times 10^{-7}$ mol/g. (2) $n_3 = 0.177 \times 10^{-7}$ mol/g. (4) $n_3 = 0.089 \times 10^{-7}$ mol/g. These distributions were calculated using $k_3 = 0.0572$ s^{-1} according to equation 2.15.
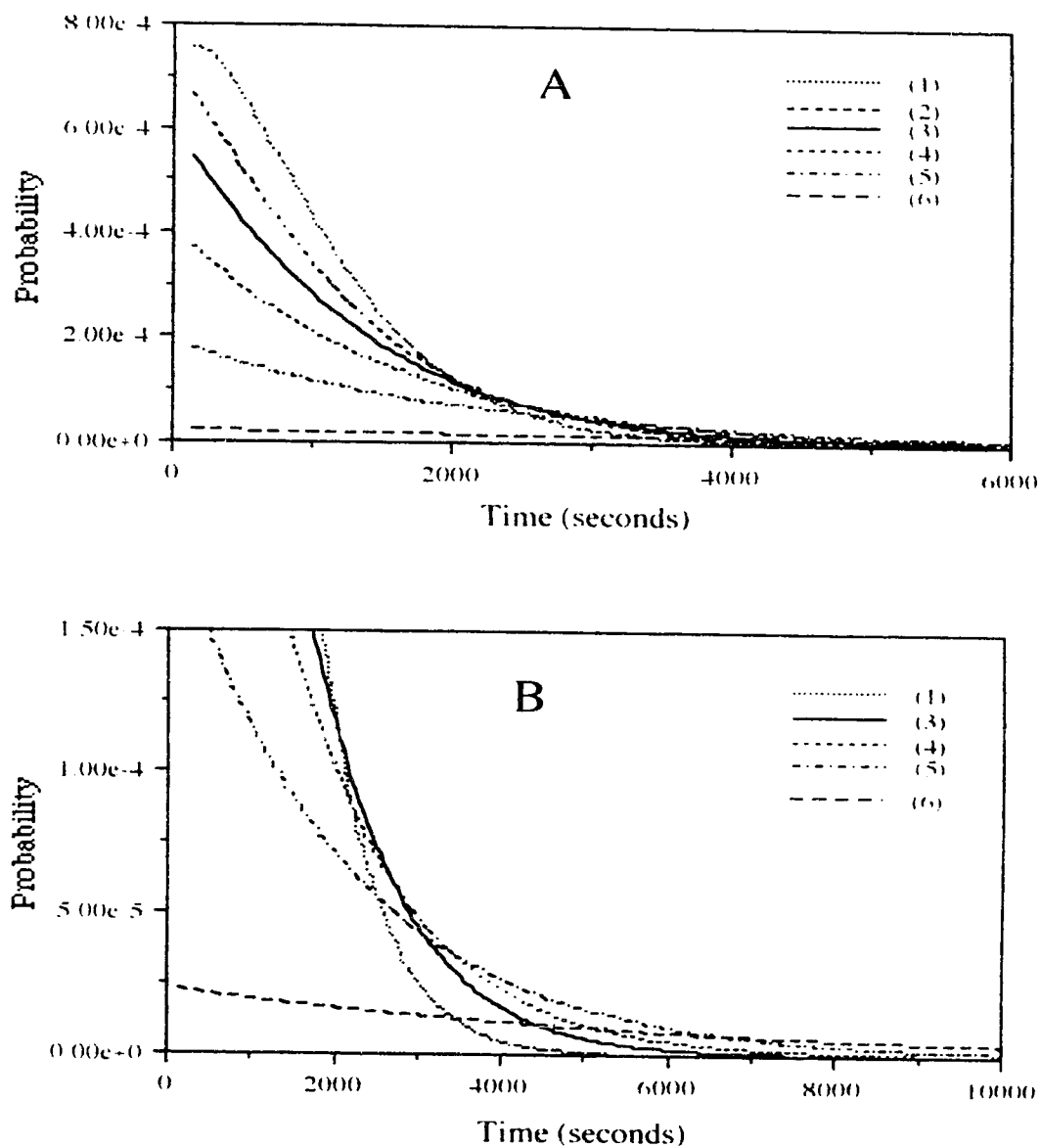
Figure 4.29 The probability distribution P3 as a function of k_3. The values of k_3 for the six distributions are as follows: (1) k_3 = 0.107 s^{-1}. (2) k_3 = 0.0738 s^{-1}. (3) k_3 = 0.0572 s^{-1}. (4) k_3 = 0.0406 s^{-1}. (5) k_3 = 0.0240 s^{-1}. (6) k_3 = 0.0074 s^{-1}. Graph (3) represents P3 predicted using the constants from Replicate 1. In these calculations n_3 = 0.353 x 10^{-7} mol/g. Graph B is a magnification of Graph A at long times Curve (2) is deleted for clarity .

effect of n_3. Second, in contrast to the effect of n_3, as k_3 decreases, the effect of P3 on the tail increases, as can be seen in Figure 4.29 and a tail extending to longer and longer times is expected.

It should be mentioned that the magnitude of error in the constants n_3 and k_3, which appears to be quite large, is not unreasonable in terms of experimental considerations. This term is associated with the portion of the sorption rate curve with exposure times greater than approximately 20 s (see Figure 4.8). In this region, the slopes of tangents to the curve are extremely small and a small degree of scatter in the experimental data can lead to large changes in the constants. Although the amount of scatter in the sorption rate data is small, it cannot be eliminated and relatively large uncertainties in the constants will always be expected.

The errors in these constants mean that there is a large uncertainty in the effect of the slowest kinetic process(es) on predicted peaks. Even in real columns, there is some evidence that the observed effect of the slowest sorption rate process varies with the history of the column, even for a constant set of experimental conditions. For instance, it was observed that, occasionally, chromatograms of naphthalene on PRP-1 were so tailing that the tailing portion appeared to be a nearly horizontal line that was vertically displaced above the baseline which was established before the peak. Such a chromatogram is shown in Figure 4.30. This type of peak was observed for the first injection in a series after the chromatographic column had been idle, at least overnight. If we assume that there are "sites" associated with each of the three sorption processes indicated by the rate curve, such behaviour is consistent with essentially "irreversible" sorption (ie. reversible but very slow to to desorb) on the slowest sites. This would be analogous to the situation in GC where a column may be "primed" by injection of a compound which will bind to strongly sorbing sites, resulting in an improvement in peak asymmetry in injections that follow [4.12]. The difficulty in relating the sorption rate experiment and the tail portion of the elution profile may be, then, a difficulty in
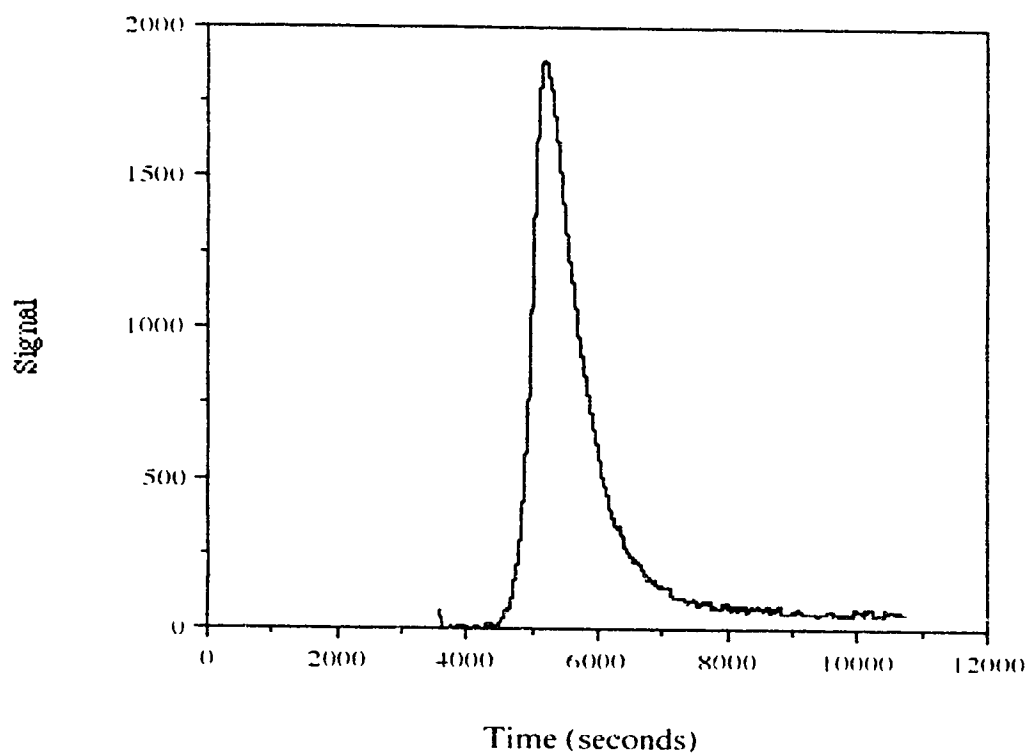
Figure 4.30   Observed elution profile of 1.002 x 10⁻³ M naphthalene on PRP-1 in 85
% MeOH. This profile illustrates the vertically offset horizontal baseline
that was observed in the first run in each series after the PRP-1 column
had been out of use at least overnight.

correctly estimating n_3 for a chromatographic column because the number of "sites" which are available depends not only on the packing itself but on the history of the column.

Assuming that we are attempting to predict the shape of peaks that do not display this sort of baseline, the examination of the individual distribution P3 can give a ball park estimate of the value of the constants that would more accurately predict the elution peak. If the experimental value of k_3 is used, the value of n_3 should be decreased, since the original set of sorption rate constants tends to overestimate the contribution of the slowest term. A modified set of sorption rate constants is contrasted, in Table 4.17, to those for Replicate 1. The major differences in the two sets of sorption rate constants are the much larger value of k_1 and much smaller value of n_3 in the modified set. The overall elution profile predicted using the modified set of tri-exponential constants is shown in Figure 4.31. This provides a much better fit to the observed profile than did the profile predicted from the rate constants associated with Replicate 1.

Also found in Table 4.17 are the EMG constants for the elution profiles predicted by the modified set of constants and by the sorption rate constants from Replicate 1. The most dramatic difference is the decrease in the τ parameter for the peak predicted by the modified set of constants. This peak is much more symmetrical. It also has a σ_G value which is lower by about a factor of 2. These EMG constants can be compared to data in Table 4.16 which show the same parameters for the experimentally observed elution peaks of naphthalene on PRP-1 at the linear velocity of 0.10 cm/s. Both the t_G and τ values for the peak predicted by the modified constants fall within the confidence interval of the same constants describing the observed signal. The agreement for the σ_G value is not as good.

There are several conclusions that can be drawn from the preceding discussion regarding the prediction of elution peaks from sorption rate measurements on

Table 4.17   The tri-exponential constants of Replicate 1 ± one standard deviation are
contrasted with the modified tri-exponential constants which are used to
generate a reasonable (ie. comparable to the observed profile) elution
profile for naphthalene on PRP-1. Also shown are the EMG
characteristics for the profiles predicted by these sets of constants. The
EMG characteristics of the observed profile are shown in Table 4.16.

type of constant	Replicate 1	modified
n_0 (x 10^{-7} mol/g)	2.75 ± 0.017	2.75
n_1 (x 10^{-7} mol/g)	1.70 ± 0.26	2.182
n_2 (x 10^{-7} mol/g)	0.697 ± 0.217	0.480
n_3 (x 10^{-7} mol/g)	0.353 ± 0.49	0.088
k_1 (s^{-1})	2.97 ± 0.38	48
k_2 (s^{-1})	0.642 ± 0.270	0.642
k_3 (s^{-1})	0.0572 ± 0.0166	0.572
t_G for predicted profile (s)	4667	5245
σ_G for predicted profile (s)	426.7	254.2
τ for predicted profile (s)	1048	419.8
M_1 for predicted profile (s)	5715	5499
M_2 for predicted profile (x $10^5 s^2$)	12.80	2.408
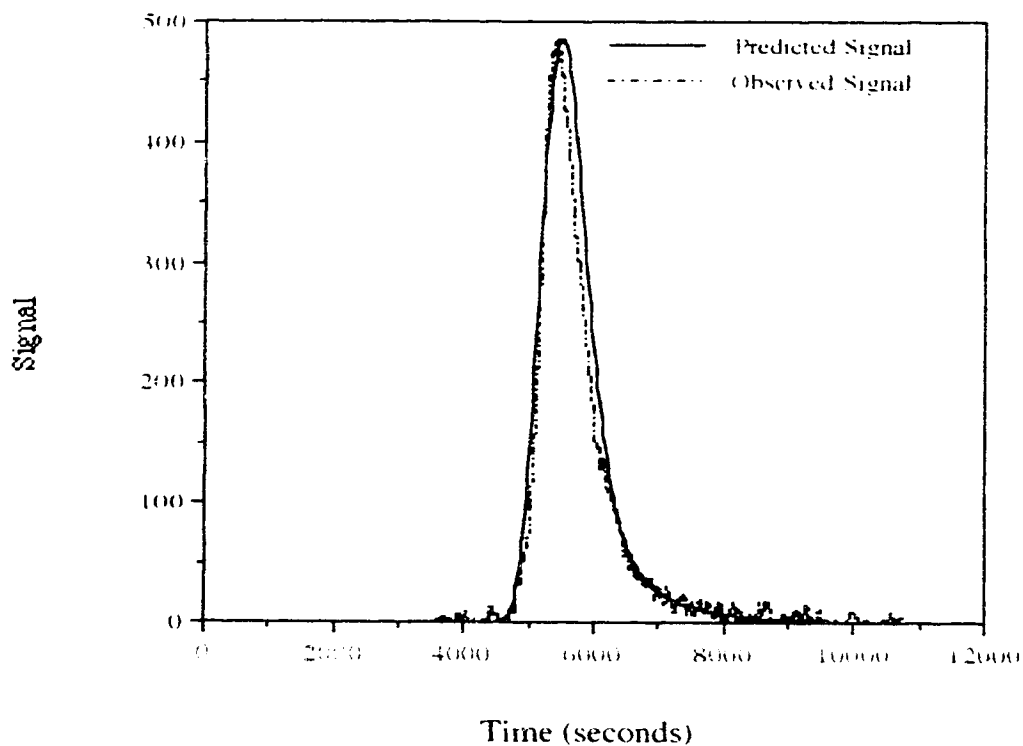
Figure 4.31   The overall distribution described in Section 4.2.6 using the modified
values of the tri-exponential constants that describe the sorption rate
curve. The actual and modified constants are shown in Table 4.17
along with the EMG parameters which fit the peaks predicted by them.
Also shown in that table are the EMG parameters of the observed peak.

microparticle HPLC packings. First, the accuracy and precision of the sorption rate data currently imposes the limit for using the proposed model. The shallow bed experiment provides accurate data for sorption reactions with intermediate rates but at both high and low exposure times, experimental errors can lead to inaccuracies and uncertainties in the constants describing the sorption rate curve. Because of the accuracy and precision limits, the model did not adequately predict the elution curves of naphthalene on PRP-1 using the experimental rate constants. It was shown, however, that using a modified set of tri-exponential constants, a reasonably accurate profile could be predicted. The imaginary rate curve that would be associated with the modified set of data and the experimental rate curve associated with Replicate 1 are compared in Figure 4.32. The major difference between these curves is the absence of the very slowly rising portion of the curve at long exposure times, which is not seen in the rate curve for the modified set of constants. This may mean that the influence of the slowest sorption process on real chromatograms is actually very small.

What the above discussion also reveals is that, taken alone, P2, which is calculated from the region for which data in the rate curve is most accurate, more or less accurately predicts one of the two peak characteristics of interest. That is, naphthalene gives experimentally observed elution peaks that are characteristically highly asymmetric and severely broadened. The constants associated with the intermediate sorption process accurately predict the observed broadened profiles in the main portion of the peak for naphthalene (see Figure 4.19). This gives unambiguous evidence that slow sorption-desorption is the major contributor to bandbroadening for naphthalene on PRP-1. The asymmetry of the peak, however, is not adequately predicted using the sorption rate data from the shallow bed experiments.

The data treatment method was also used to predict elution profiles at different linear velocities. The elution profiles predicted by the experimental tri-exponential constants from Replicate 1 are overlaid over observed naphthalene elution profiles in

The plot shows n(t) (x 10 e-7 mol/kg) on the y-axis (ranging from 0 to 3) versus Time (seconds) on the x-axis (ranging from 0 to 60).

Legend:
— Rate curve with modified constants
-- Observed rate curve

Time (seconds)
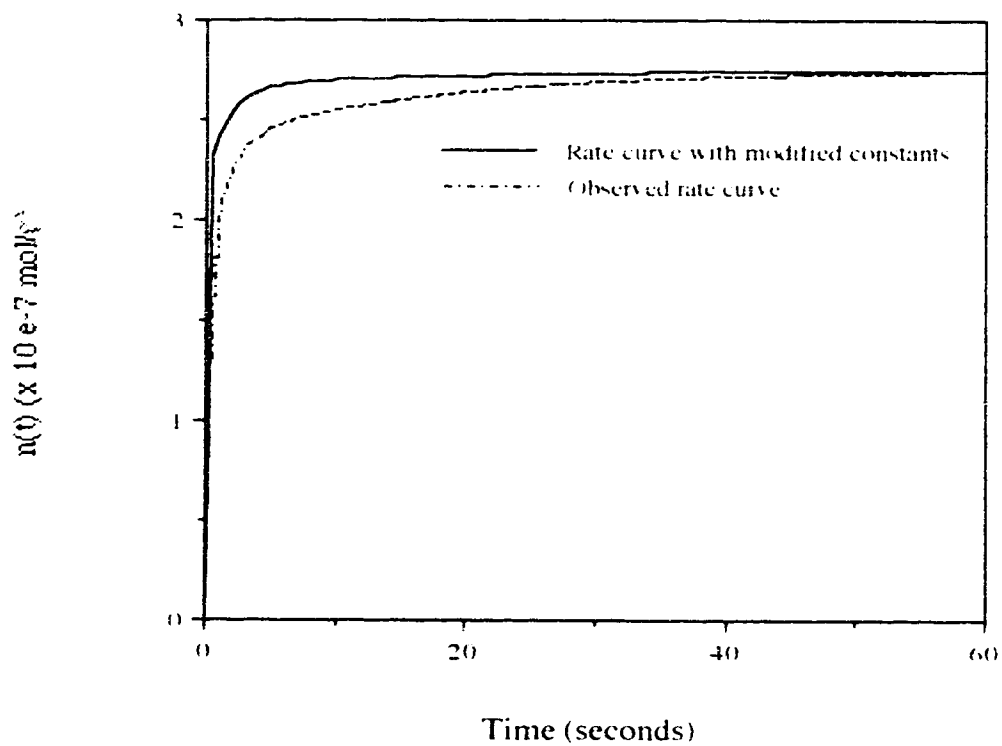
Figure 4.32   The sorption rate curve predicted by the modified tri-exponential

constants in Table 4.17 and the observed sorption rate curve described

by the experimental tri-exponential constants.

Figures 4.33 to 4.35. These represent the peaks at the linear velocities 0.20, 0.30 and 0.40 cm/s respectively. In all cases, the predicted profile has a time of peak maximum less than the observed peak and is much wider and has more tailing. Also illustrated in these figures are the P2 distributions at each linear velocity. Once again, the distribution has been artificially shifted down the time axis so that the peak maximum coincides with the maximum for the observed signal. P2 in all cases gives a better estimate for the main part of the observed peak but the estimate is not perfect. From these figures it is difficult to tell if the agreement between P2 and the observed peak is linear velocity dependent.

In Figure 4.14, it was shown that the elution profiles predicted at $u_o = 0.10$ cm/s from the four replicate sorption rate constants were very similar. Although it has not been shown in the Figure, because all the curves are so similar, it can be concluded that, like the profile predicted by the results of Replicate 1, which was discussed in detail above, all are substantially wider than the observed chromatographic peak and all have peak maxima which occur at shorter times than in the observed peak. In Figure 4.36, the distributions P2 calculated from each of the Replicates are shown along with the observed profile at a mobile phase linear velocity of 0.10 cm/s. In all cases, this distribution is a reasonable approximation of the main part of the observed elution peak.

This section has demonstrated that it is possible to generate elution profiles based on the hypothetical three column model. The profiles, in this case, do not match the observed elution profiles well either in width or asymmetry characteristics. If the tri-exponential constants are modified either within the random error calculated by the non-linear least squares curve fitting program or, in the case of k_1, considering the systematic error in the shallow bed experiment, the predicted profile can be made to better match the observed profile. It appears that the effect of the slow sorption-desorption kinetics associated with the second term in the equation describing the sorption rate curve more accurately predicts the width of the main part of the peak. At
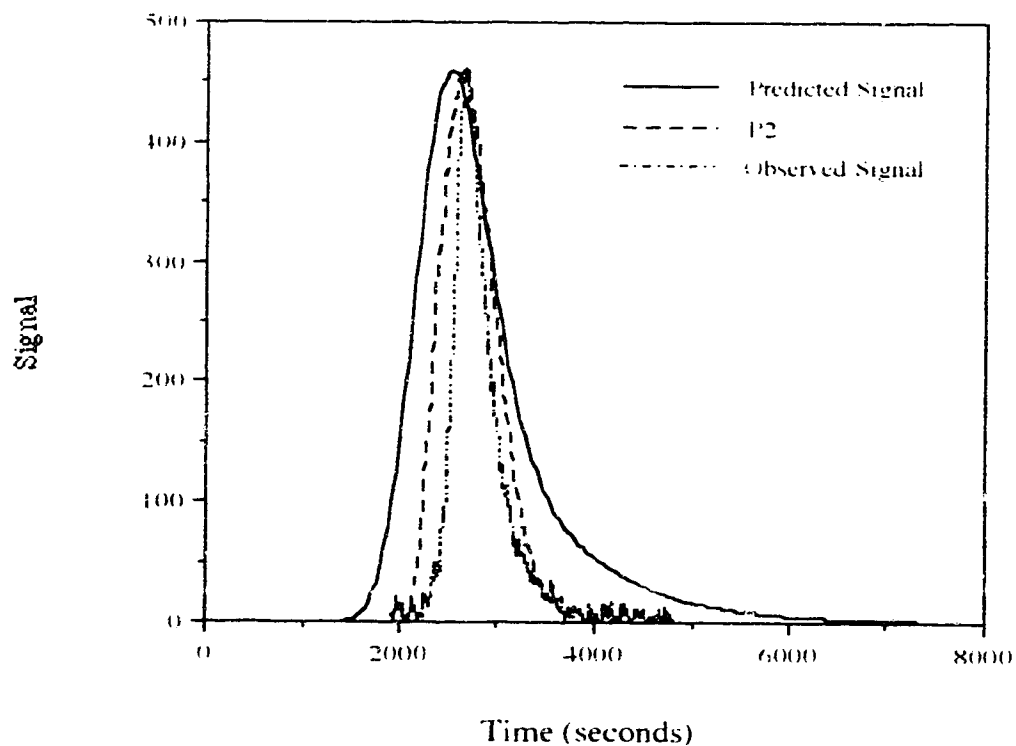
Figure 4.33   The overall distribution predicted from the tri-exponential constants of
Replicate 1 at a mobile phase linear velocity of 0.20 cm/s. The
probability distribution P2, calculated for Replicate 1 at this linear
velocity is illustrated shifted down the time axis so that the maxima
coincides with that of the observed peak. The observed signal is the
result of injection of 2.504×10^{-4} M naphthalene on PRP-1 in 85 %
MeOH.
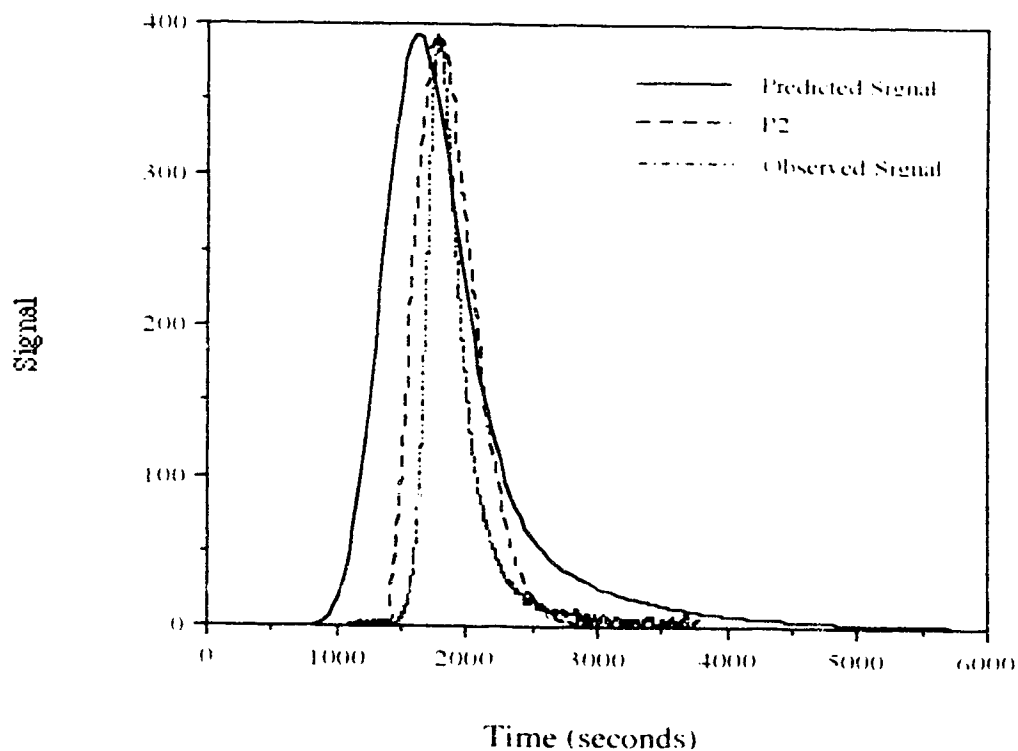
Figure 4.3 4   The overall distribution predicted from the tri-exponential constants of
Replicate 1 at a mobile phase linear velocity of 0.30 cm/s. The
probability distribution P2, calculated for Replicate 1 at this linear
velocity is illustrated shifted down the time axis so that the maxima
coincides with that of the observed peak. The observed signal is the
result of injection of 2.504×10^{-4} M naphthalene on PRP 1 in 85 %
MeOH.
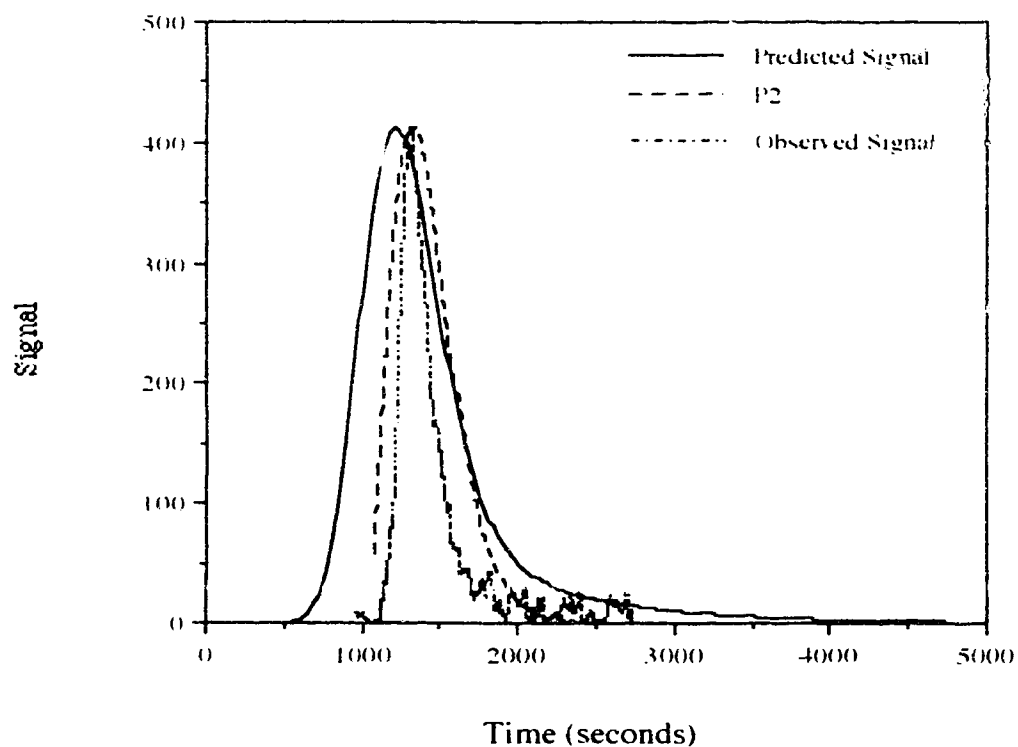
Figure 4.35   The overall distribution predicted from the tri-exponential constants of Replicate 1 at a mobile phase linear velocity of 0.40 cm/s. The probability distribution P2, calculated for Replicate 1 at this linear velocity, is illustrated shifted down the time axis so that the maxima coincides with that of the observed peak.   The observed signal is the result of injection of 2.504 x 10^{-4} M naphthalene on PRP-1 in 85 % MeOH.
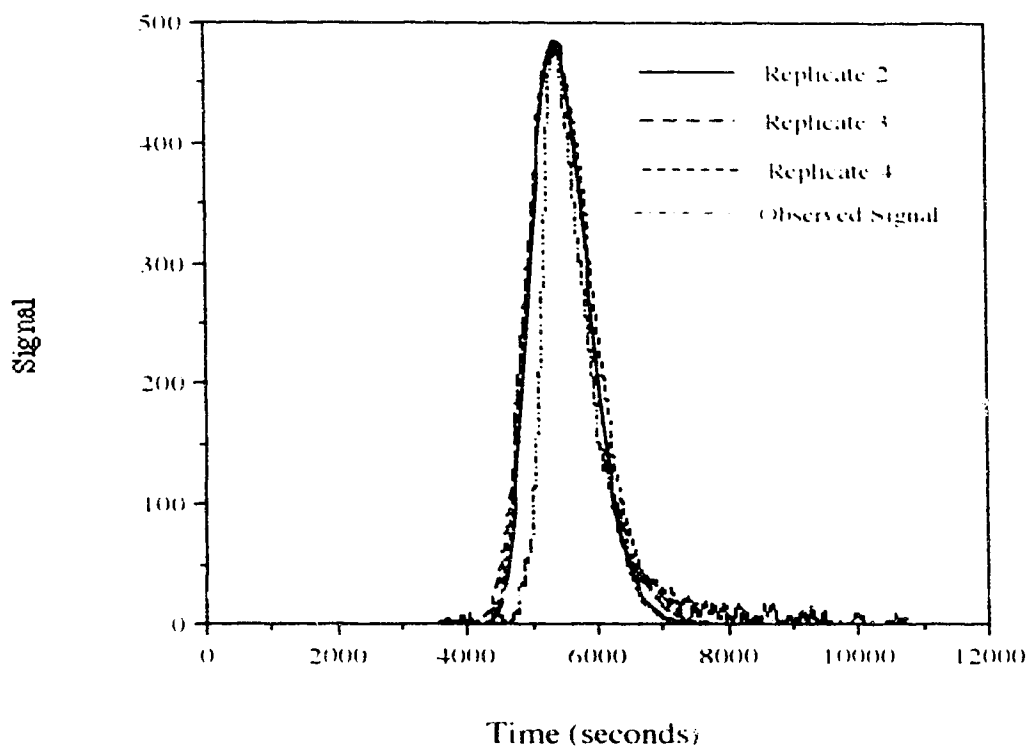
Figure 4.36   The probability distribution P2 calculated from the sorption rate data for
Replicates 2, 3 and 4 at u_0 = 0.10 cm/s. The P2 signals have been
artificially shifted down the time axis so that their peak maxima coincide
with that of the observed signal. The observed signal is obtained by
injection of 2.504 x 10^{-4} M naphthalene on a 15 cm long column.

present the evaluation of the model is limited by the accuracy of the sorption rate data.

4.3   Partisil-10 ODS-3 as a Sorbent

4.3.1   Introduction

A study parallel to those discussed above was conducted with a silica-based stationary phase. The silica-based packing, as previously discussed is a microparticle with characteristics shown in Table 3.1.

4.3.2   Characterization of Elution Profiles on Partisil-10 ODS-3

Figure 4.37 shows a typical chromatogram for naphthalene from a column of the silica-based packing. The peak was obtained at a linear velocity similar to the one used to measure the elution peak of naphthalene from PRP-1, as shown in Figure 4.2. These signals are the output of the ASYST data processing and collecting program. The solvent system used is 52.5% MeOH: an eluent weaker than that used on PRP-1 was necessary to maintain a relatively high k'. as Partisil is a weaker sorbent than the polymeric packing. A discussion of the measured k' value is found in Section 4.3.3.

In comparing the peaks in Figures 4.2 and 4.37, it is pertinent to note that the time scales are different. The naphthalene peak on Partisil is a relatively narrow and symmetric peak compared to the very broad and asymmetric peak on PRP-1. It is interesting that while the peaks eluted from PRP-1 were largely impossible to process using the moments analysis program previously described, no such difficulty was encountered with peaks eluted from Partisil. For comparison's sake, however, the profiles were fit to an EMG function in the manner described in Sections 2.3.8 and 4.2.1.2. Table 4.18 shows the EMG constants and the first and second statistical moments for the elution of a sample of 2.574×10^{-4} M naphthalene at a mobile phase linear velocity of 0.167 cm/s. Table 4.19 gives the same information for three mobile
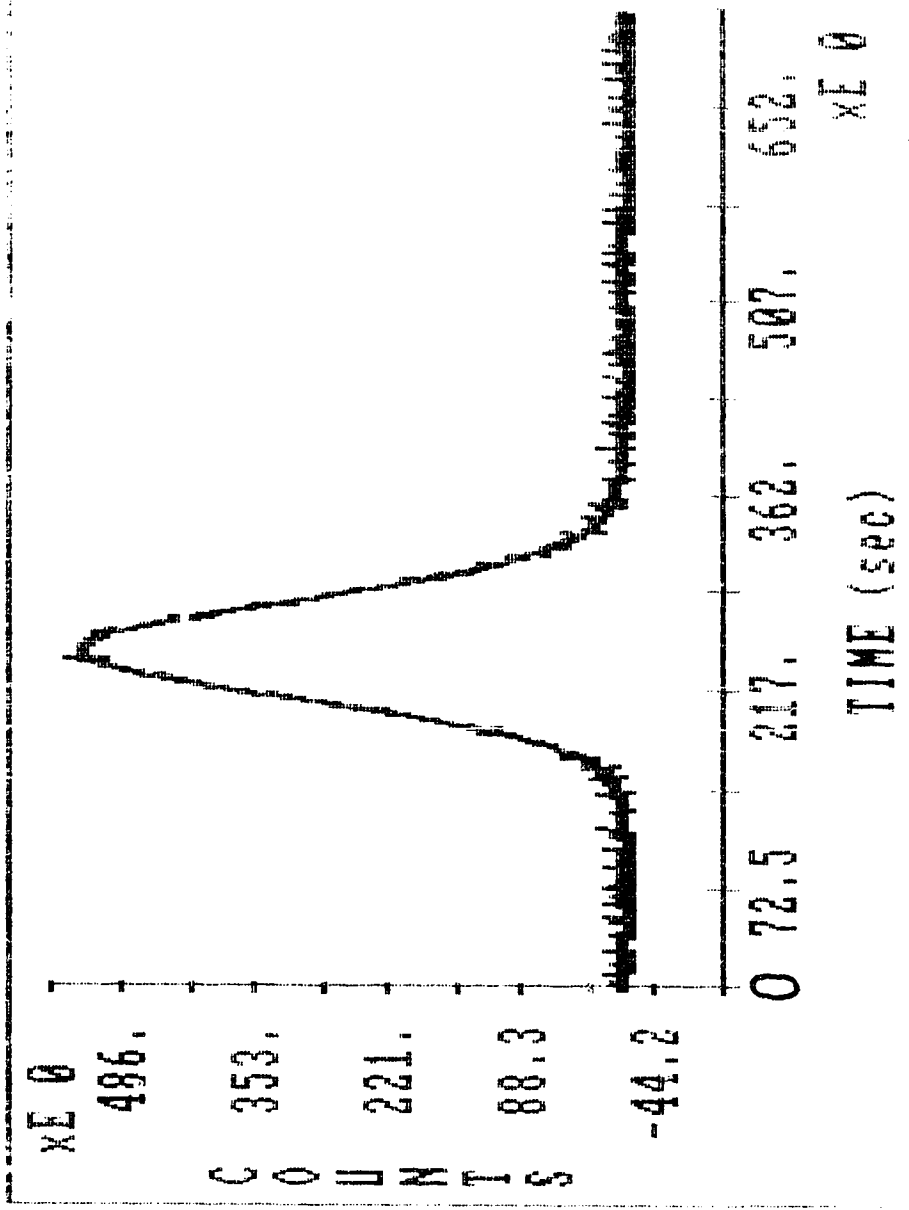
Figure 4.37 Chromatogram of $2.574 \pm 0.0058 \times 10^{-4}$ M naphthalene in 52.5 % MeOH on Partisil-10 ODS-3 with a mobile phase flow rate of 1.0 mL/min. The chromatogram is shown as the unsmoothed output from the data collection program written in ASYST. The zero mark on the time axis corresponds to the initiation of data collection. This zero is acutally 50 minutes after injection. The u_0 in this case is 0.167 cm/s.

Table 4.18   EMG characteristics of elution profile of 2.574 x 10^{-4} M naphthalene in 52.5 % MeOH on Partisil-10 ODS-3 at a mobile phase velocity of 0.167 cm/s.

Run no.	t_G (s)	σ_G (s)	τ (s)	M_1 (s)	M_2 (s^2)
1	3357	32.53	20.33	3373	1472
2	3375	32.59	19.91	3391	1454
3	3375	32.59	19.86	3391	1455
avg.	3368	32.54	20.03	3385	1460
RSD (%)	1.0	0.05	1.3	0.30	0.67

Table 4.19   EMG characteristics of experimentally observed chromatograms of 2.574 x 10^{-4} M naphthalene in 52.5 % MeOH on Partisil-10 ODS-3 at three mobile phase linear velocities, u_0, shown as ± one standard deviation. The information for $u_0 = 0.167$ cm/s was given previously in Table 4.18.

u_0 (cm/s)	0.167 ± 0.009	0.27 ± 0.01	0.35 ± 0.01
t_G (s)	3368	2062	1633
RSD t_G (%)	1.0	0.17	0.29
σ_G (s)	32.54	21.89	18.1
RSD σ_G (%)	0.05	0.29	2.2
τ (s)	20.03	13.31	11.53
RSD τ (%)	1.3	1.5	3.3
M_1 (s)	3385	2072	1643
RSD M_1 (%)	0.30	0.14	0.28
M_2 (s^2)	1460	648	464
RSD M_2 (s^2)	0.67	0.33	0.13

phase linear velocities. In general, the constants are highly reproducible, with RSD values for each being under 4 %.

A comparison of Table 4.7, which shows the EMG parameters of elution profiles on PRP-1, and Table 4.19, which shows the same parameters of elution profiles on Partisil-10 ODS-3, shows that the EMG fitting routine gives better precision with the relatively narrow, symmetrical profiles eluted from the silica-based packing. Because both the k' of naphthalene and the linear velocity of the mobile phase are different for the two columns, direct visual comparisons of the peaks in Figure 4.2 and 4.37 do not reveal the relative bandbroadening experienced by naphthalene on these two columns. Nor do direct comparisons of the parameters σ_G and τ between Tables 4.7 and 3.19. Qualitatively, though, the width of the parent Gaussian peak is larger on the PRP-1 profiles at comparable linear velocities. There is also an approximately order of magnitude difference in the degree of tailing, as expressed by the parameter τ. The two packings can be directly compared by examining the plate heights as calculated by equation 4.2. A plot of H vs u_o for PRP-1 was shown in Figure 4.5. A comparable plot for the Partisil column is shown in Figure 4.38. This plot illustrates the good precision associated with the EMG characteristics of the profiles eluted from Partisil. Notice the difference in the vertical axis in the two plots. There is almost two orders of magnitude difference in the plate heights. These plots illustrate the large difference in efficiency obtained on the two packings.

4.3.3   Equilibrium Sorption of Naphthalene on Partisil-10 ODS-3

4.3.3.1 Measurement of the Sorption Isotherm of Naphthalene on Partisil-10 ODS-3

The isotherm for the sorption of naphthalene on Partisil-10 ODS-3 in 52.5 % MeOH was measured by the column equilibration method described in Section 3.4.4. The isotherm, illustrated in Figure 4.39, is linear in the region studied, for the
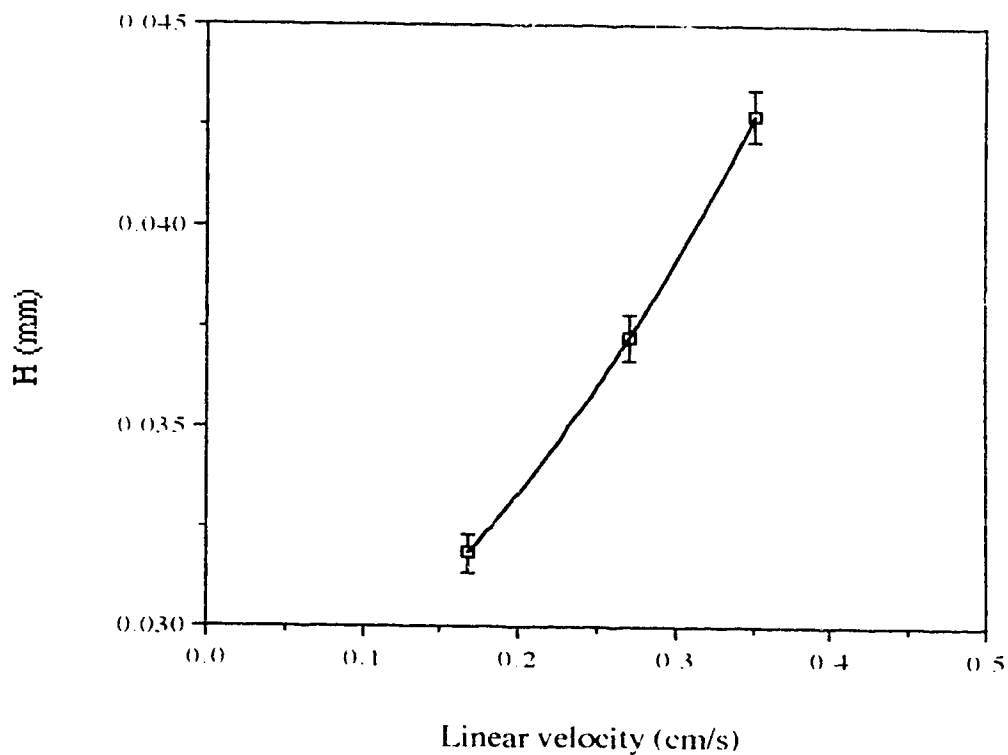
Figure 4.38   Plot of height equivalent of a theoretical plate against mobile phase linear

velocity for napthalene on Partisil-10 ODS-3 in 52.5 % MeOH. The

plate height, H, calculated from equation 4.2. The data shown represent

the average of three injections at each linear velocity. The error bars are

1.5 % of the average plate height at each linear velocity.

concentration range from 0 to at least 4 x 10^{-5} M. The linear regression constants are shown with confidence limits in the caption to the figure.

The slope of the isotherm, D, in L/g, was used to calculate the capacity factor, k' for the chromatographic column described above using equation 4.3.

$$k' = D \frac{W}{V_m}$$

eqn. 4.3

In this case, W, the weight of stationary phase in the chromatographic column, is determined from the packing density, which is, according to the manufacturer's information, "approximately" 0.55 g/mL. The accuracy of this figure is not known: the value is quoted for all bulk Partisil packings. Specific information for the column is not available. The error in this term was assumed to be ± 0.01 g/mL. W was calculated by multiplying the density by the volume of the overall column (calculated from column dimensions). An error of 1 % in each of the column dimensions was assumed. W was therefore calculated to be 2.28 g with an error of ± 0.07 g, calculated by propagation

A nominal hold-up volume, V_m, was quoted by the manufacturer as 2.67 mL. The hold-up volume for the column was measured by injection of $Ca(NO_3)_2$ to be 2.39 ml, with an error of 0.12 mL.

From the isotherm, D = 3.47 ± 0.08 x 10^{-2} L/g. Therefore, k' was calculated to be 33.1 with an error of 2.0. Therefore, the value of k' measured from the sorption isotherm is 33.1 ± 4.3 at the 95 % confidence level. The relatively large uncertainty is a reflection of propagation of error from the column characteristics.

4.3.3.2   Calculation of k' from Elution Profiles of Naphthalene on Partisil-10 ODS-3

Elution profiles of naphthalene on Partisil-10 ODS-3 were fit to an EMG function as previously discussed in Section 4.2.1.2. The capacity factor as calculated according to equation 4.4 has a value of 21.81 ± 0.06. The high degree of precision
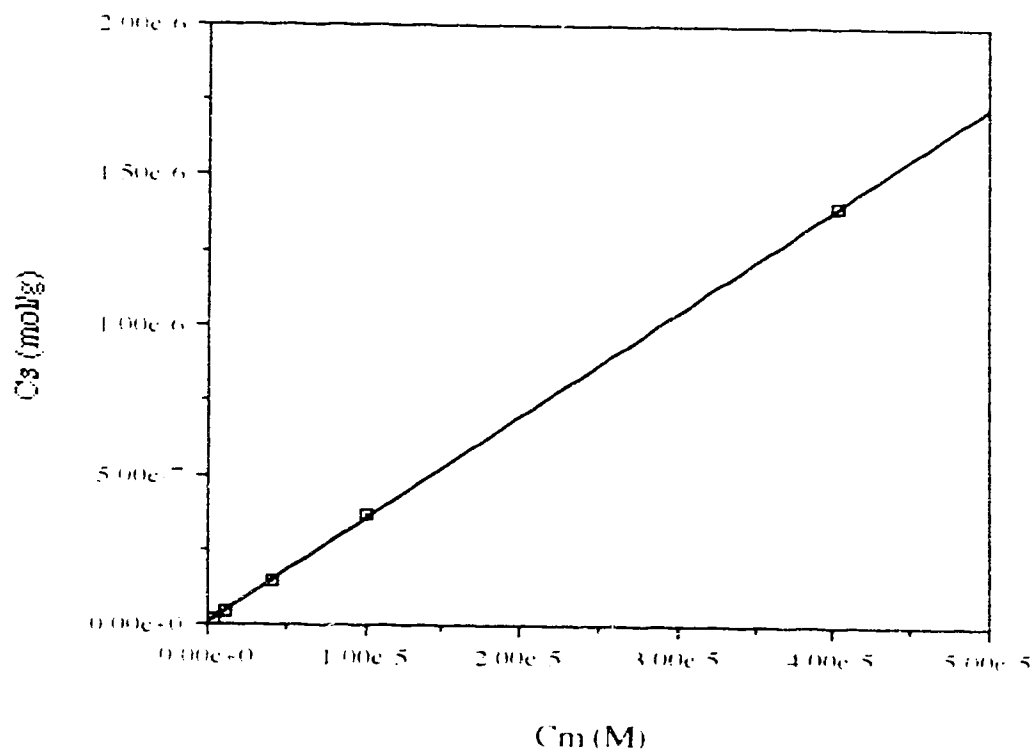
Figure 4.39   Sorption isotherm for napthalene on Partisil-10 ODS-3 in 52.5 %
MeOH. The isotherm is linear in the region studied. The isotherm has
an intercept of 9.08 ± 13.27 x 10^{-9} mol/g and a slope of 3.471 ± 0.085
x 10^{-2} L/g. The slope is used to determine the k' of napthalene under
these conditions.

indicates that the EMG curve fitting routine gives reliable values of the profile characteristics.

The agreement between the two calculated values of k' is rather poor. The capacity factor of 33.1 ± 4.3 determined from the sorption isotherm is higher than that calculated from the elution profiles. This may be due to inaccurate column characteristics such as the manufacturer's "approximate" value of the packing density, which is not known to the user with any accuracy.

4.3.3.3 The Effect of Changing the Solvent Composition on the Diffusion

Characteristics and Bandbroadening of a Naphthalene Sample Zone

The use of a weaker eluent on ODS than on PRP-1 was designed to maintain a relatively high k' on the reversed-phase packing. The large k' value is necessary so that mass transfer characteristics which are k' dependent will be comparable for the compound on the two packings. One difficulty in changing the solvent composition is that diffusional characteristics of the solute are affected, which could affect the bandbroadening. MeOH/H$_2$O solvent mixtures have a viscosity which varies with composition. The viscosity changes for MeOH/H$_2$O mixtures are shown in Figure 4.40 [4.13]. The viscosity of a solvent, η, is related to the diffusion coefficient D$_m$, by the Wilke-Chang equation, shown as equation 4.14 [4.14].

$$D_m = \frac{7.4 \times 10^{-8}(\psi_s M_s)^{0.5} T}{\eta(V_a)^{0.6}}$$

eqn. 4.14

The factor, ψ_s, is the "association factor" of the solvent S, which has a value of 2.6 for water and 1.9 for MeOH. M$_s$, is the molecular weight of the solvent. For mixed solvent systems, the term ($\psi_s M_s$) is equal to he average values of $\psi_s M_s$ for each constituent solvent weighted according to their volume fractions. The diffusion coefficient is temperature dependent; T is the temperature in Kelvin. V$_a$ is the molar
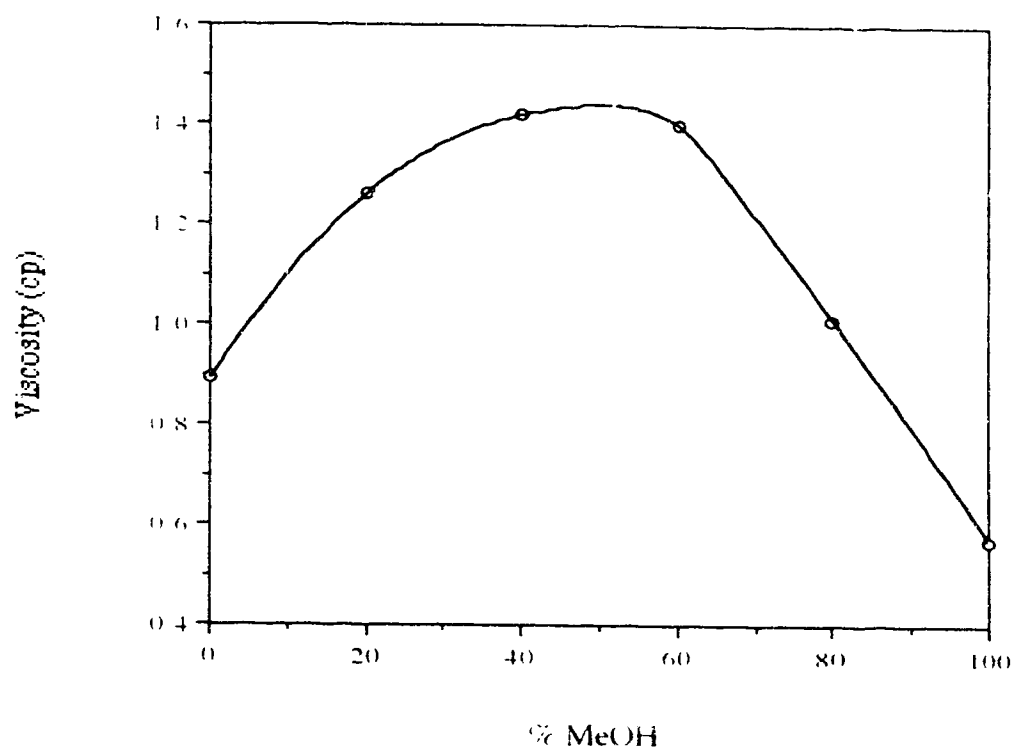
Figure 4.40   Viscosity of MeOH/H₂O solutions as a function of MeOH content
[4.13].

volume of the solute a, which was calculated from the density, ω', of the solute and MW, the molecular weight of the solute according to equation 4.15.

$$V_a = \frac{MW}{\omega'}$$

Naphthalene, with a molecular weight of 128.19 g/mol and a density of 1.0253 g/ml, as measured at 20 °C [4.15], has a calculated molar volume of 125 ml/mol. The diffusion coefficient of naphthalene, as calculated by equation 4.14 is shown in Figure 4.41. The diffusion coefficient of naphthalene in 52.5 % MeOH is read off the curve as 0.64 x 10^{-5} cm^2/s and in 85 % MeOH, it is read off the curve as 1.04 x 10^{-5} cm^2/s. The mass transfer terms in the overall bandbroadening equation that depend on the diffusion coefficient are the longitudinal diffusion contribution (equation 2.2), the resistance to mass transfer in the mobile phase term (equation 2.4), and the resistance to mass transfer in the stagnant mobile phase (equation 2.7). Previously, the longitudinal diffusion term was shown to be negligible for HPLC conditions. The plate height contribution due to the resistance to mass transfer term in the mobile phase is inversely proportional to the diffusion coefficient. In 52.5 % MeOH, this contribution is expected to be larger than in 85 % MeOH. The resistance to mass transfer in the stagnant mobile phase is also inversely proportional to the diffusion coefficient. The value of this term is expected to increase with a decreasing diffusion coefficient. In other words, the rate of diffusion through the stagnant mobile phase should be proportional to the diffusion coefficient. As discussed in the previous section, the plate height for Partisil columns is much smaller than for similar polymeric columns, even when using a solvent with higher viscosity. This is the opposite of what is predicted simply on the basis of the change in diffusion coefficients. Thus, the observed dramatic decrease in column efficiency between Partisil and PRP-1 is not due to the fact that the diffusion coefficient in 52.5 % MeOH is lower than that in 85 % MeOH.
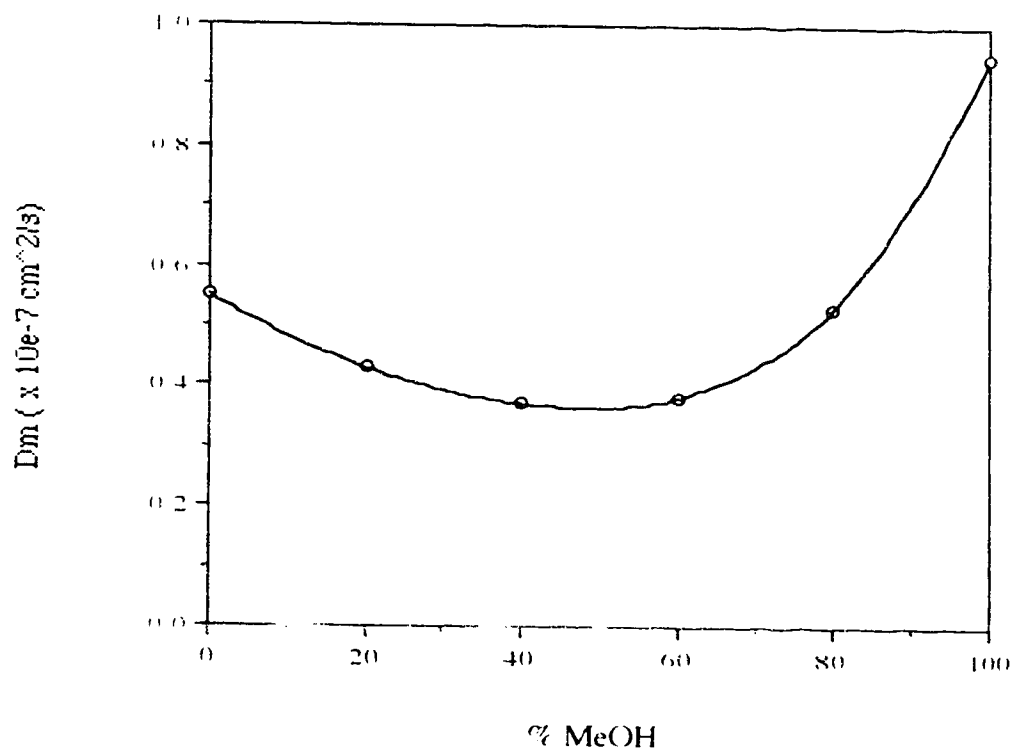
Figure 4.41   Diffusion coefficient of napthalene as calculated from the Wilke-Chang
equation [4.14] assuming that the molar volume of napthalene is 125
mL/mol.

4.3.4   Sorption Rate of Naphthalene on Partisil-10 ODS-3

In order to measure the sorption rate of naphthalene on Partisil-10 ODS-3 using the technique described in Section 3.4, some additional considerations were necessary. Because of the increased viscosity of the solvent in comparison to that used for the PRP-1 sorption experiments, the possibility of not meeting shallow bed conditions increased. The pump used to deliver the sample solution was a constant pressure pump, limited by the regulator on the nitrogen source tank to 120 psi. For 85 % MeOH, this pressure was sufficient to deliver solvent at a rate of approximately 0.3 ml /s to the shallow bed. As seen in Figure 4.40, the viscosity of MeOH/H_2O mixtures reaches a maximum around 50 % MeOH content, implying that a lower flow rate will be achieved with the constant pressure system set at the same pressure. Therefore, in an attempt to meet shallow bed conditions, the height of the shallow bed was decreased decreasing the weight of packing used) in order to minimize the resistance to flow to minimize the possibility of axial concentration gradients during exposure. The characteristics of the shallow bed used for the experiments discussed below are shown in Table 3.2.

A typical sorption rate curve measured on Partisil is shown in Figure 4.42. The rate curve fits a bi-exponential equation of the form given in equation 2.17.

$$n(t) = n_0 - n_1 e^{-k_1 t} - n_2 e^{-k_2 t}$$

eqn. 2.17

Assuming for the moment the the sorption rate is independent of solvent composition, the contrast between this curve and the curve for sorption on PRP-1 (Figure 4.8) is striking. First of all, as previously mentioned, the curve on Partisil can be fit to a bi-exponential equation of the form shown in equation 2.17. The bi-exponential rate constants and their relative standard deviations are given in Table 4.20. These may be comped to the tri-exponential constants of the rate curves on PRP-1 shown in Table 4.12. In the case of sorption on Partisil, the curve appears to reach the
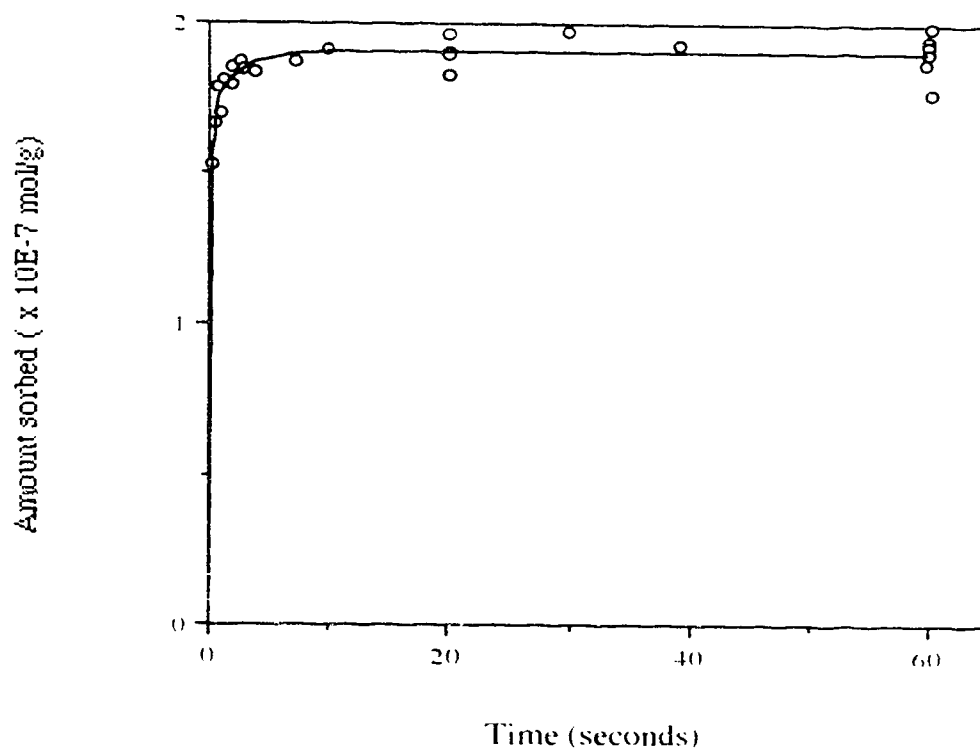
Figure 4.42   Sorption rate curve for Napthalene on Partisil-10 ODS 3 in 52.5 %
MeOH. The experimental data point (o) are overlaid by a solid line
representing the bi-exponential function that fits them. The tri-
exponential constants for this sorption rate curve are shown in Table
4.20.

Table 4.20   Bi-exponential constants describing the sorption rate curve of 5.255 x 10^{-6} M naphthalene in 52.5 % MeOH on Partisil-10 ODS-3. The constants shown are for the curve which fits the experimental data in Figure 4.42. The standard deviation is the error in the constant of interest as calculated by the curve fitting routine. The relative standard deviation is expressed in terms of percent .

constant	value	standard deviation	relative standard deviation (%)
n_o (x 10^{-7} mol/g)	1.910	0.031	0.78
n_1 (x 10^{-7} mol/g)	1.707	0.089	5.2
n_2 (x 10^{-7} mol/g)*	0.203*	0.120	59.1 %
k_1 (s^{-1})	6.76	1.30	19.2
k_2 (s^{-1})	0.39	0.27	62.8

*n_2 is determined by difference where $n_2 = n_0 - n_1$.

limiting value of n_0 much faster than the curve of the polymeric phase. Examination of the "rate constants" in Table 4.20 shows that the smallest rate constant, which contributed the gently sloping portion of the rate curve is absent for Partisil. The equilibrium value is reached relatively quickly on Partisil. The relative contributions of the two terms to the overall rate curve on Partisil are shown in Figure 4.43.

Although the first two rate constants are not very different on the two packings, the relative contribution of each to the overall sorption curve is very different. This can be seen in comparing the fractional "number of sites" associated with each term.

For Partisil: $n_1/n_0 = 0.89$ and $n_2/n_0 = 0.11$

For PRP-1: $n_1/n_0 = 0.62$ and $n_2/n_0 = 0.25$

The relative contributions of the two terms to the overall rate curve on Partisil are shown in Figure 4.43. The majority of sites are associated with the faster process and the majority of the sorption rate curve is determined by the term containing the larger rate constant. Before comparing the rate constants for the two rate curves, an examination of the experimental errors in the sorption rate measurement on Partisil is indicated.

It is unlikely that shallow bed conditions were met in this experiment. In Section 4.2.4, the initial rate of sorption was measured at different linear velocities through the shallow bed on PRP-1. On PRP-1 using a solvent of 85 % MeOH, a u of approximately 14 cm/s was achievable. At that linear velocity, it was not possible to demonstrate that shallow bed conditions had been achieved. Because a solvent system of 52.5 % MeOH was used for the Partisil, the flow rate achievable through the shallow bed is much less. A maximum u of about 9.8 cm/s is achievable in this system. Other works [2.22] suggest that the sorption on reversed-phase packings is much faster than the slowest sorption time possible. The consequence is that the sorption will change the solution concentration and a concentration gradient may well be established along the axis of the shallow bed, causing error in the rate curve at low
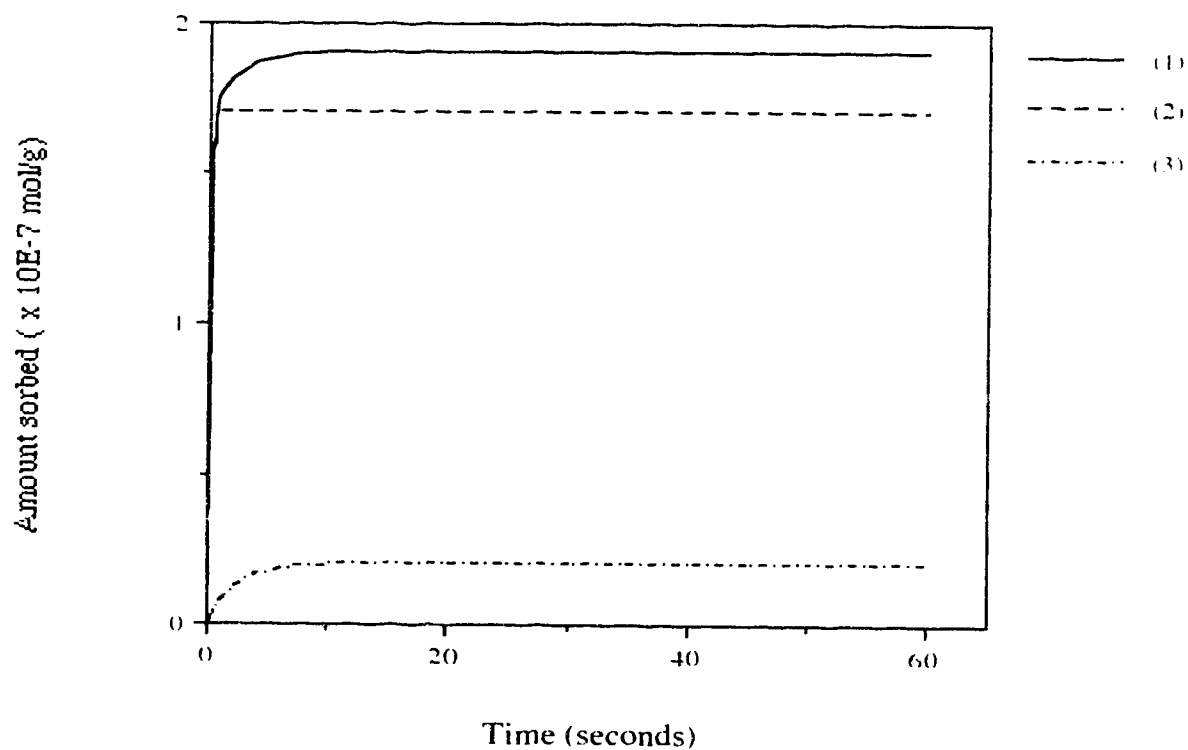
Figure 4.43   Contributions of the two exponential terms to the overall sorption rate
curve of Napthalene on Partisil-10 ODS-3 in 52.5 % MeOH. The
curves are labelled as follows: (1) the overall bi-exponential :urve; (2)
the contribution to the curve from the first term in the bi-exponential; (3)
the contribution to the curve from the second term in the bi-exponential.

exposure times.

Figure 4.42 suggests another experimental difficulty in using Partisil as the packing material. The smallest exposure time that is accessible is approximately 0.35 s, a time limited by how quickly the shallow bed can be moved in and out of the flowing sample stream by the lever system. At this time, the amount sorbed is approximately 85 % of the limiting value. Even if shallow bed conditions were met, because much of the sorption rate curve is inaccessible, the errors associated with the curve fitting process can be expected to be relatively large. For sorption on PRP-1, the reaction proceeded only to about 50 % of the limiting value at the shortest possible exposure times. As in the case of sorption on PRP-1, the experimental uncertainty in the fastest term of the bi-exponential equation may be large. Because the variables are not independent, the second term is also likely to be affected by this error. In Table 4.21, for the three replicate experiments, the random error associated with k_2 in the curve fitting alone is over 5%. These factors combine to cause a negative bias and a relatively large uncertainty in the sorption rate measurements. That is, the actual sorption is faster than the measured rate.

Bearing in mind the above possible sources of error associated with the measurement of sorption on the silica-based packing, the elution profiles were predicted using the model described in Chapter 3. This exercise is described in the next section.

The sorption rate data was also used to calculate the capacity factor of naphthalene on the reversed phase packing as discussed in Section 4.2.3. The value of n_0 is the amount of naphthalene sorbed at infinite exposure time, or at equilibrium. Table 4.21 shows the n_0 values for three replicate sorption rate experiments where the weight of the shallow bed is 1.06 ± 0.05 mg. The average n_0 value is 2.01×10^{-7} mol/g. The quantity C_s was determined from equation 4.13 where $v_p = 0.57$ mL/g (see Appendix 2) and $C_m = 5.255 \times 10^{-6}$ M. The quantity D is from the ration C_s/C_m to be 3.77×10^{-2} with an error of 0.28×10^{-2} L/g. For the HPLC column discussed above,

Table 4.21   A comparison of the bi-exponential constants of three replicate runs of the measurement of the sorption rate of naphthalene on Partisil from 52.5 % MeOH. The relative standard deviation is shown in brackets below the value of the constant.

Replicate	1	2	3
n_0 (x 10^{-7} mol/g)	1.908 (1.1 %)	1.910 (0.78 %)	2.21 (0.62 %)
n_1 (x 10^{-7} mol/g)	1.69 (2.7 %)	1.71 (5.2%)	2.08 (1.3 %)
n_2 (x 10^{-7} mol/g)*	0.218* (30.6 %)	0.200* (52.0 %)	0.130* (21.8 %)
k_1 (s^{-1})	7.25 (18.1 %)	6.76 (19.2 %)	4.46 (5.7 %)
k_2 (s^{-1})	0.164 (66.5 %)	0.394 (62.8 %)	0.147 (56.3%)

*n_3 is determined by difference where $n_2 = n_0 - n_1$

k' calculated by equation 4.3 is therefore 35.4 with an error of ± 3.4. The 95 % confidence limit is ± 8.4. The large degree of uncertainty is the result of propagation of error from the packing characteristics and the relative small number of replicate measurements.

It is impossible to distinguish a statistically significant difference between the value for k' evaluated in this manner and the value 3.1 ± 4.3 determined from the sorption isotherm. The value 21.81 ± 0.06 determined from the chromatograms is significantly different than these two values. Elution chromatography does, however, provide the most precise measurement of k'.

4.3.5 Prediction of Elution Profiles from Sorption Rate Curves of Naphthalene on Partisil-10 ODS-3

The results of the three replicate sorption rate experiments shown in Table 4.21 were used to predict the profile of naphthalene eluting from a Partisil-10 ODS-3 column according to the model discussed in Chapter 3. In this case, the elution column is modelled by two hypothetical columns. In the first column, the sorption process is described by the constant k_1. In the second column, the sorption process is described by the constant k_2. In each column, the non-interacting fraction of sample, Φ, passing through the column, can be calculated. It is found, as discussed in detail below, that only in the second column does a significant fraction of sample molecules pass through without undergoing at least one sorption-desorption cycle. The complete data treatment is therefore that which is appropriate for the case described fully in Section 2.3.5.

Briefly, the distribution due to the sorption process in the first column, P1 is calculated using the approximation equation 4.13. This is appropriate, as k_1 is relatively large and Φ_1 approaches zero at all linear velocities of interest. The distribution P2, due to sorption is calculated using equation 2.15. For the three replicate runs of the sorption rate experiment, these distributions are illustrated in

Figure 4.44. Note that although k_2 for the second term is on the same order of magnitude as found on PRP-1, the distributions P2 on the two packings appear to be much different. This is due primarily to the small fraction of sites associated with this term on the ODS. The distributions P1 and P2 are then convolved to get P1/2, the distribution profile of sample that passes through both columns after undergoing at least one sorption-desorption cycle of each type of process. However, because some sample will pass through the column without undergoing the slowest process, the distribution P1 is scaled and added to P1/2 to obtain the final predicted elution profile.

Table 4.22 shows the Φ_2 values for the three replicate experiments at the lowest linear velocity studied, 0.167 cm.s. For Replicates 1 and 3, 7 and 29 % of the sample respectively will not interact with the second column and for Replicate 2 only 0.26 % does not interact with the second column. As the value of Φ_2 decreases, the method of predicting elution profiles will still be valid because of the scaling of the area of the profiles. If Φ_2 is very small, almost all the sample will undergo both sorption processes and, because of the scaling of the profiles P1/2 and P1 before addition, the overall profile will approach that of P1/2. This is illustrated in Figure 4.45 where graph A shows the scaled distribution P1 and P1/2 for Replicate 1 where $\Phi_2 = 0.07$ and graph B shows the same distributions for Replicate 3 where $\Phi_2 = 0.29$. By inspection, it is obvious that the addition of P1 in either of these cases alters the shape of P1/2 very little. Note that as u_o increases, the fraction Φ_2 will also increase because at higher linear velocities, the samples stay in the column for less time and are therefore less likely to be sorbed.

The overall elution profiles calculated from these sorption rate curves show the same basic characteristics as those predict by the sorption on PRP-1 in comparison to actual observed elution peaks. The profile predicted using the constants for Replicate 2 (see Table 4.21) is shown in Figure 4.46 along with the observed elution profile. Once again, the predicted profile is much wider than the observed signal. While the time of
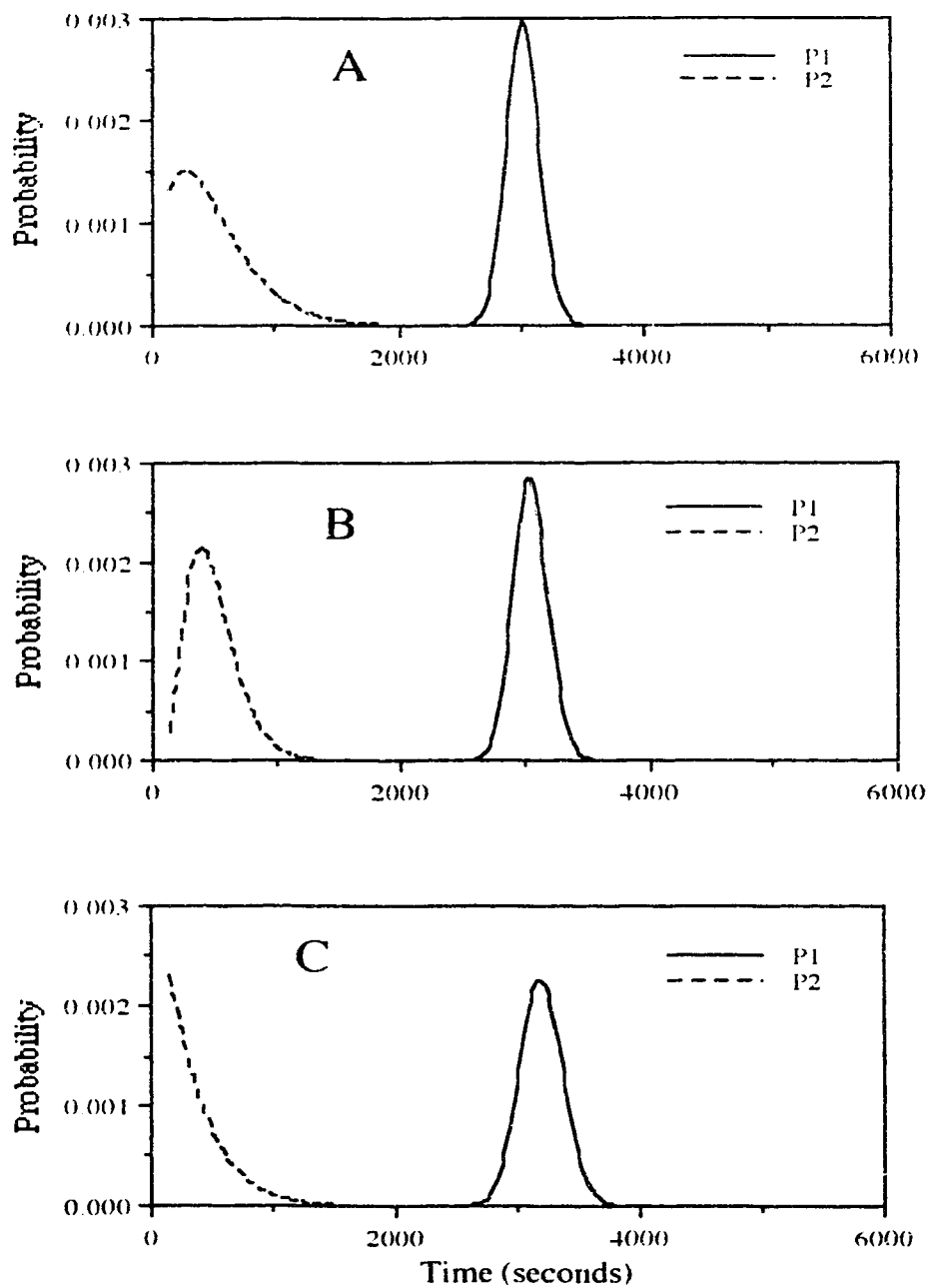
Figure 4.44   The probability distributions P1 and P2 for napthalene on Partisil.
Curves A, B and C correspond to the results using the constants for
Replicates 1, 2 and 3 from Table 4.21 respectively.

Table 4.22   The fraction Φ_2. which represents the fraction of sample which does not undergo at least one sorption-desorption cycle in the hypothetical column 2 representing the slowest sorption process at $u_o = 0.167$ cm/s. The sorption process discussed here is for naphthalene on Partisil-10 ODS-3. The values of the fraction are significant and the data treatment process is therefore applicable at this lowest linear velocity studied.

Replicate	Φ_2
1	0.0707
2	0.00257
3	0.293

A

Probability

0.02

0.01

0.00

- - - - - PI 2
——— PI

0   2000   4000   6000

Time (seconds)

B

Probability

0.004

0.003

0.002

0.001

0.000

- - - - - PI 2
——— PI

0   2000   4000   6000

Time (seconds)
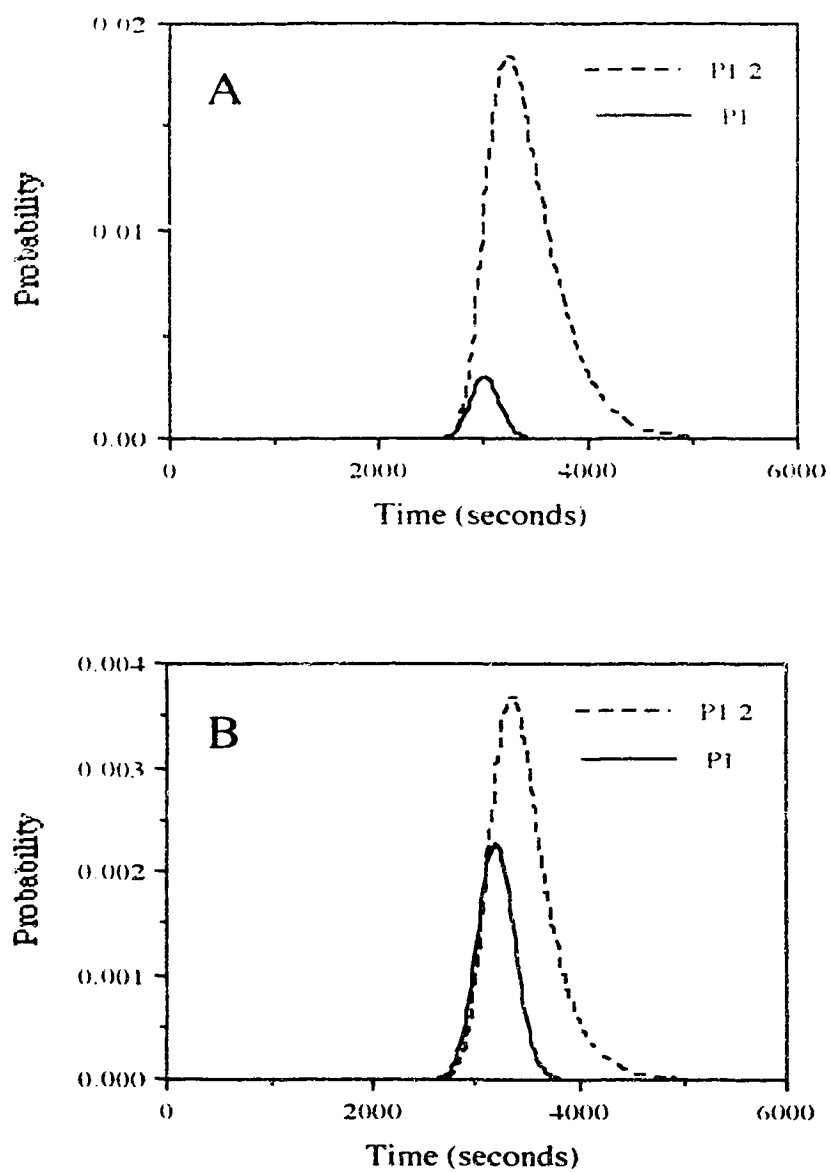
Figure 4.45   The probability distributions PI and PI/2 for napthalene on Partisil.
Curves A and B uses the exponential constants for Replicates 1 and 3
respectively. The non-interacting fraction Φ_2 for Curves A and B are
0.707 and 0.293 respectively.
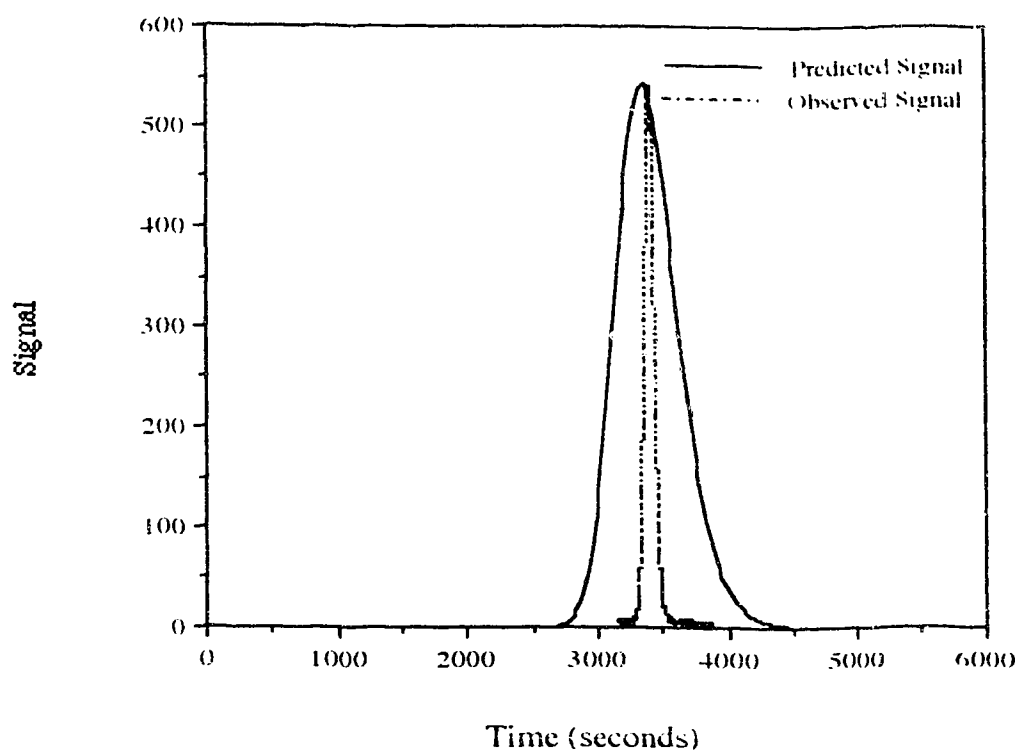
Figure 4.46   The predicted elution profile for naphthalene in 52.5 % MeOH on
Partisil-10 ODS-3 at a mobile phase linear velocity of 0.167 cm/s. The
profile is predicted using the bi-exponential constants for Replicate 2 as
shown in Table 4.21. The observed signal results from the injection
of 2.574×10^{-4} M naphthalene under the same elution conditions.

peak maxima are not coincident, they are close although this time is consistently shifted to the left for the predicted profile. It should be recalled that the profile was predicted on the basis of the actual elution conditions, that is, for a 25 cm long column packed with the same stationary phase as was used in the sorption rate experiment) at a linear velocity of 0.167 cm/s.

The three replicate rate curves predict elution profiles having somewhat differing shape. This is illustrated in Figure 4.47, for a mobile phase linear velocity of 0.167 cm/s. The elution profile predicted by Replicate 1 is less symmetrical and more tailed than the other profiles. This may be associated with the relatively small k_2 value combined with the relatively large n_2. The tailing of the profile predicted by Replicate 2 is much less because the value of k_2 here is relatively large. The profile of Replicate 3 is intermediate; although the value of k_2 is relatively small, the fraction of "sites" associated with the slow process (expressed by the fraction n_2/n_0) is much less than for the other two replicates (by about a factor of 2). As a result the influence of the second slower process is less.

The magnitude of these differences can be seen in the EMG characteristics of the predicted profiles. For $u_0 = 0.167$ cm/s, these characteristics are shown individually in Table 4.23. For all u_0 of interest, the averages from the peaks predicted by the three replicates are shown in Table 4.24. In general, the characteristics describing the character of the parent Gaussian peak are fairly reproducible, with the centre of gravity having less than 4 % RSD at all three flow rates. Less reproducible is the tailing characteristic, τ, which has a RSD greater than 25 %. This leads to a large uncertainty in the M_2 values which depend on the square of τ. It is not surprising that the tailing portion of the peak is associated with the most uncertainty, considering that it is determined mostly by the slowest rate constant and also the relatively large error in that quantity as calculated by the non-linear least squares fit program.
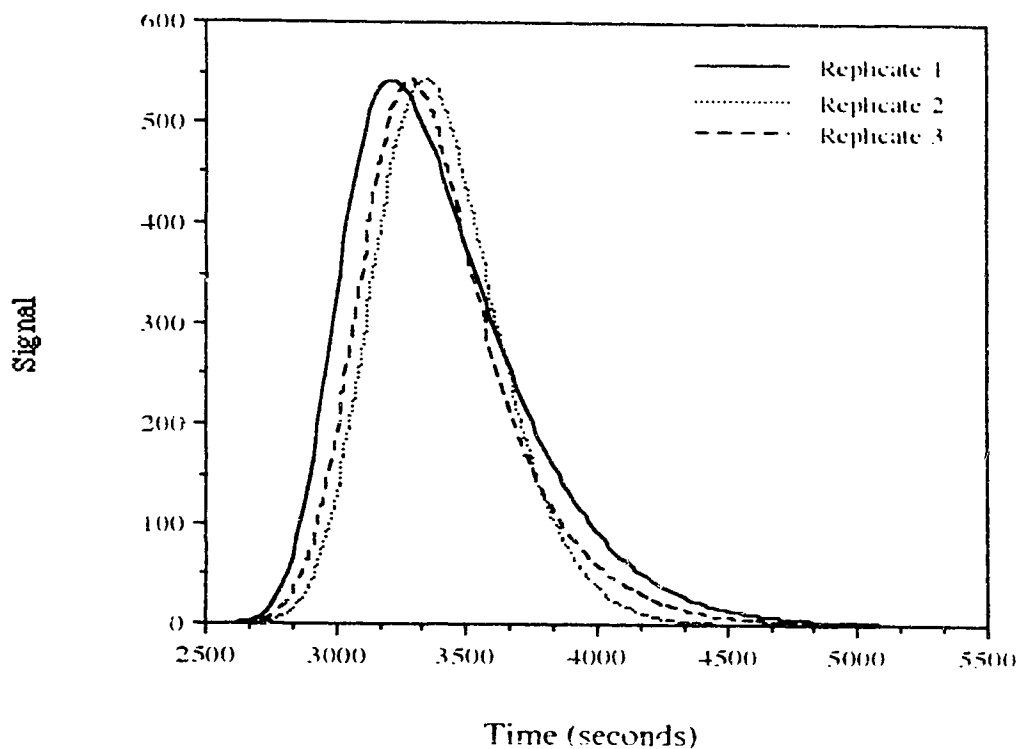
Figure 4.47   The elution profiles predicted by the three replicate bi-exponential
sorption rate curves for naphthalene on Partisil-10 ODS -3 in 52.5 %
MeOH. The individual sets of constants are shown in Table 4.21. The
profiles are predicted for a mobile phase linear velocity of 0.167 cm/s in
a 25 cm long column. The EMG characteristics of these three profiles
are shown in Table 4.23. This plot illustrates the difference in the shape
of the overall profiles.

Table 4.23   EMG characteristics of the elution profiles predicted by the three replicate bi-exponential sorption rate curves for naphthalene on Partisil-10 ODS-3 in 52.5 % MeOH for a mobile phase linear velocity of 0.167 cm.s. The elution profiles are modelled on a column which is 25 cm long containing a stationary phase identical to that used in the shallow bed experiment. Also shown are the observed values for a real elution profile acquired by the injection of 2.574 x 10^{-4} M naphthalene. See Table 4.24 for error estimates. The data in this table can be compared to data in Table 4.18 which shows the EMG characteristics of real elution profiles of naphthalene on Partisil-10 ODS-3.

Replicate	1	2	3	Observed
t_G (s)	3052	3223	3141	3270
σ_G (s)	168.2	185	165.8	29.25
τ (s)	373.1	184.5	262.9	16.52
M_1 (s)	3425	3408	3404	3286
M_2 (x 10^4 s^2)	16.75	6.826	9.661	0.1128

4.3.6   Comparison of the Predicted and Observe Elution Profiles of Naphthalene on
Partisil-10 ODS-3

Tables 4.19 and 4.24 show the EMG characteristics of the observed and
predicted elution profiles of naphthalene on Partisil-10 ODS-3, respectively. The only
parameters which are comparable are the centres of gravity which are fairly close. The
parameters which are associated with the width of the main part of the peak, namely σ_G
and with the asymmetry and tailing, namely, τ, are much larger for the predicted
profiles at all flow rates. Here again, the sources of error which include the possibility
of not meeting shallow bed conditions, inability to measure the fastest sorption rates
and the possible overestimation of the effect of slow sorption-desorption kinetics on
elution profiles using the proposed model, are consistent with the large width
characteristics for predicted profiles.

4.4   Summary

The work presented here has demonstrated that PRP-1 and Partisil-10 ODS-3
differ as sorbents in at least two major areas. First, the efficiency of PRP-1, as
demonstrated by the elution of naphthalene, is much lower than the efficiency of the
silica-based packing. Secondly, the sorption rate of naphthalene on the polymeric
phase was much slower than the rate on ODS, as measured by the shallow bed method.
Specifically, the ODS packing reaches equilibrium with a naphthalene solution fairly
quickly, at measured times of about 10 seconds whereas PRP-1 approaches equilibrium
asymptotically after 60 seconds. In the absence of other differences in these packings
and using information from the model use here to predict the shape of elution profiles
on the two packings, the difference in efficiency in the two packings is due primarily to
the difference in rate of sorption. In other words, the slow sorption (which includes

Table 4.24   Average EMG characteristics of elution profiles predicted by the three
replicate bi-exponential sorption rate curves for naphthalene on Partisil-
10 ODS-3 in 52.5 % MeOH. The characteristics are shown for three
different mobile phase linear velocities, u_o, which is shown ± one
standard deviation. The information in this table can be compared to
that found in Table 4.19 which shows the analogous quantities for real
elution profiles of naphthalene on Partisil-10 ODS-3.

u_o (cm/s) ± s	0.167 ± 0.009	0.27 ± 0.01	0.35 ± 0.01
t_G (s)	3155	1864	1451
RSD t_G (%)	2.9	3.25	3.27
σ_G (s)	173	116.74	98.09
RSD σ_G (%)	6.0	15.3	17.4
τ (s)	274	211	180
RSD τ (%)	34.6	31.3	26.6
M_1 (s)	3412.2	2074.9	1634.7
RSD M_1 (%)	0.33	0.42	0.41
M_2 (x 10^5 s^2)	1.1079	0.61209	0.43891
RSD M_2 (%)	46.1	42.3	35.2

adsorption and diffusion through the pores of the polymeric packing) is the primary cause of the broadened and tailed elution profiles observed when naphthalene is eluted off PRP-1. At this point, however, it is not possible to use the sorption rate information as measured to accurately predict the shape of the elution profile. It is unclear whether this is the result of inaccurate sorption rate determinations (due to failure to meet shallow bed conditions and to the inability to measure sorption at very short exposure times) or whether this is the result of failure of the model. This question and a possible approach to its solution are addressed in Chapter 5.

CHAPTER 5

Conclusions and Future Work

The work presented in this thesis concentrated on three major areas including: (1) the characterization of elution peaks; (2) the development of the shallow bed apparatus an its use to measure sorption rates on HPLC stationary phases; and (3) the use of a model based on probability theory to predict elution profiles based on sorption rate data acquired in the shallow bed experiment. The conclusions and future work associated with these areas are discussed below.

First, experimental HPLC peaks which were broadened and severely tailed, such as those of naphthalene on PRP-1, were shown to be well fit by an EMG function, despite problems with baseline errors such as noise. The EMG characteristics of peaks can be used to characterize the efficiency of an HPLC column. One improvement to the data processing as described in this thesis would be the development of a data collection system for the Macintosh, where the EMG curve fit program is used. The current system requires transfer of data between an IBM clone to a Macintosh, which is tedious and prone to errors in translation.

The major undertaking of the research was the design and development of the shallow bed apparatus. This apparatus has been shown to give reproducible sorption rate data for reasonably fast reactions,which occur in the time range of approximately 0.4 to 60 s. The measured sorption rate curves were shown to be well fit to multi-exponential equations. The accuracy of the method is currently limited by the failure to meet shallow bed conditions with the apparatus. This systematic error in the experiment has the greatest effect on the steeply rising portion of the sorption rate curve. A possible solution to this problem is the use of solvent systems of lower viscosity or a solution delivery system capable of higher pressure. Both of these

measures would result in a higher linear velocity through the shallow bed. The weight of packing could also be reduced as long as a radially uniform bed is formed within the slider.

A second major source of error is the limited ability of the apparatus to measure sorption at very short exposure times. The smallest exposure time, limited by the lever system which moves the slider containing the shallow bed is about 0.4 s. Sorption reactions that are complete or near-complete before this time are inaccessible. For the sorption rate curves studied here, if one of the processes is fast, the steeply rising portion of the curve will be poorly defined, resulting in erroneous rate constants in this region. A modification of the lever system might make shorter exposure times possible.

One obvious avenue open for investigation is the link between diffusion characteristics of solute molecules and their rates of sorption on polymeric packings as measured by this experiment. The slow sorption of naphthalene on PRP-1 is suspected to be a result of slow diffusion within the micropores of the polymer. If the sorption rate of a sample which is large enough to be excluded from the micropores were found to be larger than that of naphthalene, this could be taken as evidence to support this concept. The study of sorption rates of compounds which have much larger and much smaller diffusion coefficients than naphthalene could be undertaken. Also of interest is the correlation of the measured sorption rates to observed efficiencies. Polyaromatic species are observed to give especially poor efficiencies on PRP-1. Sorption rate measurements for molecules with similar diffusion characteristics to those of naphthalene but which are not polyaromatic are therefore appropriate.

The shallow bed apparatus could also be used to measure sorption rates for materials on other types of packings. The sorption rates associated with ion-exchange or affinity chromatography might be investigated by this method, assuming that the rates are in the range accessible by the shallow bed technique.

The third major area of investigation was the development of a model which uses the results of the shallow bed experiments to predict elution profiles. The model was successfully applied only qualitatively or semi-quantitatively. However, by using only one of the three sorption terms measured, the main portion of the elution profile of naphthalene on PRP-1 was successfully modelled. Poor accuracy of sorption measurements at short-exposure times means that the first term in the tri-exponential is probably underestimated. Poor precision in the curve fit at long exposure times leads to large uncertainties in the constants describing the slowest process. Improvements in the shallow bed experiment that were suggested above, which may result in meeting shallow bed conditions, may also improve prove the quantitative accuracy of the model. Another possibility in testing the model is increasing the accuracy of the shallow bed experiment by studying slower sorption processes. If sorption is a diffusion-limited process, the rate can be decrease by increasing the particle diameter, effectively increasing the diffusion distance. This work is currently underway in this laboratory.

The application of sorption rate data to HPLC columns using the Giddings type model also appears to be limited because of the apparent difference in availability of the slowest "sites", depending on the column history. In columns that are "primed", that is, where sample has been injected and is occupying the "sites" associated with the slowest kinetic process, the fraction of sites available in subsequent injections is probably not the same fraction as measured by the sorption rate experiment. For the most part, except where elution occurs off of an "unprimed" column, the effect on the chromatogram of the slowest sorption process measured in the sorption rate may be small.

BIBLIOGRAPHY

1.1 L.C. Sander and S.A. Wise. "Recent Advances in Bonded Phases for Liquid Chromatography". CRC Critical Reviews in Analytical Chemistry. 18, 299-415 (1987).

1.2 M.P. Rigney, E.F. Funkenbusch and P.W. Carr. "Physical and Chemical Characterization of Microporous Zirconia", J. Chromatogr. , 499, 291-304 (1990).

1.3 U. Bien-Vogelsang et.al., "Synthesis of Stationary Phases for Reversed-Phase LC Using Silanization and Polymer Coating", Chromatogr. 19, 170-179 (1984).

1.4 R. M. Chicz, Z. Shi and F.E. Regnier, "Preparation and Evaluation of Inorganic Anion-Exchange Sorbents Not Based on Silica". J. Chromatogr. , 359, 121-131 (1986).

1.5 M.P. Rigney, T.P. Weber and P.W.Carr. "Preparation and Evaluation of Zirconia Reversed-phase Chromatographic Support", J. Chromatogr. , 484, 273-291 (1989).

1.6 B. Gawdzik, J. Gawdzik and U. Czerwinska-Bil. "Copolymer of Di(Methylacryloxymethyl) Naphthalene and Divinylbenzene as a Column Packing for High-Performance Liquid Chromatography", Chromatogr., 26, 399-407 (1990).

1.7 R. M. Smith et.al., "Determination of Trace Levels of Ethylenethiourea by HPLC Following Derivatisation with Phenacyl Halides", Chromatogr., 19, 411-414 (1984).

1.8 D.J. Pietrzyk. "Organic Polymeric Stationary Phases", Chem. Anal. (N.Y.). 98, 223-276 (1989).

1.9 K. Wolfs et.al., "Separation of Tetracycline and Related Substances by High-Performance Liquid Chromatography on Poly(Styrene-Divinylbenzene)". J. Chromatogr., 358, 444-447 (1986).

1.10 H.J.E.M. Reeuwijk. "High-Performance Liquid Chromatography of Tetracyclines", J. Chromatogr.. 353, 339-350 (1986).

1.11 W.A. Moats, "Effect of the Silica Support of Bonded Reversed-Phase Columns on Chromatography of Some Antibiotic Compounds", J. Chromatogr., 366, 69-78 (1986).

1.12 K.A. Tweeten and T.N. Tweeten. "Reversed-Phase Chromatography of Proteins on Resin-Based Wide Pore Packings", J. Chromatogr., 359, 111-117 (1986).

1.13 I.O. Kibwage et.al., "Separation of Erythromycin and related substances by High-Performance Liquid Chromatography", J. Chromatogr., 330, 275-286 (1985).

1.14   S.E.Tett, D.J. Cutler and K.F. Brown, "High-Performance Liquid
        Chromatographic Assay for Hydroxychlorquine and Metabolites in Blood and
        Plasma using a Stationary Phase of Poly(Styrene-Divinylbenzene) and a
        Mobile Phase at pH 11, with Fluorometric Detection", J. Chromatogr., 344,
        241-248 (1985).

1.15   R.M. Cassidy and S. Elchuk, "Dynamically Coated Columns for the Separation
        of Metal Ions and Anions by Ion Chromatography", Anal. Chem., 54, 1558-
        1563 (1982).

1.16   J.W. O'Laughlin, "Separation of Cationic Metal Chelates of 1,10 -
        Phenanthroline by Liquid Chromatography", Anal. Chem., 54, 178-181
        (1982).

1.17   R.L. Smith and D.J. Pietrzyk, "Retention of Inorganic and Organic Cations on
        a Poly(styrene-divinylbenzene) Adsorbent in the Presence of Alkylsulfonate
        Salts", Anal. Chem., 56, 1572-1577 (1984).

1.18   M. Dreux and M. Lafosse, "Measurement of Sub Parts-per Million of Inorganic
        Anions in Water by Nonsuppressed Ion Exchange Chromatography with
        Conventional HPLC Instrumentation", J. High Resolut. Chrom., 9, 122-???
        (1986).

1.19   P.G. Rigas and D.J. Pietrzyk, "Liquid Chromatographic Separation and
        Indirect Detection of Inorganic Anions Using Iron(II) 1,10- Phenanthroline as a
        Mobile Phase Additive", Anal. Chem., 58, 2226-2233 (1986).

1.20   S.Coppi and A. Betti, "Liquid Chromatographic Separation and Behaviour of
        some Triazines on Styrene-divinylbenzene Columns", J. Chromatogr., 472,
        406-410 (1989).

1.21   J.R. Benson and D.J. Woo, "Polymeric Columns in Liquid Chromatography",
        J. Chromatogr. Sci., 22, 386-399 (1990).

1.22   D.P. Lee, "Reversed-Phase HPLC from pH 1 to 13", J. Chromatogr. Sci., 20,
        203-208 (1982).

1.23   R.M. Smith and D.R. Garside, "Effect of Organic Modifier on the Separation
        and Efficiencies of Homologues on Porous Columns", J. Chromatogr., 407,
        19-35 (1987).

1.24   F. Nevejans and M. Verzele, "On the Structure and Chromatographic
        Behaviour of Poystyrene Phases", J. Chromatogr., 406, 325-342 (1987).

1.25   C. Grobe-Rhode, H.G. Kicinski and A. Kettrup, "Modified Polystyrene,
        Stationary Phases for the Separation of Different Aromatic Hydrocarbon Types
        by HPLC", Chromatogr., 26, 209-214 (1990).

1.26   Y.B. Yang and M. Verzele, "New Water-Compatible Modified Polystyrene as a
        Stationary Phase for High-Performance Liquid Chromatography;
        Characterization and Application", J. Chromatogr., 387, 197-205 (1987).

1.27   D.P. Lee, "Chromatographic Evaluation of Large-Pore and Non-Porous

Poymeric Reversed Phases", J. Chromatogr., 443, 143-153 (1988).

1.28   F. Nevejans and M. Verzele, "Porous Polystyrene Packings: Characterization Through Pore Structure Determination", Chromatogr., 20, 173-178 (1985).

1.29   L.D. Bowers and S.Pedigo, "Solvent Strength on Polystyrene-Divinylbenzene Columns", J. Chromatogr., 371, 243-251 (1986).

2.1   J.C. Giddings, Dynamics of Chromatography, Marcel Dekker, New York, 1965.

2.2   C. Horvath and H.-J. Lin, "Band Spreading in Liquid Chromatography", J. Chromatogr., 149, 43-70 (1978).

2.3   J.-C. Chen and S.G. Weber, "Theoretical and Experimental Determination of Band Broadening in Liquid Chromatography", Anal. Chem. 55, 127-134, (1983).

2.4   J.C. Giddings, Dynamics of Chromatography, Marcel Dekker, New York, 1965, pps. 35, 36.

2.5   J.H. Knox and L. McLaren, "A New Gas Chromatographic Method for Measuring Gaseous Diffusion Coefficients and Obstructive Factors", Anal. Chem., 36, 1477-1482, (1964).

2.6   T. Dubetz, Ph.D. Thesis, "Study of the Origin of Excessive Bandbroadening on PRP-1", University of Alberta, Edmonton, Canada, 1988, pps. 54-59.

2.7   J.C. Giddings, Dynamics of Chromatography, Marcel Dekker, New York, 1965, pps. 49-52.

2.8   R.M. Miller, Separation Methods in Chemical Analysis, Wiley-Interscience, Toronto, 1975, pg. 123.

2.9   R. Endele, I. Halasz and K. Unger, "Influence of d_p on Column Efficiencies", J. Chromatogr., 99, 377-393 (1974).

2.10   J.C. Giddings, Dynamics of Chromatography, Marcel Dekker, New York, 1965, pps. 40-47.

2.11   R.P.W. Scott, "Contemporary Liquid Chromatography" in Techniques in Chemistry, Vol. XI, Wiley-Interscience, Toronto, 1976, Chapter 2.

2.12   J.C. Giddings, Dynamics of Chromatography, Marcel Dekker, New York, 1965, pps. 52-61.

2.13   J.C. Giddings, " Isolation of Peak Broadening Factors in Exclusion Chromatography", Macromolecules, 10, 443-448 (1977).

2.14   D.J. Anderson and R.R. Walters, "Equilibrium and Rate Constants of Immobilized Concanavalin A Determined By High-Performance Affinity Chromatography", J. Chromatogr., 376, 69-85 (1986).

2.15   J.C. Giddings, Dynamics of Chromatography, Marcel Dekker, New York,

1965, pps. 36-39.

2.16   S.J. Hawkes, "Mass Transfer Terms in Porous Layers and Particles", J. Chromatogr., 68, 1-8 (1972).

2.17   E. Grushka, L.R. Snyder and J.H.Knox, "Advances in Band Spreading Theories", J. Chromatogr. Sci., 13, 25-36 (1975).

2.18   Rohm and Haas, personal communication.

2.19   T. Dubetz, Ph.D. Thesis, "Study of the Origin of Excessive Bandbroadening on PRP-1", University of Alberta, Edmonton, Canada, 1988.

2.20   F.G. Helfferich in Mass Transfer and Ion Exchange, L. Liberti and F.G. Helfferich, eds., Martinus Nijhoff Publishers, Boston, 1983, Chapter 5.

2.21   O. Grubner in Advances in Chromatography, Vol. 6, J.C. Giddings and R.A. Keller, eds., Dekker, NY, 1968, Chapter 4.

2.22   D.B. Marshall, J.W. Burns and D.E. Connolly, "Direct Measurement of Liquid Chromatographic Sorption-Desorption Kinetics and the Kinetic Contribution to Band Broadening," J. Chromatogr., 360, 13-25 (1986).

2.23   G.E. Boyd, A.W. Adamson and L.S.Myers, Jr., "The Exchange Adsorption of Ions from Aqueous Solutions by Organic Zeolites. II. Kinetics", J. Amer. Chem. Soc., 69, 2836-2848 (1947).

2.24   P.A. Riveros and W.C. Cooper, "Kinetic Aspects of the Ion Exchange Extraction of Gold, Silver, And Base Metal Cyano Complexes", Solvent Extraction and Ion Exchange, 6, 479-503 (1988).

2.25   G.M. Harris, Chemical Kinetics, D.C. Heath, Boston, 1966, pps 68-70.

2.26   J.R. Conder and C.L. Young, Physicochemical Measurement by Gas Chromatography, John Wiley and Sons, Toronto, 1976, p. 354.

2.27   C.H. Lochmuller et.al., "Bound Pyrene Excimer Photophysics and the Organization and Distribution of Reaction Sites on Silica", J. Amer. Chem. Soc., 106, 4077-4082 (1984).

2.28   D.B. Marshall, "Statistical Considerations in the Analysis of Dispersive Kinetics Data as Discrete or Continuous Distributions of Rate Constants", Anal. Chem., 61, 660-665 (1989).

2.29   J.C. Giddings, " Kinetic Origin of Tailing in Chromatography", Anal. Chem., 35, 1999-2002 (1963).

2.30   B.A. Bidlingmeyer and F.V. Warren, Jr., "Column Efficiency Measurements", Anal. Chem., 56, 1581A-1596A (1984)

2.31   D.J. Anderson and R.R. Walters, " Effect of Baseline Errors on the Calculation of Statistical Moments of Tailed Chromatographic Peaks", J. Chromatogr. Sci., 22, 353-359 (1984).

2.32   J.P. Foley and J.G. Dorsey, "A Review of the Exponentially Modified Gaussian (EMG) Function : Evaluation and Subsequent Calculation of Universal Data", J. Chromatogr. Sci., 22, 40-46 (1984).

2.33   S.N. Chesler and S.P. Cram, "Iterative Curve Fitting of Chromatographic Peaks", Anal. Chem., 45, 1354-1359 (1973).

3.1   S. May, R.A. Hux, and F.F. Cantwell, "Measurement of Sorption Isotherms by On-Stream Precolumn Equilibration Liquid Chromatography", Anal. Chem., 54, 1279-1282 (1980).

3.2   B.L. Karger, L.R. Snyder and C. Horvath, An Introduction to Separation Science, Interscience, New York, 1973, Chapter 3.

3.3   J.C. Giddings, Dynamics of Chromatography, Marcel Dekker, New York, 1965.

3.4   L.C. Sander, C. J. Glinka and S.A. Wise, "Recent Advances in the Characterization of Bonded Phases", National Bureau of Standards publication.

3.5   C.A. Lucy, Ph.D. Thesis, "Solvent Extraction - Flow Injection Analysis: Application and Speed of Analysis", University of Alberta, Edmonton, Alberta, Canada, 1988.

3.6   J.R. Conder and C.L. Young, Physicochemical Measurement by Gas Chromatography, Wiley, Toronto, 1979, pps. 57-62.

4.1   J. Marsden and A. Weinstein, Calculus: Single Variable, Benjamin/Cummings, Don Mills, Ont, 1981, pg. 531.

4.2   E. Grushka et.al., "Computer Characterization of Chromatographic Peaks by Plate Height and Higher Central Moments, Anal. Chem., 41, 889-892 (1969).

4.3   T. Petitclerc and G.Guichon, "Determination of Higher Moments of a Non-Symmetrical Chromatographic Signal" J. Chromatogr. Sci., 14, 531-535 (1976).

4.4   S.N. Chesler and S.P. Cram, "Effect of Peak Sensing and Random Noise on the Precision and Accuracy of Statistical Moment Analysis from Digital Chromatographic Data", Anal. Chem., 43, 1922-1933 (1971).

4.5   J.J Kirkland et.al., "Sampling and Extra-Column Effects on High-Performance Liquid Chromatography; Influence of Peak Skew on Plate Count Calculations", J. Chromatogr. Sci., 15, 303-316 (1977).

4.6   P.R. Rony and J.E. Funk, "Retention Time and the First Time Moment in Elution Chromatography", J. Chromatogr. Sci., 9, 215-219 (1971).

4.7   C. Vidal-Madjar and G. Guichon, "Experimental Characterization of Elution Profiles in Gas Chromatography Using Statistical Moments, " J. Chromatogr., 142, 61-86 (1977).

4.8   J.J. van Deemter, F.J. Zuiderweg and A. Klinkenberg, " Longitudinal Diffusion and Resistance to Mass Transfer as Causes of Non-ideality in

Chromatography". Chem. Eng. Sci., 5 271-289 (1956).

4.9 E. Katz, K. Logan and R.P.W. Scott, "Liquid Chromatographic Column Design", J. Chromatogr., 289, 65-83 (1984).

4.10 E. Katz, K. Logan and R.P.W. Scott, "Peak Dispersion and Mobile Phase Velocity in LC", J. Chromatogr., 270, 51-75 (1983).

4.11 J.C. Giddings and H. Eyring, "A Molecular Dynamic Theory of Chromatography", J. Chem. Phys., 59, 416-421 (1955).

4.12 D.M. Ottenstein, "Chromatographic Support in Gas Chromatography", J. Chromatogr. Sci., 11, 136-144 (1973).

4.13 L.R. Snyder and J.J. Kirkland, Introduction to Modern Liquid Chromatography, Wiley-Interscience, Toronto, 1979, pg. 838.

4.14 L.R. Snyder "A Rapid Approach to Selecting the Best Experimental Conditions for High-Speed Column Chromatography", J. Chromatogr. Sci., 15, 441-449 (1971).

4.15 J.G. Graselli and W.M. Ritchey, editors, Atlas of Spectral Data and Physical Constants for Organic Compounds, 2nd edition, CRC Press, Boca Raton, FA., 1975.

APPENDIX 1

Calculation of Contributions to the Total Plate Height from Individual Rate Processes

The contributions to the plate height that have been calculated for an HPLC column containing 10 μm spherical, porous particles are shown in the following discussion.

The diffusion coefficient was calculated from the Wilke-Chang equation [4.14] for naphthalene which was assumed to have a molar volume of 125 mL/mol. D_m is assumed to have a value of 1.0×10^{-5} cm^2/s. The mobile phase is considered to be 85 % MeOH. Section 4.6.3.3 describes the calculation for the diffusion coefficient of this sample molecule under these circumstances. The k' of the molecule is assumed to be 35 under these conditions. The linear velocity of the mobile phase, u_o, is 0.4 cm/s.

1. Plate Height Contribution due to Longitudinal Diffusion

Using equation 2.2 and using an obstruction factor, γ, of 0.6 [2.5], H_{LD} is calculated be

$$H_{LD} = \frac{2\gamma D_m}{u_o} = \frac{2\ (0.6)\ 10^{-5}\ cm^2/s}{0.4\ cm/s} = 3 \times 10^{-5}\ cm$$

2. Plate Height Contribution due to Eddy Diffusion

Using equation 2.3 and a column packing factor of 2.5 [2.9], H_{eddy} is calculated to be

$$H_{eddy} = 2\lambda d_p = 2(2.5)(0.001\ cm) = 0.005\ cm$$

The packing factor was determined experimentally by Endele et.al. using spherical silica particles in the range of 5 to 35 μm. The value of the packing factor is calculated from a plot of plate height vs linear velocity at relatively high linear velocity. Equation 2.11 reduces to a linear function with an intercept equal to $2\lambda d_p$. This is an estimate, as the packing factor is expected to depend on the quality of packing as well

as the particle diameter.

3. Plate Height Contribution due to Resistance to Mass Transfer in the Mobile

Phase

Using equation 2.4 and a packing factor of 1.3 [2.8], H_m is calculated to be

$$H_m = \frac{\omega d_p^2 u_o}{D_m} = \frac{1.3(0.001 cm)^2(0.4\ cm/s)}{10^{-5} cm^2/s} = 0.052\ cm$$

This term is fairly large due to the small diffusion coefficient for the sample in the liquid

mobile phase.

4. Plate Height Contribution due to Coupled Term

Using equation 2.5 and results shown above, H_{couple} is calculated to be

$$H_{couple} = \left[\frac{1}{H_{eddy}} + \frac{1}{H_m} \right]^{-1}$$

$$H_{couple} = \left[\frac{1}{0.005\ cm} + \frac{1}{0.052\ cm} \right]^{-1} = 0.0046\ cm$$

5. Plate Height Contribution due to Resistance to Mass Transfer in the Stagnant

Mobile Phase

In order to use equation 2.7, the fraction of mobile phase locate in the pores, f,

must be calculated. This is given by the ratio of the pore volume of the column to the

total pore and intraparticle volume. For PRP-1, the specific pore volume and the total

specific volume are given by the manufacturer.

$$f = \frac{pore\ vol.}{pore\ vol.\ +\ interparticle\ vol.} = \frac{0.79\ mL/g}{1.53\ mL/g} = 0.52$$

The fct(f,k') can then be calculated using equation 2.8

$$fct(f,k') = \frac{(1 - f + k')^2}{30(1 - f)(1 + k')^2} = \frac{(1 - 0.52 + 35)^2}{30(1 - 0.52)(1 + 35)^2} = 0.067$$

This result can be used in equation 2.7 assuming γ' is 1.

$$H_{sm} = \frac{fct\ (f,\ k')\ d_p^2\ u_o}{\gamma' D_m}$$

$$= \frac{(0.067)\ (0.001\ cm)^2(0.4\ cm/s)}{1(10^{-5}\ cm^2/s)} = .0027\ cm$$

6. Plate Height Contribution due to Resistance to Mass Transfer in the Stationary Phase

Equation 2.7 was used to calculate this contribution, assuming that the desorption rate constant was the inverse relaxation time found by Marshall et.al. to be on the order of 500 s^{-1} [2.22].

$$H_s = 2\ \frac{k'}{(1 + k')^2}\ \frac{u_o}{k_d}$$

$$= 2\ \frac{35}{(1 + 35)^2}\ \frac{(0.4\ cm/s)}{500\ s^{-1}} = 4.3\ x\ 10^{-5}\ cm$$

7. Total Plate Height

The total plate height is therefore the sum of the above individual contributions.

$$H = H_{LD} + H_{couple} + H_{sm} + H_s$$

$$= (3\ x\ 10^{-5} + 0.0046 + 0.0027 + 4.3\ x\ 10^{-5})\ cm$$

$$H = 0.0073\ cm$$

APPENDIX 2

Calculation of Specific Pore Volume for Partisil-10 ODS-3

Sander et.al. [3.4] used size exclusion chromatographic techniques to determine the specific pore volumes of a variety of bonded phase. They describe the synthesis of phases of different chain lengths in so-called monomeric and polymeric (which results in cross-linking of the stationary phase) syntheses. They demonstrate that the decrease in pore volume associated with surface derivatization of silica is independent of the type of synthesis used and is dependent only on the percentage carbon loading, % C. From their published data. equation A.2.1 relates the pore volume of the bonded phase to % C.

$$v'_p = v_{p,Si} - \frac{0.0169 \text{ mL}}{\text{g Si}}(\% \text{ C})$$

<div align="right">eqn. A2.1</div>

Here, $v_{p,Si}$ is the specific pore volume of the original, underivatized silica. This is usually the only information available about pore volume for commercially available bonded phases. As further explained below, v'_p is the pore volume of the bonded phase with respect to the weight of the original silica in the bonded phase.

For the Partisil-10 ODS-3 used in the experiments, $v_{p,Si}$ is approximately 0.8 mL/g Si and the % C loading is 10.5 %. Therefore, v'_p is 0.62 mL/g Si. In order to calculate the pore volume with respect to the weight of the stationary phase as a whole, it is necessary to calculate the relative weight of original silica in the bonded phase.

In the derivatization process, octadecyl-silyl groups, Si-$C_{18}H_{37}$, are bonded to the silica surface by Si-O-Si linkages. The derivatization process is assumed to be the only source of C. In 100 g of derivatized packing, there are 10.5 g of carbon, corresponding to 0.874 mol. The amount of H added by the derivatization can be calculated from the ratio of C:H in ODS and is 1.8 g. Some silica is added in the derivatization process, in this case 0.049 mol or 1.4 g. In 100 g packing, the amount

of original silica is then given by equation A2.2

$$\text{g Si in pkg} = 100 \text{ g} - \text{g C} - \text{g H} - \text{p added Si} \qquad \text{eqn A2.2}$$

For Partisil-10 ODS-3, there are 86 g of origi: :a in 100 g of packing. The pore volume with respect to the weight of the bonded phase is calculated using A2.3

$$v_p = v_p' \; \frac{\text{g Si in pkg}}{\text{g pkg}}$$

$$\text{eqn A2.3}$$

For Partisil-10 ODS-3, v_p is calculated to be 0.54 mL/ g pkg. A typical shallow bed with a weight of 1.06 ± .04 mg will have a pore volume of 0.57 µL.

PRP-1, the porous polymeric packing, has a specific pore volume of 0.79 mL/g pkg. A typical shallow bed with a weight of 1.82 ± .04 mg will have a pore volume of 1.43 µL.

APPENDIX 3.1

The program shown below, written in MATLAB by David Gowanlock is referred to in
the text as EXPGAUSS and calculates the Exponentially-modified Gaussian function
that best fits data from an elution curve. The data are entered with their time values in
the brackets following the Data command.

```
echo off
clc
clear
Data = ...
[];
numberofpoints = 40;
t = Data(:,1);
y = Data(:,2);
[Ymax,indexYmax] = max(y);
[Ymin1,indexYmin1] = min(y(1:indexYmax));
[Ymin2,index] = min(y(indexYmax:length(y)));
indexYmin2 = index + indexYmax - 1;


[M0,M1,M2,M3] = moments(t,y);


retenttime_exp = (M3 ./ 2) .^ 0.3333
retenttime_gaus = M1 - retenttime_exp
variance_exp = retenttime_exp .^ 2
variance_gaus = M2 - variance_exp
fit_indecies = linspace(1,length(y),numberofpoints);
round(fit_indecies);
global FitData_t
FitData_t = t(fit_indecies);
global FitData_y
FitData_y = y(fit_indecies) ./ M0;  % area of dist. normalized to unit area
axis([t(1) t(length(t)) 0 (Ymax ./ M0 .* 1.05)]);
plot(t,y ./ M0,FitData_t,FitData_y,'o');
```

```
lam = |retenttime_gaus retenttime_exp (variance_gaus .^ 0.5)|';
lam = fmins('fitmy',lam,,1)

FitData_y = y(fit_indecies);

global lam_global
lam_global = lam;
lin_scaling_factor = fzero('exp_fit_diff',M0)

mintime = min(t);
maxtime = max(t);
miny = 0.0;
maxy = max(y);
t_curvefit = mintime:10:maxtime;
y_curvefit = lin_scaling_factor .* (exp(lam(3).^2 ./ (2 .* lam(2).^2)) .* ...
exp((lam(1) - t_curvefit) ./ lam(2)) ./ (2 .* lam(2)) .* ...
(1 + erf((t_curvefit-lam(1)-lam(3).^2 ./ lam(2)) ./( sqrt(2) .* lam(3)))));
axis([mintime maxtime miny (maxy .* 1.05)]);
plot(t,y,FitData_t,FitData_y,'o',t_curvefit,y_curvefit);
xlabel('Time [seconds]');
ylabel('Counts');
text(.65,.8,'numeric','sc')
text(.8,.8,'fit','sc')
text(.5,.7,'gaus tr','sc')
text(.5,.65,'gs sd.dv.','sc')
text(.5,.6,'exp tr','sc')
text(.65,.7,num2str(retenttime_gaus),'sc')
text(.65,.65,num2str(variance_gaus .^ 0.5),'sc')
text(.65,.6,num2str(retenttime_exp),'sc')
text(.8,.7,num2str(lam(1)),'sc')
text(.8,.65,num2str(lam(3)),'sc')
text(.8,.6,num2str(lam(2)),'sc')
```

APPENDIX 3.2

The program shown below, called FITMY, is referred to in the EMG curve fitting routine shown in Appendix 3.1 and is written in MATLAB by David Gowanlock.

```
function f = fitfun(lam)
%       FITFUN is used by FITDEMO.  Fitfun(lam) returns the error
%       between the data and the values computed by the current
%       function of lam.  FITFUN assumes a function of the form

%y = lam(4).*(exp(lam(3) .^2 ./ (2 .* lam(2) .^2)) .* exp((lam(1) - t) ...
%  ./ lam(2)) ./ (2 .* lam(2)) .* ...
%( 1 + erf((t-lam(1)-lam(3) .^2 ./ lam(2)) ./( sqrt(2) .* lam(3)))));
% Global Data
t = FitData_t; y = FitData_y;
A = zeros(length(t),1);
for j = 1:1
A(:,j) = (exp(lam(3).^2 ./ (2 .* lam(2).^2)) .* exp((lam(1) - t) ...
  ./ lam(2)) ./ (2 .* lam(2)) .* ...
( 1 + erf((t-lam(1)-lam(3).^2 ./ lam(2)) ./( sqrt(2) .* lam(3)))));

end
c = A\y;
z = A*c;
f = norm(z-y);


% Statements to plot progress of fitting:
%plot(t,z,t,y,'o')
%xt = max(t)/2;
%yt = max(y)/2;
%text(xt,1.2*yt,['lambda(1,2) = ' num2str(lam(1)) ' ' num2str(lam(2))])
%text(xt,1.0*yt,['lambda(3) = ' num2str(lam(3))])
%text(xt,0.8*yt,['err norm = ' num2str(f)])
```

APPENDIX 3.3

The program shown below, FZERO, is written in MATLAB by David Gowanlock and is referred to in the program peakshape shown in Appendix 4.1. It is used to find the minimum of a function.

```
function b = fzero(FunFcn,x,tol,trace)
%FZERO      Zero of a function of one variable.
%      FZERO(F,X) finds a zero of f(x).  F is a string containing the
%      name of a real-valued function of a single real variable.  X is
%      a starting guess.  The value returned is near a point where F
%      changes sign.  For example. FZERO('sin',3) is pi.  Note the
%      quotes around sin.  Ordinarily, functions are defined in M-files.
%      An optional third argument sets the relative tolerance for the
%      convergence test.  The presence of an nonzero optional fourth
%      argument triggers a printing trace of the steps.
%      C.B. Moler 1-19-86
%      Revised CBM 3-25-87, LS 12-01-88.
%      Copyright (c) 1986-88 by the MathWorks, Inc.
% This algorithm was originated by T. Dekker.  An Algol 60 version,
% with some improvements, is given by Richard Brent in "Algorithms for
% Minimization Without Derivatives", Prentice-Hall, 1973.  A Fortran
% version is in Forsythe, Malcolm and Moler, "Computer Methods
% for Mathematical Computations", Prentice-Hall, 1976.

% Initialization
if nargin < 3, trace = 0; tol = eps; end
if nargin == 3, trace = 0; end
if trace, clc, end
if x ~= 0, dx = x/20;
else, dx = 1/20;
end
a = x - dx; fa = feval(FunFcn,a);
if trace, home, init = [a fa], end
b = x + dx; fb = feval(FunFcn,b);
```

```
if trace, home, init = |b fb|, end


% Find change of sign.
while (fa > 0) == (fb > 0)
  dx = 2*dx:
  a = x - dx:  fa = feval(FunFcn,a);
  if trace, home, sign = |a fa|, end
  if (fa > 0) ~= (fb > 0), break, end
  b = x + dx;  fb = feval(FunFcn,b);
  if trace, home, sign = |b fb|, end
end


fc = fb;
% Main loop, exit from middle of the loop
while fb ~= 0
  % Insure that b is the best result so far, a is the previous
  .  value of b, and c is on the opposite of the zero from b.
  if (fb > 0) == (fc > 0)
    c = a;  fc = fa;
    d = b - a;  e = d;
  end
  if abs(fc) < abs(fb)
    a = b;   b = c;   c = a;
    fa = fb;  fb = fc;  fc = fa;
  end


  % Convergence test and possible exit
  m = 0.5*(c - b);
  toler = 2.0*tol*max(abs(b),1.0);
  if (abs(m) <= toler) + (fb == 0.0), break, end


  % Choose bisection or interpolation
  if (abs(e) < toler) + (abs(fa) <= abs(fb))
  % Bisection
    d = m;  e = m;
  else
```

```
% Interpolation
   s = fb/fa:
   if (a == c)
   % Linear interpolation
      p = 2.0*m*s:
      q = 1.0 - s:
   else
   % Inverse quadratic interpolation
      q = fa/fc:
      r = fb/fc;
      p = s*(2.0*m*q*(q - r) - (b - a)*(r - 1.0));
      q = (q - 1.0)*(r - 1.0)*(s - 1.0):
   end:
   if p > 0. q = -q: else p = -p: end:
   % Is interpolated point acceptable
   if (2.0*p < 3.0*m*q - abs(toler*q)) * (p < abs(0.5*e*q))
      e = d:  d = p/q:
   else
      d = m:  e = m:
   end:
   end % Interpolation
% Next point

   a = b:

   fa = fb:

   if abs(d) > toler, b = b + d:

   else if b > c, b = b - toler:

      else b = b + toler:

      end

   end
   fb = feval(FunFcn,b);
   if trace, home, step = |b fb|, end
end % Main loop
```

APPENDIX 3.4

The program shown below, written in MATLABby David Gowanlock is called EXP_FIT_DIFF and is used in peakshape, the program shown in Appendix 3.1 to determine the difference between the experimental data points and those calculated by the fit equation.

```
function differ = exp_fit_diff(linscale)

% Global Data
t = FitData_t; y_experimental = FitData_y;
lam = lam_global;

y_fit = linscale .* (exp(lam(3).^2 ./ (2 .* lam(2).^2)) .* exp((lam(1) - t) ...
 ./ lam(2)) ./ (2 .* lam(2)) .* ...
(1 + erf((t-lam(1)-lam(3).^2 ./ lam(2)) ./( sqrt(2) .* lam(3)))));

differ = sum(y_experimental - y_fit);
```

APPENDIX 4.1

The program shown in Appendix 4.1 is written in MATLAB by David Gownalock and uses information from the sorption rate curves to calculate the elution chromatogram. The program is called PEAK SHAPE CALC. It is based on the data treatment discussed in Section 2.3.6.

```
clear
clc
% ELUTION CHROMATOGRAM FROM KINETIC CURVE
% David Gowanlock  May 31, 1991
%
% The following is written to predict elution chromatogram profiles
% from shallow bed kinetic plots. In this case the shallow bed kinetic
% plots have been fit to a triexponential of the following form:
%
% absorbance = n0 - (n1 * exp(-k1 * t)) - (n2 * exp(-k2 * t))
%                 - (n3 * exp(-k3 * t))
%
%                         1 = fast sites
%                         2 = intermediate sites
%                         3 = slow sites
% The equation used to produce the elution profiles corresponding
% to each of the above type of sites is given in the following reference
% (see function probdist):
%    equation (1), page 1999
%    J. C. Giddings, Anal. Chem., Vol. 35, Page 1999, Dec. 1963
%
% Variable List
%    k_prime = k'
%    k = rate constant from kinetic curve
%    n = fraction of a particular type of site
%    ord = order of bessel function
%    ts = t - tm
%    tm = time for mobile phase
```

```
%   t = time from injection
%   ka = adsorption rate constant
%   kd = desorption rate constant
%   Pts = probability distribution with respect to time
%   nanalrt = used to detect NaN warnings that can arise in the
%           calculation of bessel values in the function probdist
%                            stepsz = stepsize along the time axis
%   fr_no_sl = fraction not interacting with the slow sites
%           (fraction not slow)
%   fr_sl = fraction interacting with the slow sites
%           (fraction slow)
%   theor_ratio = theoretical ratio of solute iteracting with slow sites to
%           solute not interacting with slow sites
%   act_ratio = theoretical ratio of solute iteracting with slow sites to
%           solute not interacting with slow sites
%   maxsz = maximum value of range of ts1 and ts2 values
%-----------------------------------------------------------------
% This section is where the inital parameters used throughout the rest
% of the program are entered.


stepsz = 50;
maxsz = 3000;
k_prime = 35.7
k1 = 2.79
k2 = .642
k3 = .0572
n1 = 1.70e-7
n2 = .697e-7
n3 = .356e-7
tm = 37.32


n0 = n1 + n2 + n3


%-----------------------------------------------------------------
% The following calculates the elution profile for the fast sites.
%
```

```
ord1 = 1:
ts1 = 1:stepsz:maxsz;
ka1 = k1 ./ (1 + (k_prime .^ (-1)))
kd1 = k1 ./ (k_prime + 1)
tm1 = tm .* n1 ./ n0


[Pts1,nanalrt1] = probdist(ts1,ka1,kd1,tm1,ord1);


%--------------------------------------------------------------
% The following calculates the eleution profile for the intermediate sites.
%
ord2 = 1:
ts2 = 1:stepsz:maxsz;
ka2 = k2 ./ (1 + (k_prime .^ (-1)))
kd2 = k2 ./ (k_prime + 1)
tm2 = tm .* n2 ./ n0


[Pts2,nanalrt2] = probdist(ts2,ka2,kd2,tm2,ord2);


%--------------------------------------------------------------
% The following convolves the elution profiles of sites 1 & 2 and
% calculates the maximum value of the ts3 array.
Pts1_2 = conv(Pts1,Pts2);
maxsz3 = length(Pts1_2) .* stepsz;


%--------------------------------------------------------------
% The following calculates the elution profile for the slow sites
%
ord3 = 1;
ts3 = 1:stepsz:maxsz3;
ka3 = k3 ./ (1 + (k_prime .^ (-1)))
kd3 = k3 ./ (k_prime + 1)
tm3 = tm .* n3 ./ n0


[Pts3,nanalrt3] = probdist(ts3,ka3,kd3,tm3,ord3);
%--------------------------------------------------------------
```

```
% The following convolves the elution profiles and plots the results
% along with the elution profiles for each type of site acting alone.
%
ts1_2 = 1:stepsz:maxsz3;
Pts1_2_3 = conv(Pts1_2,Pts3);
maxsz1_2_3 = length(Pts1_2_3) .* stepsz;
ts1_2_3 = 1:stepsz:maxsz1_2_3;
ymax = max([max(Pts1),max(Pts2),max(Pts3)]);
scale1_2 = 0.6 .* ymax ./ max(Pts1_2);
scale1_2_3 = 0.4 .* ymax ./ max(Pts1_2_3);

axis([0,maxsz1_2_3.*0.5,0,1.05.*ymax])
plot(ts2,Pts2,ts1,Pts1,ts1_2,Pts1_2 .* scale1_2,ts3,Pts3,ts1_2_3,Pts1_2_3 .* ...
scale1_2_3)
xlabel('ts'), ylabel('P(ts)')
pause
%-------------------------------------------------------------------
% Integration of the peaks

area1_2 = integrate_2pt(ts1_2,Pts1_2)
area1_2_3 = integrate_2pt(ts1_2_3,Pts1_2_3)
%area1 = integrate_2pt(ts1,Pts1)
%area2 = integrate_2pt(ts2,Pts2)
%area3 = integrate_2pt(ts3,Pts3)
%-------------------------------------------------------------------
% This section scales the convolution of 1 & 2 with the convolution of 1, 2, & 3

fr_no_sl = exp(-1 .* ka3 .* tm3);
fr_sl = 1.0 - fr_no_sl;
theor_ratio = fr_sl ./ fr_no_sl;
act_ratio = area1_2_3 ./ area1_2;
correction = theor_ratio ./ act_ratio;
Pts1_2_3 = Pts1_2_3 .* correction;
area1_2_3 = integrate_2pt(ts1_2_3,Pts1_2_3)
axis([0,maxsz1_2_3.*0.5,0,1.05.*max([max(Pts1_2),max(Pts1_2_3)])])
plot(ts1_2,Pts1_2,ts1_2_3,Pts1_2_3)
```

```
xlabel('ts'), ylabel('P(ts)')
pause


%---------------------------------------------------------------
%   This section addes the convolution of 1 & 2  to the convolution of 1, 2, & 3
%
for l= 1:length(Pts1_2);
Ptsnet(l) = Pts1_2(l) + Pts1_2_3(l);
end
axis([0,maxsz1_2_3.*0.5,0,1.05.*max(Ptsnet)])
plot(ts1_2,Pts1_2,ts1_2_3,Pts1_2_3,ts1_2,Ptsnet)
xlabel('ts'), ylabel('P(ts)')
pause


%---------------------------------------------------------------
%   This section plots the elution profile from time of injection, not ts
%   (ts = t - tm)
%
t1_2 = ts1_2 + tm;
axis;
plot(t1_2,Ptsnet)
xlabel('t'), ylabel('P(t)')
```

APPENDIX 4.2

The following program, called INTEGRATE_2PT, is used in the program PEAK
SHAPE CALC shown in Appendix 4.1. It was written in MATLAB by David
Gowanlock.

```
function area = integrate_2pt(X,Y)
%
%
if length(X) ~= length(Y)
  error('Can not integrate because X & Y of unequal length')
end
deltaX = X(2) - X(1);
runningarea = 0.0;
for I = 1:length(X)-1;
  Yave = (Y(I) + Y(I+1)) ./ 2;
  slicearea = deltaX .* Yave;
  runningarea = runningarea + slicearea;
end
area = runningarea;
```

APPENDIX 4.3

The program shown below, called PROBDIST is referred to in the program PEAK SHAPE CALC. shown in Appendix 4.1. It was written in MATLAB by David Gowanlock. This program calculates the function Pt_s.

```
function [Y,nanalrt] = probdist(ts,ka,kd,tm,n)
%  PROBABILITY DISTRIBUTION
%  The equation used to produce the eleution profile corresponding
%  to each type of site
%    equation (1), page 1999
%    J. C. Giddings, Anal. Chem., Vol. 35, Page 1999, Dec. 1963
%  Variable List
%    n = order of bessel function
%    ts = t - tm
%    tm = time for mobile phase
%    t = time from injection
%    ka = adsorption rate constant
%    kd = desorption rate constant
%    Pts = probability distribution with respect to time
%    nanalrt = used to detect NaN warnings that can arise in the
%              calculation of bessel values
term = sqrt(4 .* ka .* kd .* tm .* ts);
subterm = abs(((-1) .^n .* bessel(n,i .* term) .* i));
Y = ((ka .* kd .* tm) ./ ts) .^0.5 .* ...
exp(-1 .* ((ka .* tm) + (kd .* ts))) .* ...
subterm;
for l=1:length(Y);
  if Y(l) == NaN,
    Y(l) = 0.0;
        nanalrt(l) = 1;
  end;
end;
```